ELSEVIER

Journal of Molecular Structure (Theochem) 619 (2002) 143–194

THEO CHEM

www.elsevier.com/locate/theochem

How reliable could economic Hartree–Fock computations be in studying large, folded peptides? A comparative HF and DFT case study on N- and C-protected aspartic acid

Joseph C.P. Koo[a,*], Janice S.W. Lam[a], Salvatore J. Salpietro[a], Gregory A. Chass[a,b], R.D. Enriz[c], Ladislaus L. Torday[d], Andras Varro[d], Julius Gy. Papp[d,e]

[a]*Department of Chemistry, University of Toronto, Toronto, Ont., Canada M5S 3H6*
[b]*Velocet R&D, 210 Dundas St. West, Suite 810, Toronto, Ont., Canada M5G 2E8*
[c]*Department of Chemistry, National University of San Luis, Chacabuco 971, 5700 San Luis, Argentina*
[d]*Department of Pharmacology and Pharmacotherapy, Szeged University, Dóm tér 12, H-6701 Szeged, Hungary*
[e]*Division of Cardiovascular Pharmacology, Hungarian Academy of Sciences and Szeged University, Dóm tér 12, H-6701 Szeged, Hungary*

Received 23 June 2002; accepted 11 August 2002

Abstract

In this study, potential energy hypersurfaces have been generated and analyzed for each of the nine possible backbone (BB) conformations for both the *endo* and *exo* forms of *N*-acetyl-L-aspartic acid *N*′-methylamide. Ab initio calculations were carried out at RHF/3-21G, RHF/6-31G(d), and B3LYP/6-31G(d) levels for all backbone conformations. The relative energies, as well as stabilization energies exerted by the sidechain (SC) on the backbone, were calculated for all stable conformers. All sidechain–sidechain (HO···O=C), backbone–backbone (N–H···O=C), and sidechain–backbone (N–H···O=C; N–H···OH) hydrogen bond interactions were analyzed. The appearance of the traditionally absent α_L and ε_L conformers may be recognized as special geometric orientation which the aspartyl residue manifests during peptide folding or ligand docking in a receptor that contains aspartic acids in its ligand recognition sites. At all three levels of theory, there exists a trend between the hydrogen bond distance and ring size. In addition, strikingly high correlations between the torsional angles ($R^2 = 0.9937$ for RHF/6-31G(d) versus RHF/3-21G; $R^2 = 0.9967$ for B3LYP/6-31G(d) versus RHF/6-31G(d); $R^2 = 0.9914$ for B3LYP/6-31G(d) versus RHF/3-21G) and between the ΔE values in kcal/mol ($R^2 = 0.9424$ for RHF/6-31G(d) versus RHF/3-21G; $R^2 = 0.9108$ for B3LYP/6-31G(d) versus RHF/6-31G(d); $R^2 = 0.9434$ B3LYP/6-31G(d) versus RHF/3-21G) found at the different ab initio levels suggest that calculations carried out at the lower levels (i.e. at RHF/3-21G) are still significant.

Keywords: Aspartic acid residue; Density functional theory conformations; α_L Helical structure; ε_L Helical structure; Internal hydrogen bonding; External hydrogen bonding

* Corresponding author.
E-mail address: joseph.koo@utoronto.ca (J.C.P. Koo) jan.lam@utoronto.ca (J.S.W. Lam), sal.salpietro@utoronto.ca (S.J. Salpietro), gchass@fixy.org (G.A. Chass), denriz@unsl.edu.ar (R.D. Enriz), pyro@phcol.szote.u-szeged.hu (L.L. Torday), varro@phcol.szote.u-szeged.hu (A. Varro), papp@phcol.szote.u-szeged.hu (J.G. Papp).

1. Introduction

Computational molecular modeling is a field of great interest in recent years. In particular, computational studies have played a dominant role

0166-1280/02/$ - see front matter © 2002 Elsevier Science B.V. All rights reserved.
PII: S0166-1280(02)00579-1

in drug designs as well as functional studies in pharmacology [1–8]. However, results from computational modeling are often limited by computer powers. In addition, the speed of which these results were generated is also determined by the different theories that form the fundamental formulas and equations in these modeling computer programs. The more strict and less degree of freedom a particular theory has, the more accurate the results, and the computation requires a longer period of time. In quantum chemistry, the efficiency and accuracy of ab initio calculations are restricted by the above-mentioned conditions. It is important to perform ab initio studies on peptides and molecules, as they are the constituents from which proteins, ligands, and other macromolecules were formed. All amino acids can now be studied by ab initio methods. Many single amino acids have already been subjected to detailed ab initio calculations. These attempts include, among others, alanine [9–14], asparagines [15], cysteine [16,17], glycine [18,19], phenylalanine [20–22], proline [23], selenocysteine [24], serine [25–27], and valine [28]. In the past, it is always assumed that only results generated at B3LYP/6-31G(d) (or density functional theory, DFT) or higher levels would have validity while results from the Hartree–Fock levels, including the RHF/3-21G and RHF/6-31G(d), are only viewed as preliminary 'guesses' and estimates of the true values. As a result, ab initio computational studies are often time-consuming, a factor that affects the efficiency of which result analyses can be reported. In this paper, we wish to explore the answer to the question whether ab initio results generated at the RHF/3-21G and RHF/6-31G(d) levels are sufficiently accurate when compared to higher levels of theory such as DFT. Here, all stable conformers for the aspartic acid residue, *N*-acetyl-L-aspartic acid *N*′-methylamide, were computed at RHF/3-21G, RHF/6-31G(d), and B3LYP/6-31G(d). In turn, we compared the correlation of these levels of theory by comparing their torsional angles computed for all stable conformers.

2. Stereochemical background

An earlier study performed by Salpietro et al. [29] focused on the sidechain potential energy surface of *N*-formyl-L-aspartic acidamide and its conjugate base *N*-formyl-L-aspartamide in their γ_L backbone conformations. In that study, ab initio calculations were performed on all conformations of the parent aspartic acid diamide and its conjugate base with depronated sidechain. Propionic acid and priopionate ion were, respectively, used to mimic the sidechain of *N*-formyl-L-aspartamide in its neutral and anionic form. In this report, the full backbone (BB) and sidechain (SC) conformations of *N*-acetyl-L-aspartic acid *N*′-methylamide in both *endo* and *exo* forms were explored for the carboxylic acid moiety.

N-acetyl-L-aspartic acid *N*′-methylamide differs from *N*-formyl-L-aspartic acidamide by having methyl groups instead of H atoms in each of its N- and C-protective groups, as shown in Fig. 1. It is expected that the backbone geometry of *N*-acetyl-L-aspartic acid *N*′-methylamide will be analogues to that of an alanine residue. In this case, however, an H atom of the α-methyl group in alanine is replaced with a –COOH group. Previous studies on the alanine molecule [9–14] did not reveal any stable conformer in either the α_L and ε_L backbones. Because alanine is the simplest chiral amino acid whose backbone also recurred in other peptide residues, it was predicted at first that no stable α_L and ε_L conformers will exist *N*-acetyl-L-aspartic acid *N*′-methylamide.

As mentioned above, other ab initio studies have been performed on various single amino acids [9–28]. In this investigation, the 4D-Ramachandran potential energy hypersurface (PEHS) of the *N*-methylated aspartic acid, where $E = E(\phi, \psi, \chi_1, \chi_2)$, is explored by varying the backbone (ϕ, ψ) and sidechain (χ_1, χ_2). As a result, $3^2 = 9$ backbone conformations (γ_L, β_L, δ_L, α_L, ε_L, γ_D, δ_D, α_D, and ε_D) are coupled with $3^2 = 9$ sidechain orientations on a 2D-Ramachandran Map, shown in Fig. 2. Consequently, $3^4 = 81$ geometries were optimized on a 4D-Ramachandran PEHS, shown in Fig. 3, for both the *endo* and *exo* forms of *N*-acetyl-L-aspartic acid *N*′-methylamide.

N-acetyl-L-aspartic acid *N*′-methylamide exists in two forms: *endo* and *exo*. This is because its carboxyl group of the propionic acid sidechain also exist in two forms: where $\chi_3 = 180°$ denotes the *endo* orientation and $\chi_3 = 0°$ denotes the *exo* orientation, shown in Fig. 4. As a result, it is clear that the sidechain of *N*-acetyl-L-aspartic acid *N*′-methylamide can be modeled by propionic acid ($CH_3–CH_2–COOH$)

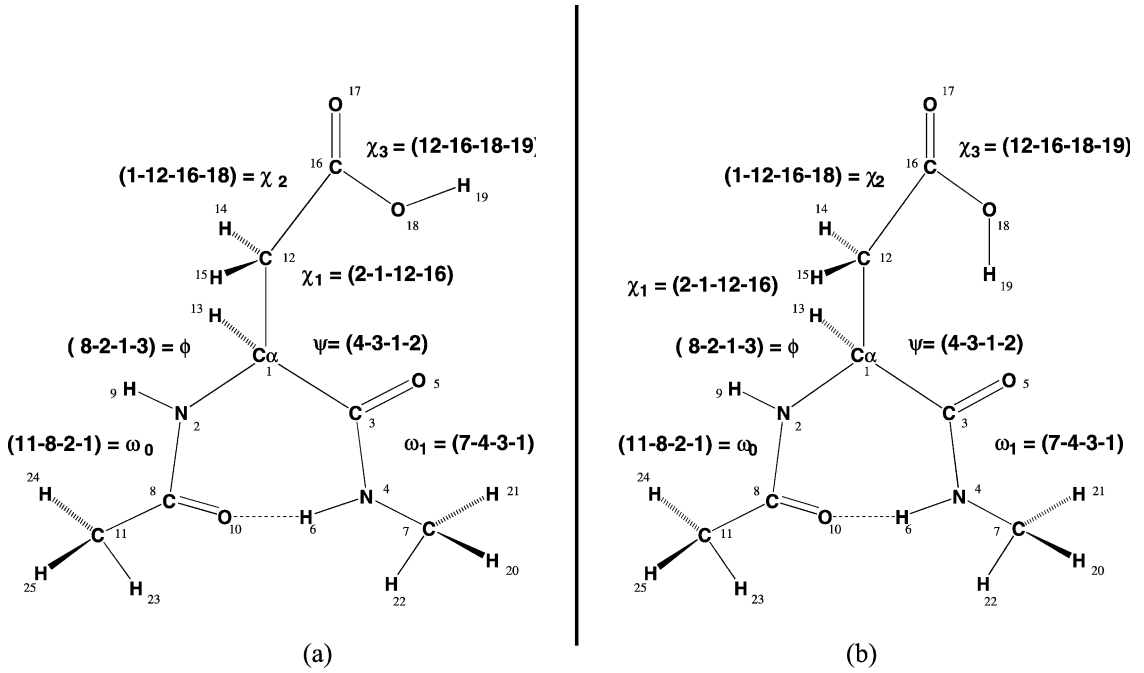

Fig. 1. Definition of torsional angles and atomic numbering for (a) the *endo* form and (b) the *exo* form of *N*-acetyl-L-aspartic acid *N*′-methylamide.

where the α-carbon on the aspartic acid residue is represented by CH_3.

In this paper, optimization results for all stable conformers found in both the *endo* and the *exo* forms of *N*-acetyl-L-aspartic acid *N*′-methylamide were reported. Studying the aspartic acid residue in both its *endo* and *exo* form is important in a biological system. For example, in its *exo* form, the peptide residue is allowed to form external hydrogen bonds and when in its *endo* form, these external hydrogen interactions may be broken to allow the formation of other stabilizing forces. These forces are especially important in a biological system involving ligand binding, substrate interactions, protein docking and protein–protein interactions; all of which are pharmacologically important on a molecular level.

3. Biological background

It is not difficult to find the many biological implications involving aspartic acid. On a molecular level, mutational studies involving the aspartic acid residue are very popular in the recent years. For example, it was shown that mutations in two aspartate regions of the human immunodeficiency virus-1 (HIV-1) *chemokine coreceptor CXCR4* would reduce the coreceptor's function in enhancing HIV-1 entry into host cells [30]. The aspartic residue is also shown to be clinically important in many situations. Neurologically, the quantification of *N*-acetylaspartate is a potential relative measurement of cellular dysfunction and neuronal loss for stroke patients suffering from cerebral injury [31]. In experiments that explore the issue of aging, it was shown that K and Mg salts of aspartic acid intake allows rats to survive longer by as much as 30% [32,33].

An ongoing list of biological applications and experiments can be contributed to researches involving aspartic acid, including lipase activities [34], probing for the binding sites of HIV-1 protease [35], immunological antiproliferative experiments [36], protein modification studies in Alzheimer's disease [37], enzyme kinetics involving bacteria [38], using aspartic acid-specific sites to probe for target proteins in their normal and disease states [39], and protein decomposition that influence rate of racemization [40]. Results from these studies often indicate that

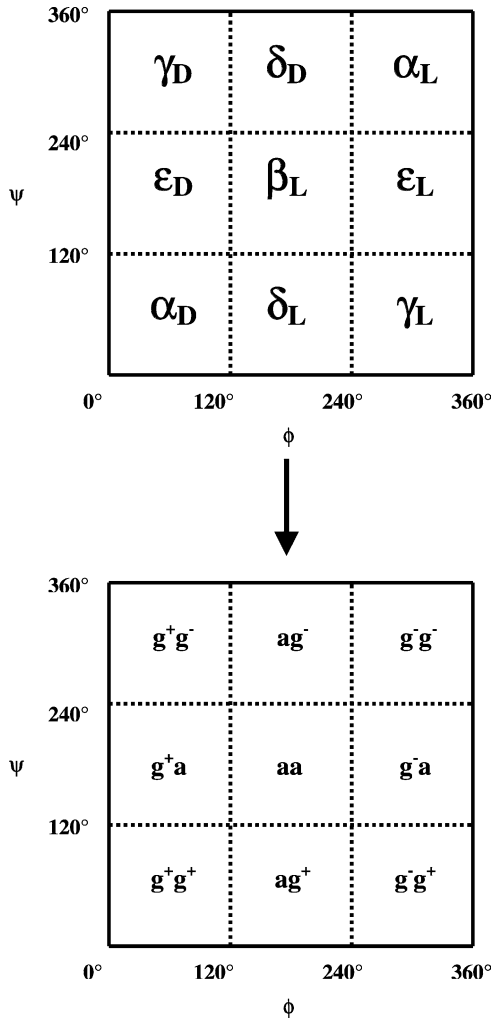

Fig. 2. A schematic representation of the 4D Ramachandran PEHS, $E = E(\phi, \psi, \chi_1, \chi_2)$. Each of the nine backbone conformations (γ_L, β_L, δ_L, α_L, ε_L, γ_D, δ_D, α_D, ε_D) has nine sidechain conformations as shown by the γ_L conformation.

specific conformations of the aspartic acid could lead to variations in the regulation of a biological system. Here, all possible sidechain and backbone conformers that may exist for the aspartic acid residue, *N*-acetyl-L-aspartic acid *N*′-methylamide, in both its *endo* and *exo* forms were reported. The sidechain carboxyl group of this particular aspartic acid residue is capable to inter- and intra-residual as well as intermolecular hydrogen bonding, characteristics that may be responsible for the peptide's many applications in biology and medicine.

One notable application of the aspartic acid residue in a biological system is shown in the RGD tripeptide. The RGD tripeptide can be separated into three components, namely, arginine (R), glycine (G), and aspartic acid (D), shown in Fig. 5 [41]. It is highly involved in molecular genetics and cell biology studies, including cell-surface recognition by receptors [42], expanding adenovirus vector tropism [43] and improving gene delivery [44,45] in gene therapy, apoptosis [46], and increasing oral bioavailability in drug production [47]. By exploring the conformation preferences of the aspartic acid (D) residue, one can examine the stabilization forces as well as molecular geometry for the RGD tripeptide.

4. Computational methods

Using GAUSSIAN 94 [48] and GAUSSIAN 98 [49], ab initio calculations were performed on all possible conformers for both *endo* and *exo* forms of *N*-acetyl-L-aspartic acid *N*′-methylamide. Specifically, these calculations were carried out on all backbone conformations (γ_L, β_L, δ_L, α_L, ε_L, γ_D, δ_D, α_D, and ε_D) of the aspartic acid residue. The ab initio results were then used to determine all minima on the PEHS. The sidechain geometry of *N*-acetyl-L-aspartic acid *N*′-methylamide can be related to that of propionic acid, $CH_3{-}CH_2{-}COOH$. Here, the carboxyl group can be in the *endo* or *exo* form, where χ_3 is 180 or 0°, respectively (Fig. 4). As a result, $9 \times 9 = 81$ initial conformers were calculated at the RHF/3-21G level of theory for each of the *endo* and *exo* forms of *N*-acetyl-L-aspartic acid *N*′-methylamide. Subsequently, all stable conformers found at RHF/3-21G were then subjected to optimizations at RHF/6-31G(d) level of theory. Likewise, all stable conformers found at the RHF/6-31G(d) level were then subjected to geometry optimization at B3LYP/6-31G(d) level of theory, the results of which were previously published [50,51]. All calculations were performed at tight geometry settings using Berny Optimization: FOPT = TIGHT, Z-Matrix; which at termination produced critical points that have gradients of less than 1.5×10^{-5} a.u.

In addition, partially relaxed PEHS scan calculations, where $E = E(\chi_1, \chi_2)$ and FOPT = Z-Matrix, were performed on both the *endo* and the *exo* forms of *N*-acetyl-L-aspartic acid *N*′-methylamide at

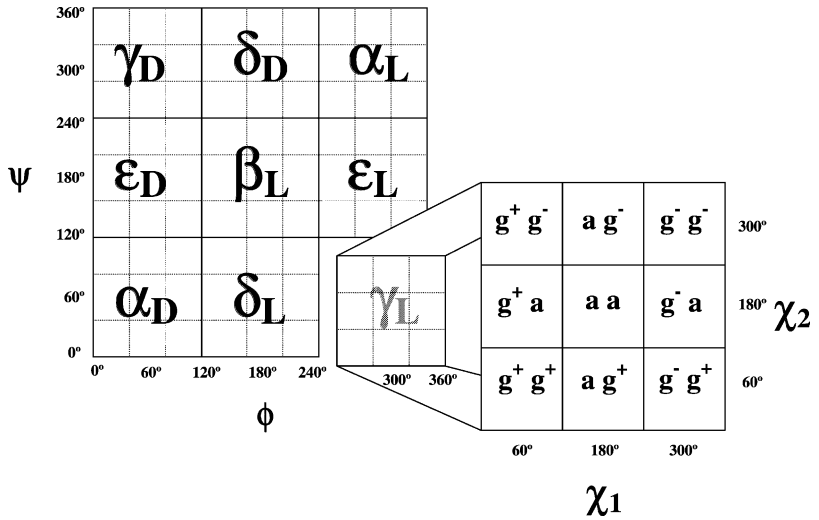

Fig. 3. 2D topology of a Ramachandran PEHS, $E = E(\phi, \psi)$ of an amino acid residue in a peptide. (Top) conformers are designated by traditional conventions; (bottom) conformers are designated by IUPAC conventions.

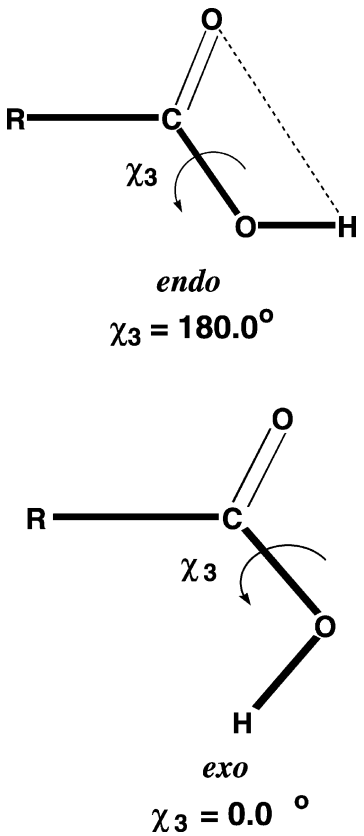

Fig. 4. Definitions of *endo* (top) and *exo* (bottom) forms for the propionic sidechain of *N*-acetyl-L-aspartic acid *N*′-methylamide.

RHF/3-21G. Here, setting and specifying the ϕ, ψ, and χ_3 torsional angles allow the backbone of the aspartic acid residue to be fixed to either the *endo* or the *exo* form as well as to their respective backbone conformations (γ_L, β_L, δ_L, α_L, ε_L, γ_D, δ_D, α_D, and ε_D). In turn, all critical points for these scan calculations had gradients of less than 4.5×10^{-4} a.u.

The stabilization or destabilization energy exerted by the sidechain on the backbone was calculated using

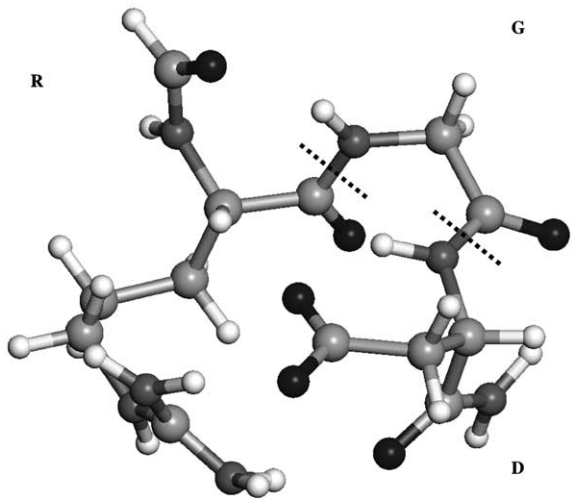

Fig. 5. An Arg-Gly-Asp (RGD) conformer obtained by preliminary optimization.

the following isodesmic reactions with respect to the γ_L and the β_L backbones of the glycine residue:

$$\begin{aligned} &CH_3{-}CO{-}(NH{-}\underset{\gamma_L}{CH_2}{-}CO){-}NHCH_3 + CH_3{-}R \\ &\quad \rightarrow CH_3CO{-}(NH{-}\underset{\text{any conformation}}{CHR}{-}CO){-}NHCH_3 \\ &\quad + CH_4 + \Delta E^{\text{stabil}}(\gamma_L) \end{aligned} \tag{1}$$

$$\begin{aligned} &CH_3{-}CO{-}(NH{-}\underset{\beta_L}{CH_2}{-}CO){-}NHCH_3 + CH_3{-}R \\ &\quad \rightarrow CH_3CO{-}(NH{-}\underset{\text{any conformation}}{CHR}{-}CO){-}NHCH_3 \\ &\quad + CH_4 + \Delta E^{\text{stabil}}(\beta_L). \end{aligned} \tag{2}$$

Here, $CH_3{-}R$ stands for $CH_3{-}CH_2{-}COOH$ and $CH_3CO{-}(NH{-}CHR{-}CO){-}NHCH_3$ stands for *N*-acetyl-L-aspartic acid *N*′-methylamide. Table 1 shows the energies for each component of the isodesmic reaction (excluding *N*-acetyl-L-aspartic acid *N*′-methylamide, whose optimized energies for each stable conformer found will be tabulated in Tables 2–7). Fig. 6 provides an example of the stabilization energy calculation. Note that the two stabilization values (from Eqs. (1) and (2)) are shifted with respect to each other by 0.66 kcal/mol at RHF/3-21G, by 0.031 kcal/mol at RHF/6-31G(d), and by 1.13 kcal/mol [50,51] at B3LYP/6-31G(d). This shift in stabilization energy corresponds to the difference in relative energies between the β_L and γ_L backbone conformation for the glycine diamide:

RHF/3-21G

$$\Delta E^{\text{stabil}}(\beta_L) - \Delta E^{\text{stabil}}(\gamma_L) = 0.66 \text{ kcal/mol} \tag{3}$$

RHF/6-31G(d)

$$\Delta E^{\text{stabil}}(\beta_L) - \Delta E^{\text{stabil}}(\gamma_L) = 0.031 \text{ kcal/mol} \tag{4}$$

B3LYP/6-31G(d)

$$\Delta E^{\text{stabil}}(\beta_L) - \Delta E^{\text{stabil}}(\gamma_L) = 1.13 \text{ kcal/mol.} \tag{5}$$

In the past, $\Delta E^{\text{stabil}}(\gamma_L)$ was favored in stabilization calculations as the global minima for most of the single amino acid diamides in the gas phase are usually located at the γ_L backbone. Interestingly, when fully extended the β_L conformation is highly symmetrical and it represents a unique structure on the Ramachandran map. As a result, $\Delta E^{\text{stabil}}(\beta_L)$ is becoming a more accepted parameter for stabilization energy calculations [52–54].

5. Results and discussions

All optimized results, including the dihedral angles, the relative energies and the stabilization energies for both the *endo* and the *exo* forms *N*-acetyl-L-aspartic acid *N*′-methylamide were tabulated in Tables 2–7. At all three levels of theory, 81 possible

Table 1
Components in the isodesmic reaction that were used to calculate the stabilization energy of various conformers found for both *endo* and *exo* forms of *N*-acetyl-L-aspartic acid *N*′-methylamide. All components were individually optimized at the three levels of theory: RHF/3-21G, RHF/6-31G(d), and B3LYP/6-31G(d)

Components of the isodesmic reaction	E_{min}		
	RHF/3-21G (Hartree)	RHF/6-31G(d) (Hartree)	B3LYP/6-31G(d) (Hartree)
$CH_3{-}CO{-}(NH{-}\underset{\gamma_L}{CH_2}{-}CO){-}NHCH_3$	−451.2942437	−453.8237506	−456.5375150
$CH_3{-}CO{-}(NH{-}\underset{\beta_L}{CH_2}{-}CO){-}NHCH_3$	−451.2931883	−453.8237997	−456.5357122
$CH_3{-}R$ *endo*	−265.3567876	−266.8465482	−268.3966238
$CH_3{-}R$ *exo*	−265.3440785	−266.8354509	−268.3872059
CH_4	−39.9768776	−40.19517190	−40.5183829

Table 2
Optimized conformers of *N*-acetyl-L-aspartic acid *N'*-methylamide in its *endo* form for all its stable backbone (γ_L, β_L, δ_L, α_L, γ_D, δ_D, α_D, and ε_D) conformation computed at the RHF/3-21G level of theory. Shown here are the optimized torsional angles, computed energy values, relative energies, and stabilization energies

Final conform.	Optimized parameters										
BB [$\chi_1\chi_2$]	ϕ	ψ	ω_0	ω_1	χ_1	χ_2	χ_3	E_{min} (Hartree)	ΔE (kcal/mol)	ΔE^{stabil} (kcal) γ_L	ΔE^{stabil} (kcal) β_L
γ_L Backbone conformation											
γ_L [g^+s^+]	−86.54	68.85	−178.11	−177.98	59.15	145.48	−178.71	−676.6905014	0.000	−10.2580	−10.9202
γ_L [g^+g^-]	−86.81	68.93	−177.74	−178.32	69.45	−42.59	176.18	−676.6875087	1.878	−8.3800	−9.0423
γ_L [*as*]	−85.88	65.69	−175.63	−179.50	177.98	28.89	−177.17	−676.6819477	5.368	−4.8904	−5.5527
γ_L [*aa*]	−86.16	69.00	−176.45	−179.56	−171.53	−169.18	178.94	−676.6827908	4.838	−5.4195	−6.0818
γ_L [g^-g^+]	−83.43	69.39	−174.01	−178.84	−49.09	81.79	178.60	−676.6822089	5.204	−5.0543	−5.7166
γ_L [g^-g^+]	−97.61	8.58	−170.57	177.23	−53.18	83.43	179.19	−676.6737116	10.536	0.2778	−0.3845
γ_L [g^-a]	−87.82	65.47	−171.45	−179.09	−69.97	169.60	177.20	−676.6815484	5.618	−4.6399	−5.3021
γ_L [g^-s^-]	−84.08	70.15	−171.84	−178.48	−41.15	−124.82	−177.36	−676.6828537	4.799	−5.4590	−6.1212
γ_L [g^-g^-]	−84.91	67.70	−174.84	−179.01	−55.44	−70.03	178.10	−676.6823949	5.087	−5.1711	−5.8333
γ_L [g^-g^-]	−116.57	25.83	−172.39	176.12	−61.30	−57.92	177.77	−676.6762169	8.964	−1.2943	−1.9566
β_L Backbone conformation											
β_L [g^+g^+]	−169.95	170.13	−178.51	176.98	54.96	76.93	−174.25	−676.6784956	7.534	−2.7242	−3.3865
β_L [g^+a]	−166.71	−176.90	177.16	−179.82	63.86	−173.36	−179.71	−676.6786647	7.428	−2.8303	−3.4926
β_L [*as*]	−169.46	168.76	177.30	178.24	−172.54	28.46	171.50	−676.6832670	4.540	−5.7183	−6.3806
β_L [*aa*]	−169.94	171.34	176.74	179.83	−162.37	174.19	−178.43	−676.6879710	1.588	−8.6701	−9.3324
β_L [*aa*]	−169.89	170.76	176.79	179.59	−161.90	174.43	−178.36	−676.6880484	1.539	−8.7187	−9.3810
δ_L Backbone conformation											
δ_L [g^+a]	−130.74	36.35	−173.74	177.68	60.24	167.20	−179.06	−676.6854098	3.195	−7.0629	−7.7252
δ_L [g^+g^-]	−126.96	42.20	−173.35	177.35	72.20	−30.10	176.19	−676.6819374	5.374	−4.8840	−5.5462
δ_L [ag^+]	−135.26	39.36	−174.15	176.58	−176.79	35.75	−177.53	−676.6767391	8.636	−1.6220	−2.2843
δ_L [a*a*]	−138.35	46.79	−175.01	176.79	−168.58	−160.28	179.56	−676.6767888	8.605	−1.6532	−2.3154
δ_L [s^-s^+]	−168.36	44.10	−176.30	176.26	−101.54	146.29	−179.82	−676.6721066	11.543	1.2850	0.6227
δ_L [g^-g^-]	−142.26	33.50	−170.54	176.32	−65.68	−73.27	170.07	−676.6760032	9.098	−1.1602	−1.8225
α_L Backbone conformation											
α_L [g^-s^-]	−70.29	−26.01	−169.94	−179.17	−54.73	−132.44	−178.26	−676.6742455	10.201	−0.0572	−0.7195
γ_D Backbone conformation											
γ_D [ag^+]	73.89	−53.47	175.99	−177.00	−168.59	56.36	−175.04	−676.6747454	9.887	−0.3709	−1.0332
γ_D [ag^+]	74.64	−53.94	175.80	−177.29	−168.36	56.27	−175.11	−676.6747365	9.893	−0.3653	−1.0276
γ_D [a*a*]	76.36	−65.94	178.06	179.76	−155.27	−161.97	−178.26	−676.6739166	10.407	0.1492	−0.5131
γ_D [a*a*]	74.17	−76.20	179.76	179.47	−173.93	−175.75	−179.83	−676.6738807	10.430	0.1717	−0.4906
γ_D [g^-a]	73.47	−58.91	172.99	−178.65	−65.92	178.73	179.13	−676.6803159	6.391	−3.8665	−4.5287
γ_D [g^-g^-]	72.59	−59.63	175.05	−178.70	−58.91	−47.94	−177.93	−676.6774479	8.191	−2.0668	−2.7290

(*continued on next page*)

Table 2 (*continued*)

Final conform.	Optimized parameters										
BB [$\chi_1\chi_2$]	ϕ	ψ	ω_0	ω_1	χ_1	χ_2	χ_3	E_{min} (Hartree)	ΔE (kcal/mol)	ΔE^{stabil} (kcal) γ_L	ΔE^{stabil} (kcal) β_L
δ_D Backbone conformation											
δ_D [sg^+]	−153.01	−62.32	176.64	179.36	24.90	64.75	178.62	−676.6705819	12.500	2.2417	1.5794
δ_D [g^+s]	121.52	−2.95	175.72	−179.41	65.23	15.35	179.67	−676.6684883	13.813	3.5555	2.8932
δ_D [g^+a]	−163.58	−49.46	177.17	179.43	50.76	−171.14	−179.76	−676.6775156	8.149	−2.1092	−2.7715
δ_D [g^+g^-]	−172.55	−49.25	−179.86	−178.71	66.16	−40.03	−173.06	−676.6697533	13.020	2.7617	2.0994
δ_D [ag^+]	178.92	−39.96	172.20	−175.30	−176.59	53.79	−175.95	−676.6682117	13.987	3.7290	3.0668
δ_D [aa]	−179.53	−46.96	172.05	−176.97	−164.09	−157.96	−177.06	−676.6667564	14.900	4.6423	3.9800
δ_D [g^-g^+]	−154.38	−56.93	178.01	−179.39	−66.55	87.55	−172.27	−676.6643590	16.405	6.1466	5.4844
δ_D [g^-g^-]	−170.00	−50.52	173.92	−177.36	−80.67	−51.48	171.58	−676.6671680	14.642	4.3840	3.7217
α_D Backbone conformation											
α_D [g^+s^+]	28.97	66.58	157.07	−171.56	59.79	142.97	−178.07	−676.6651020	15.938	5.6804	5.0181
α_D [g^+g^-]	55.61	38.91	167.38	179.69	49.34	−73.91	179.12	−676.6661590	15.275	5.0171	4.3549
α_D [ag^+]	61.63	35.39	174.93	179.12	−172.23	36.32	−176.48	−676.6749103	9.784	−0.4744	−1.1367
α_D [aa]	61.92	36.63	175.50	178.80	−162.44	−155.51	178.63	−676.6757864	9.234	−1.0242	−1.6864
α_D [g^-s]	61.23	34.49	172.72	179.01	−60.24	−26.22	−176.19	−676.6758499	9.194	−1.0640	−1.7263
α_D [g^-a]	61.23	35.50	171.49	179.11	−63.61	−178.56	179.68	−676.6798427	6.688	−3.5695	−4.2318
ε_D Backbone conformation											
ε_D [g^+g^+]	68.82	171.79	−163.69	177.23	76.42	46.61	−167.26	−676.6643520	16.409	6.1510	5.4888
ε_D [g^+g^+]	53.83	−123.13	−175.80	−178.23	50.20	89.60	−169.69	−676.6699202	12.915	2.6569	1.9947
ε_D [g^+s^-]	55.77	−131.66	−173.52	−177.38	64.65	−94.37	172.82	−676.6707814	12.374	2.1165	1.4543
ε_D [aa]	67.63	175.10	−160.89	179.99	−151.80	168.39	179.03	−676.6777138	8.024	−2.2336	−2.8959
ε_D [s^-g^-]	65.35	−176.81	−162.80	−179.63	−134.59	−43.56	−179.95	−676.6724414	11.333	1.0749	0.4126
ε_D [g^-a]	65.02	178.61	−167.13	−179.28	−71.30	168.99	179.28	−676.6710500	12.206	1.9480	1.2857
ε_D [g^-g^-]	62.59	−175.09	−166.69	−178.91	−58.21	−53.07	179.87	−676.6697134	13.045	2.7867	2.1244

Table 3
Optimized conformers of *N*-acetyl-L-aspartic acid *N′*-methylamide in its *exo* form for all its stable backbone (γ_L, β_L, δ_L, γ_D, δ_D, α_D, and ε_D) conformation computed at the RHF/3-21G level of theory. Shown here are the optimized torsional angles, computed energy values, relative energies, and stabilization energies

Final conform.	Optimized parameters										
BB [$\chi_1\chi_2$]	ϕ	ψ	ω_0	ω_1	χ_1	χ_2	χ_3	E_{min} (Hartree)	ΔE (kcal/mol)	ΔE^{stabil} (kcal) γ_L	ΔE^{stabil} (kcal) β_L
γ_L Backbone conformation											
γ_L [g^+g^+]	−87.38	76.81	−176.83	−177.11	39.69	43.19	22.15	−676.6851664	3.348	−14.8853	−15.5476
γ_L [g^+g^+]	−81.50	63.94	−172.24	179.98	51.00	89.06	−23.41	−676.6896522	0.533	−17.7002	−18.3624
γ_L [ag^+]	−86.48	67.91	−176.69	−179.07	177.80	37.16	6.04	−676.6610996	18.450	0.2169	−0.4454
γ_L [ag^-]	−85.15	64.56	−172.48	−179.67	−167.11	−69.85	3.64	−676.6808379	6.064	−12.1691	−12.8314
γ_L [g^-g^+]	−82.06	74.60	175.26	−178.62	−70.48	36.19	−0.88	−676.6672684	14.579	−3.6541	−4.3164
γ_L [g^-a]	−88.83	65.59	−168.34	−178.97	−66.14	177.71	2.04	−676.6695026	13.177	−5.0561	−5.7184
γ_L [g^-s^-]	−83.91	68.36	−170.89	−178.64	−43.12	−121.57	0.83	−676.6702313	12.720	−5.5134	−6.1756
β_L Backbone conformation											
β_L [g^+g^+]	−168.29	−176.69	−178.95	−174.85	59.47	74.45	1.41	−676.6648105	16.121	−2.1118	−2.7740
β_L [g^+a]	−169.88	−176.43	176.91	179.51	63.70	−164.81	6.85	−676.6663164	15.176	−3.0567	−3.7190
β_L [ag^+]	−165.97	166.30	177.81	176.24	−176.14	45.45	32.11	−676.6702094	12.733	−5.4996	−6.1619
β_L [aa]	−173.06	172.01	175.92	179.84	−161.54	172.17	−4.23	−676.6769545	8.501	−9.7322	−10.3945
β_L [aa]	−173.12	172.65	175.87	−179.93	−161.96	171.90	−4.26	−676.6769286	8.517	−9.7160	−10.3783
δ_L Backbone conformation											
δ_L [g^+a]	−130.38	33.55	−173.77	177.98	60.32	164.49	−9.88	−676.6740529	10.322	−7.9115	−8.5737
δ_L [s^-g^+]	−164.33	51.49	−177.84	177.18	−121.17	46.70	12.47	−676.6710723	12.192	−6.0411	−6.7034
δ_L [g^-g^-]	−140.37	34.46	−179.17	176.30	−71.97	−30.17	56.08	−676.6697746	13.006	−5.2268	−5.8891
γ_D Backbone conformation											
γ_D [g^+g^+]	66.34	−58.66	171.40	177.21	60.56	71.34	−26.29	−676.6587310	19.936	1.7032	1.0409
γ_D [s^+g^-]	96.91	−77.77	−178.37	178.07	102.79	−64.39	−12.47	−676.6663410	15.161	−3.0722	−3.7344
γ_D [ag^+]	73.89	−59.87	178.08	−177.05	−172.00	66.23	3.19	−676.6563803	21.411	3.1783	2.5160
γ_D [ag^+]	74.56	−59.93	177.92	−177.13	−171.99	65.88	2.97	−676.6563797	21.412	3.1786	2.5164
γ_D [aa]	76.50	−68.39	178.90	179.32	−157.18	−166.38	4.60	−676.6611624	18.411	0.1775	−0.4848
γ_D [aa]	74.85	−75.02	−179.68	179.59	−170.69	−172.91	3.83	−676.6611313	18.430	0.1970	−0.4653
γ_D [ag^-]	72.04	−78.63	176.43	175.39	−178.83	−69.29	2.40	−676.6652082	15.872	−2.3613	−3.0236
γ_D [g^-a]	73.93	−57.40	172.34	−178.95	−64.82	175.17	−1.71	−676.6688080	13.613	−4.6202	−5.2825
γ_D [g^-g^-]	76.94	−53.03	162.39	−178.46	−55.17	−79.81	−10.13	−676.6639563	16.657	−1.5757	−2.2380
δ_D Backbone conformation											
δ_D [g^+g^+]	−168.58	−50.00	−174.89	177.23	39.74	85.15	16.86	−676.6561993	21.525	3.2919	2.6296
δ_D [g^+a]	−165.98	−49.33	177.76	179.34	49.65	−168.17	3.75	−676.6667681	14.893	−3.3402	−4.0024
δ_D [g^+g^-]	−157.27	−48.33	166.32	−178.07	63.92	−41.74	−7.58	−676.6629634	17.280	−0.9527	−1.6150
δ_D [aa]	−167.40	−67.99	173.28	−179.14	175.51	171.19	−6.37	−676.6534401	23.256	5.0233	4.3610
δ_D [s^-g^+]	−170.81	−54.45	174.81	−177.77	−122.95	52.85	11.12	−676.6671813	14.634	−3.5995	−4.2617
δ_D [g^-s]	−140.79	−61.80	171.60	179.91	−70.60	−29.79	55.06	−676.6631427	17.168	−1.0652	−1.7275

(*continued on next page*)

Table 3 (*continued*)

Final conform.	Optimized parameters											
BB [$\chi_1\chi_2$]	ϕ	ψ	ω_0	ω_1	χ_1	χ_2	χ_3	E_{min} (Hartree)	ΔE (kcal/mol)	ΔE^{stabil} (kcal)	γ_L	ΔE^{stabil} (kcal) β_L
α_D Backbone conformation												
α_D [g^+g^+]	48.19	52.74	162.59	−177.97	55.55	84.13	−22.40	−676.6725960	11.236	−6.9972		−7.6595
α_D [g^+g^-]	54.89	37.74	172.17	179.31	31.15	−64.72	−0.20	−676.6482748	26.498	8.2646		7.6023
α_D [$a\,g^-$]	64.05	32.27	171.91	178.78	−150.55	−59.78	−3.39	−676.6749987	9.728	−8.5050		−9.1672
α_D [g^-a]	61.62	35.58	171.55	178.93	−63.18	179.32	0.15	−676.6700644	12.824	−5.4086		−6.0709
ε_D Backbone conformation												
ε_D [g^+g^-]	42.82	−126.48	−166.54	−178.59	57.27	−84.00	12.45	−676.6551743	22.168	3.9350		3.2728
ε_D [$a\,a$]	68.31	173.61	−159.69	179.90	−153.52	174.81	0.94	−676.6675821	14.382	−3.8510		−4.5132
ε_D [g^-a]	67.31	174.63	−166.00	−179.65	−70.72	157.30	−8.66	−676.6604377	18.865	0.6322		−0.0301

conformers were initially expected to be found for the aspartic acid residue. At the RHF/3-21G level, there were 49 stable conformers found for the *endo* form while 37 were found for the *exo* form (Tables 2 and 3). At the RHF/6-31G(d) level, there were 40 stable conformers found for the *endo* form while 31 were found for the *exo* form (Tables 4 and 5). Finally, at the B3LYP/6-31G(d) level, 37 stable conformers were found for the *endo* form while 27 were found for the *exo* form (Tables 6 and 7). Sidechain PESs, $E = E(\chi_1, \chi_2)$, were generated for all nine backbone conformations (γ_L, β_L, δ_L, α_L, γ_D, δ_D, α_D, ε_D) for both the *endo* and *exo* forms of *N*-acetyl-L-aspartic acid *N*′-methylamide at RHF/3-21G. These PESs revealed numerous minima for each backbone conformation, shown in landscape and contour representations (Figs. 7–15). However, subsequent optimizations on these 'apparent' minima revealed that only some were 'true' minima. This discrepancy can be explained, as both the ϕ and ψ torsional angles were frozen when the PESs were generated. Also, grid points are optimized at fixed χ_1 and χ_2 values (in our case, 30° increments of both χ_1 and χ_2 from 0 to 360°) in a double-scan PESs such as $E = E(\chi_1, \chi_2)$. As a result, any minimum appearing on a particular PES surface may not be a true minimum on the hypersurface, as these semi-rigid optimizations do not precisely correspond to true optimized structures. In these cases, the 'false' minima may reflect higher order critical points, such as transition structures. It is also worth noting that a minimum appearing on a surface may be shifted somewhat to a regional neighbor. In addition to landscape and contour representations, topology diagrams were generated to illustrate the stable conformers found for both *endo* and *exo* forms of *N*-acetyl-L-aspartic acid *N*′-methylamide at RHF/3-21G (Figs. 7–15).

In Tables 2–7, optimized results showed that sometimes there are noticeable shifts in the torsional angle away from the typical g^+ value (60°) or from the typical g^- value (−60°) toward the anti orientation (+180 or −180°). In these cases, the planar −COOH moiety was rotated against the tetrahedral β-carbon (χ_2). Values that fell within the range of +90 and +150° (i.e. +120 ± 30°) were categorized as *syn*$^+$ (s^+), which indicates that the oxygen of −OH in the carboxyl moiety was in *syn* orientation arrangement with the proton attached to

Table 4
Optimized conformers of *N*-acetyl-L-aspartic acid *N'*-methylamide in its *endo* form for all its stable backbone (γ_L, β_L, δ_L, α_L, γ_D, δ_D, α_D, and ε_D) conformation computed at the RHF/6-31G(d) level of theory. Shown here are the optimized torsional angles, computed energy values, relative energies, and stabilization energies

Final conform.	Optimized parameters										
BB [$\chi_1\chi_2$]	ϕ	ψ	ω_0	ω_1	χ_1	χ_2	χ_3	E_{min} (Hartree)	ΔE (kcal/mol)	ΔE^{stabil} (kcal) γ_L	ΔE^{stabil} (kcal) β_L
γ_L Backbone conformation											
γ_L [g^+s^+]	−86.13	67.15	179.93	−178.00	59.99	146.35	179.15	−680.4826738	0.000	−4.7358	−4.7049
γ_L [g^+g^-]	−86.51	71.14	179.30	−176.92	67.88	−39.35	179.12	−680.4775689	3.203	−1.5324	−1.5016
γ_L [*as*]	−85.91	72.96	178.53	−177.07	−178.29	24.53	−179.78	−680.4755867	4.447	−0.2885	−0.2577
γ_L [*aa*]	−85.75	77.61	176.69	−177.03	−172.52	−167.44	−179.48	−680.4780650	2.892	−1.8437	−1.8129
γ_L [g^-s^+]	−85.14	77.16	−179.71	−175.19	−60.48	106.57	−179.58	−680.4759197	4.238	−0.4975	−0.4667
γ_L [g^-a]	−89.37	74.07	−171.72	−175.05	−68.77	167.13	177.31	−680.4763858	3.946	−0.7900	−0.7592
γ_L [g^-g^-]	−86.77	73.88	−175.31	−175.52	−55.62	−85.52	178.26	−680.4774970	3.248	−1.4873	−1.4564
γ_L [g^-g^-]	−87.77	73.56	−170.93	−175.41	−56.23	−86.60	178.37	−680.4774861	3.255	−1.4804	−1.4496
β_L Backbone conformation											
β_L [g^+s^+]	−166.46	145.06	−168.69	178.75	58.09	108.65	−177.16	−680.4740676	5.400	0.6647	0.6955
β_L [g^+a]	−152.98	−177.39	172.03	−175.47	65.26	−172.27	−179.40	−680.4742037	5.315	0.5793	0.6101
β_L [ag^+]	−159.40	159.74	175.70	179.14	−172.59	36.46	174.58	−680.4755791	4.452	−0.2838	−0.2529
β_L [*aa*]	−160.51	163.15	173.97	178.17	−160.64	177.93	−178.48	−680.4811329	0.967	−3.7688	−3.7380
δ_L Backbone conformation											
δ_L [g^+s]	−137.58	33.62	−168.99	174.34	70.01	−22.09	178.41	−680.4745853	5.076	0.3399	0.3707
δ_L [g^+a]	−136.26	32.10	−168.80	178.32	62.68	165.63	179.68	−680.4802297	1.534	−3.2021	−3.1712
δ_L [ag^+]	−146.22	38.90	−169.50	172.96	−173.49	34.53	179.61	−680.4716220	6.935	2.1994	2.2302
δ_L [g^-g^+]	−137.85	27.48	−165.77	172.75	−66.59	81.12	−178.43	−680.4710249	7.310	2.5740	2.6049
δ_L [g^-s^-]	−137.67	24.59	−163.30	173.31	−58.22	−91.65	175.62	−680.4739890	5.450	0.7140	0.7449
α_L Backbone conformation											
α_L [g^-s^-]	−83.98	−12.33	−164.67	175.46	−58.28	−104.83	179.00	−680.4733488	5.852	1.1158	1.1466
γ_D Backbone conformation											
γ_D [ag^+]	74.66	−50.42	179.60	−174.81	−167.93	63.63	−176.90	−680.4695010	8.266	3.5303	3.5611
γ_D [a*a*]	71.00	−88.48	−173.64	174.11	−169.06	−169.92	−178.78	−680.4701740	7.844	3.1080	3.1388
γ_D [g^-a]	76.44	−43.19	166.92	−176.47	−63.68	178.79	179.14	−680.4753736	4.581	−0.1548	−0.1240
γ_D [g^-g^-]	74.17	−50.32	171.96	−177.42	−56.97	−48.89	−177.72	−680.4715568	6.976	2.2403	2.2711
δ_D Backbone conformation											
δ_D [g^+s]	132.04	−7.86	169.72	−173.73	65.57	13.02	179.08	−680.4635646	11.991	7.2555	7.2863
δ_D [g^+g^+]	−159.11	−23.59	168.02	−175.02	46.99	48.12	176.76	−680.4649266	11.137	6.4008	6.4316
δ_D [g^+a]	−154.13	−43.81	174.44	−175.97	54.33	−171.36	−179.46	−680.4723052	6.506	1.7706	1.8015
δ_D [g^+g^-]	−160.89	−44.89	179.21	−174.62	66.76	−36.95	−175.41	−680.4641405	11.630	6.8941	6.9249
δ_D [ag^+]	−164.39	−41.51	167.42	−170.82	178.24	66.27	−176.77	−680.4652722	10.920	6.1839	6.2147
δ_D [as^-]	−164.82	−40.79	166.98	−171.06	−178.77	−99.88	176.19	−680.4637103	11.900	7.1640	7.1948

(*continued on next page*)

Table 4 (*continued*)

Final conform.	Optimized parameters											
BB [$\chi_1\chi_2$]	ϕ	ψ	ω_0	ω_1	χ_1	χ_2	χ_3	E_{min} (Hartree)	ΔE (kcal/mol)	ΔE^{stabil} (kcal) γ_L	ΔE^{stabil} (kcal) β_L
δ_D [g^-s^+]	−146.42	−54.72	175.77	−174.61	−70.07	91.82	−174.67	−680.4619070	13.031	8.2956	8.3264
δ_D [g^-g^-]	−144.62	−57.05	180.21	−175.41	−62.08	−79.34	172.33	−680.4640699	11.674	6.9384	6.9692
α_D Backbone conformation											
α_D [g^+s^+]	57.36	38.29	162.26	−175.32	45.38	101.21	−176.46	−680.4652539	10.931	6.1954	6.2262
α_D [g^+g^-]	57.59	35.82	164.67	−175.59	55.27	−77.32	178.31	−680.4617149	13.152	8.4162	8.4470
α_D [ag^+]	64.57	34.56	167.57	−176.26	−166.29	35.33	−179.68	−680.4690305	8.561	3.8255	3.8564
α_D [aa]	65.34	35.91	168.43	−176.85	−157.79	−151.63	−179.28	−680.4717819	6.835	2.0990	2.1298
α_D [g^-a]	65.49	32.93	164.87	−176.47	−62.46	−179.47	179.48	−680.4760321	4.168	−0.5680	−0.5372
α_D [g^-g^-]	65.47	31.27	165.66	−176.39	−56.08	−42.85	−176.56	−680.4708365	7.428	2.6923	2.7231
ε_D Backbone conformation											
ε_D [g^+g^+]	51.50	−131.49	−168.45	177.43	53.11	87.73	−174.10	−680.4656585	10.677	5.9415	5.9723
ε_D [g^+s^-]	53.94	−137.68	−164.44	178.66	67.87	−98.90	176.04	−680.4684261	8.941	4.2048	4.2356
ε_D [s^-a]	66.93	−178.87	−158.06	−174.75	−148.12	168.66	178.88	−680.4728813	6.145	1.4091	1.4399
ε_D [s^-g^-]	64.10	−167.71	−160.46	−174.74	−132.37	−51.70	−179.22	−680.4659488	10.495	5.7593	5.7902

the β-carbon, positioned at about +120°. Similarly, values that fell within the range of −90 and −150° (i.e. −120 ± 30°) were labeled as *syn*$^-$ (s^-), indicating that the –OH oxygen of the carboxyl moiety was in *syn* orientation with the proton attached to the β-carbon, position at about −120°.

For the *endo* form of the aspartic acid residue, it is interesting to note that a g^-s^- conformer, shown in Fig. 16, as found in the α_L backbone conformation at RHF/3-21G. In this particular g^-s^- conformer, it is found that, besides the sidechain–sidechain (SC/SC) hydrogen bond (calculated to be 2.362 Å), a sidechain–backbone (SC/BB) hydrogen bond calculated to be 2.052 Å, may contribute to the stabilizing forces of the conformer at RHF/3-21G. This g^-s^- conformer was found also at RHF/6-31G(d) and at B3LYP/6-31G(d). At all three levels of theory, the same SC/SC (Type 1, calculated to be 2.272 Å at RHF/6-31G(d) and 2.281 Å at B3LYP/6-31G(d)) and SC/BB (Type 3A, calculated to be 2.293 Å at RHF/6-31G(d) and 2.121 Å at B3LYP/6-31G(d)) hydrogen bonds were found. In addition, it is interesting to note that there exists a rather unusual hydrogen bond, $N^2\cdots H^6$, which has an intermolecular distance of 2.291 Å at RHF/3-21G, 2.325 Å at RHF/6-31G(d), and 2.276 Å [51] at B3LYP/6-31G(d) (results not tabulated but shown in Fig. 16), may also contribute to the stabilizing force that allows for the existence of this g^-s^- conformer. Fig. 17 shows the various 'traditional' hydrogen bonds that may exist in the *endo* form of *N*-acetyl-L-aspartic acid *N*′-methylamide. There exist three kinds of stabilizing hydrogen bonds: sidechain–sidechain (SC/SC), backbone–backbone (BB/BB), or sidechain–backbone (SC/BB). In total, there exist one SC/SC, two BB/BB, and four SC/BB hydrogen bond interactions for the *endo* form. The corresponding distances for these hydrogen bond interactions were tabulated in Tables 8, 10 and 12.

For the *exo* form of the aspartic acid residue, it is interesting to note that initially no stable conformers can be found in the α_L and ε_L backbones at RHF/3-21G. However, at both RHF/6-31G(d) and B3LYP/6-31G(d) levels, a g^-g^+ conformer was found at the α_L backbone conformation, as shown in Fig. 18. In this particular g^-g^+ conformer, there exists a weak backbone–backbone internal hydrogen bond, calculated to be 2.476 Å at RHF/6-31G(d) and 2.297 Å [50]

Table 5
Optimized conformers of *N*-acetyl-L-aspartic acid *N'*-methylamide in its *exo* form for all its stable backbone (γ_L, β_L, δ_L, ε_L, γ_D, δ_D, α_D, and ε_D) conformation computed at the RHF/6-31G(d) level of theory. Shown here are the optimized torsional angles, computed energy values, relative energies, and stabilization energies

Final conform.	Optimized parameters										
BB [χ_1 χ_2]	ϕ	ψ	ω_0	ω_1	χ_1	χ_2	χ_3	E_{min} (Hartree)	ΔE (kcal/mol)	ΔE^{stabil} (kcal) γ_L	ΔE^{stabil} (kcal) β_L
γ_L Backbone conformation											
γ_L [g^+g^+]	−85.33	62.09	−169.71	179.81	51.48	87.25	−16.58	−680.4785887	2.563	−9.1360	−9.1052
γ_L [ag^-]	−86.59	68.55	−172.81	−178.21	−166.56	−74.85	5.70	−680.4731593	5.970	−5.7290	−5.6982
γ_L [g^-a]	−92.63	70.66	−162.97	−175.88	−64.33	−175.85	1.51	−680.4661419	10.374	−1.3255	−1.2947
γ_L [g^-s^-]	−88.87	69.81	−167.64	−176.16	−55.37	−97.05	−3.09	−680.4663875	10.220	−1.4796	−1.4488
β_L Backbone conformation											
β_L [g^+g^+]	−178.13	−171.67	−159.41	177.96	62.50	79.37	−1.04	−680.4617018	13.160	1.4607	1.4915
β_L [g^+a]	169.71	175.19	−157.10	−175.35	65.51	−150.99	5.96	−680.4635102	12.025	0.3259	0.3567
β_L [$a\,a$]	−162.62	164.33	173.01	178.29	−160.10	175.37	−2.36	−680.4711439	7.235	−4.4643	−4.4335
β_L [s^-g^+]	174.30	179.61	−168.85	−179.55	−131.15	75.52	−4.60	−680.4767330	3.728	−7.9715	−7.9407
δ_L Backbone conformation											
δ_L [g^+a]	−136.55	31.02	−168.58	179.12	63.51	159.55	−8.66	−680.4706011	7.576	−4.1237	−4.0929
δ_L [s^-g^+]	−163.64	44.63	−175.11	171.72	−124.31	54.00	4.19	−680.4627730	12.488	0.7885	0.8193
δ_L [g^-g^-]	−131.47	22.20	−174.36	172.69	−54.97	−32.30	15.27	−680.4638043	11.841	0.1414	0.1722
ε_L Backbone conformation											
ε_L [g^-g^+]	−79.30	148.28	161.92	−179.27	−69.79	42.55	−3.62	−680.4655327	10.756	−0.9432	−0.9124
γ_D Backbone conformation											
γ_D [g^+g^+]	68.43	−64.15	168.73	175.08	57.30	74.80	−16.88	−680.4551001	17.303	5.6033	5.6342
γ_D [s^+g^-]	82.81	−54.23	−177.57	−173.52	109.19	−82.77	8.76	−680.4594361	14.582	2.8825	2.9133
γ_D [ag^+]	74.03	−57.83	−176.93	−175.43	−172.56	72.22	−0.22	−680.4549002	17.428	5.7288	5.7596
γ_D [ag^+]	74.78	−57.40	178.38	−175.55	−172.82	71.57	−0.66	−680.4548321	17.471	5.7715	5.8023
γ_D [aa]	72.01	−87.48	−173.23	174.35	−167.92	−170.61	2.93	−680.4590778	14.807	3.1073	3.1381
γ_D [ag^-]	71.95	−84.52	176.58	172.58	−170.66	−75.55	3.36	−680.4606718	13.806	2.1071	2.1379
γ_D [g^-a]	76.13	−33.49	165.48	−176.02	−62.08	176.32	−0.59	−680.4655035	10.775	−0.9249	−0.8941
δ_D Backbone conformation											
δ_D [g^+a]	−157.75	−42.67	175.09	−176.09	53.69	−169.05	2.41	−680.4629789	12.359	0.6593	0.6901
δ_D [g^+a]	−158.84	−43.49	−179.92	−176.11	53.52	−169.93	2.14	−680.4629534	12.375	0.6753	0.7061
δ_D [g^+g^-]	−151.86	−42.53	162.49	−173.05	64.60	−50.32	−1.70	−680.4579405	15.520	3.8210	3.8518
δ_D [s^-g^+]	−167.14	−47.86	170.63	−172.41	−125.58	58.87	3.81	−680.4609358	13.641	1.9414	1.9722
δ_D [g^-s]	−131.15	−60.53	167.76	−175.83	−65.98	−17.71	18.34	−680.4583677	15.252	3.5529	3.5837
α_D Backbone conformation											
α_D [g^+g^+]	52.39	49.36	160.04	−173.81	57.48	81.53	−15.20	−680.4673923	9.589	−2.1101	−2.0793
α_D [g^+g^-]	52.06	34.32	172.89	−176.37	48.05	−78.28	0.37	−680.4447479	23.799	12.0994	12.1303

(*continued on next page*)

Table 5 (*continued*)

Final conform.	Optimized parameters											
BB [χ_1 χ_2]	ϕ	ψ	ω_0	ω_1	χ_1	χ_2	χ_3	E_{min} (Hartree)	ΔE (kcal/mol)	ΔE^{stabil} (kcal) γ_L	ΔE^{stabil} (kcal) β_L
α_D [s^-g^-]	68.04	31.35	165.56	−178.41	−145.80	−67.22	2.40	−680.4688675	8.664	−3.0358	−3.0050
α_D [g^-a]	66.03	33.29	164.97	−176.88	−61.61	179.18	0.22	−680.4674263	9.568	−2.1315	−2.1007
ε_D Backbone conformation											
ε_D [s^+g^-]	70.08	179.51	−161.04	178.00	116.46	−68.81	1.18	−680.4657620	10.612	−1.0871	−1.0563
ε_D [s^-a]	68.15	179.02	−157.22	−175.16	−149.61	174.98	0.36	−680.4641156	11.645	−0.0540	−0.0232
ε_D [g^-s^+]	74.67	172.20	−154.23	−176.90	−53.19	98.22	−9.90	−680.4650164	11.080	−0.6192	−0.5884

at B3LYP/6-31G(d), which may contribute in stabilizing the conformer (results not tabulated but shown in Fig. 18). In addition, a rather unusual hydrogen interaction, $H^{19}\cdots N^{2}$, calculated to have an intermolecular distance of 2.039 Å at RHF/6-31G(d) and 1.918 Å [50] at B3LYP/6-31G(d) was found, which could also stabilize the conformer. Fig. 19 shows the various traditional hydrogen bonds that may exist in the *exo* form of *N*-acetyl-L-aspartic acid *N*′-methylamide. Here, since the carboxyl group in the sidechain is in the *exo* form, there can be no sidechain–sidechain interaction in the aspartic acid residue. Hence, there exist two kinds of stabilizing hydrogen bonds: backbone–backbone (BB/BB) or sidechain–backbone (SC/BB). In total, there exist two BB/BB and four SC/BB hydrogen bond interactions for the *exo* form. The corresponding distances for these hydrogen bond interactions were tabulated in Tables 9, 11 and 13.

When examining Tables 8–13, it was found that the existence of hydrogen bond interactions is prominent among all stable conformers found for both *endo* and *exo* forms of *N*-acetyl-L-aspartic acid *N*′-methylamide. This suggests that hydrogen bonding is significant in stabilizing most of the conformers found for the aspartic acid residue. It is also worth noting that hydrogen bond interactions are more common in the *exo* forms of the aspartic acid residue than in the *endo* forms (comparing Tables 9, 11 and 13 for *exo* versus Tables 8, 10 and 12 for *endo*). External hydrogen bondings are significant when the aspartyl residue participates in intra- or inter-molecular interactions, such as in the RGD tripeptide. This way, the presence or absence of these stabilizing forces may directly affect the folding patterns of the RGD tripeptide moiety. Here, we propose that while the BB/BB interaction can be considered as an internal stabilizing factor for the *exo* forms of the aspartic acid residue, its sidechain can participate in external interactions with other substrates. This phenomenon can be applied to the docking of a specific molecule to receptors that express the aspartic acid residue on its surface. This way, one can explain why a point mutation in a receptor will significantly affect its recognition capabilities for certain ligands. This proposed mechanism does not imply that the *endo* forms of the aspartic acid residue are ‘useless’ in such ligand/

Table 6
Optimized conformers of *N*-acetyl-L-aspartic acid *N*′-methylamide in its *endo* form for all its stable backbone (γ_L, β_L, δ_L, α_L, γ_D, δ_D, α_D, and ε_D) conformation computed at the B3LYP/6-31G(d) level of theory. Shown here are the optimized torsional angles, computed energy values, relative energies, and stabilization energies

Final conform.	Optimized parameters									
BB [$\chi_1\chi_2$]	ϕ	ψ	ω_0	ω_1	χ_1	χ_2	E_{min} (Hartree)	ΔE (kcal/mol)	ΔE^{stabil} (kcal) γ_L	ΔE^{stabil} (kcal) β_L
γ_L Backbone conformation										
γ_L [g^+s^+]	−82.63	69.39	−179.63	−176.47	58.85	144.19	−684.4260542	0.000	−6.4623	−7.5936
γ_L [g^+g^-]	−83.22	70.88	−179.64	−176.59	67.76	−41.53	−684.4210847	3.118	−3.3439	−4.4751
γ_L [*as*]	−83.13	69.16	−178.12	−177.73	−176.54	27.91	−684.4178720	5.134	−1.3279	−2.4591
γ_L [*aa*]	−82.80	71.63	−179.13	−177.93	−169.19	−163.60	−684.4199177	3.851	−2.6116	−3.7428
γ_L [g^-s^+]	−83.30	71.37	−173.51	−176.48	−55.28	90.31	−684.4190950	4.367	−2.0953	−3.2266
γ_L [g^-a]	−84.30	66.13	−173.78	−177.94	−72.14	157.14	−684.4189046	4.486	−1.9758	−3.1071
γ_L [g^-s^-]	−83.95	72.82	−170.48	−175.81	−45.07	−119.39	−684.4217674	2.690	−3.7723	−4.9035
β_L Backbone conformation										
β_L [g^+s^+]	−170.22	150.84	−169.30	175.92	58.82	107.24	−684.4154168	6.675	0.2128	−0.9185
β_L [g^+a][a,b]	−157.77	−177.22	173.48	−179.57	66.22	−171.49	−684.4153786	6.699	0.2368	−0.8945
β_L [ag^+]	−164.40	162.84	177.73	177.71	−173.28	32.25	−684.4184974	4.742	−1.7203	−2.8516
β_L [*aa*]	−163.51	167.73	175.07	178.61	−161.48	173.27	−684.4240236	1.274	−5.1881	−6.3193
δ_L Backbone conformation										
δ_L [g^+s]	−130.53	32.86	−170.39	176.65	69.12	−26.01	−684.4164380	6.034	−0.4280	−1.5593
δ_L [g^+a][a,b]	−130.74	30.06	−170.27	177.91	60.44	162.32	−684.4215144	2.849	−3.6135	−4.7448
δ_L [ag^+]	−135.53	34.83	−170.11	175.22	−172.91	37.96	−684.4130412	8.166	1.7035	0.5722
δ_L [g^-g^+]	−135.08	25.11	−164.18	174.86	−67.72	82.47	−684.4133097	7.997	1.5350	0.4037
δ_L [g^-s^-]	−133.61	22.39	−161.57	175.51	−56.89	−98.79	−684.4155795	6.573	0.1107	−1.0206
α_L Backbone conformation										
α_L [g^-s^-][a,b]	−81.20	−13.35	−164.10	176.83	−55.35	−119.10	−684.4153827	6.696	0.2342	−0.8971
γ_D Backbone conformation										
γ_D [ag^+]	73.01	−53.01	175.99	−176.30	−170.77	65.87	−684.4128945	8.258	1.7956	0.6643
γ_D [as^-][a,b]	74.54	−65.87	178.99	177.75	−155.29	−145.77	−684.4128963	8.257	1.7944	0.6632
γ_D [g^-a]	73.63	−49.71	168.25	−178.12	−64.89	179.52	−684.4181554	4.957	−1.5057	−2.6370
γ_D [g^-g^-]	72.81	−53.52	172.24	−178.73	−59.41	−37.44	−684.4146876	7.133	0.6704	−0.4609
δ_D Backbone conformation										
δ_D [g^+g^+][a,b]	−155.89	−38.80	171.16	−175.78	43.03	44.58	−684.4069299	12.001	5.5384	4.4071
δ_D [g^+a][a,b]	−156.90	−48.59	174.77	−176.77	54.07	−168.35	−684.4146306	7.168	0.7061	−0.4251
δ_D [g^+g^-]	−164.26	−45.65	176.01	−175.35	67.67	−35.23	−684.4075771	11.595	5.1323	4.0010
δ_D [ag^+]	−169.53	−39.89	168.72	−171.72	178.57	65.29	−684.4067348	12.123	5.6608	4.5296
δ_D [as^-]	−173.40	−36.11	167.19	−172.40	−172.30	−117.79	−684.4058219	12.696	6.2337	5.1024
δ_D [g^-g^-][a,b]	−144.09	−61.07	178.05	−176.94	−61.73	−79.40	−684.4052097	13.080	6.6178	5.4866
α_D Backbone conformation										
α_D [g^+s^+]	58.20	35.63	161.69	−175.78	42.53	102.03	−684.4070563	11.921	5.4591	4.3278

(*continued on next page*)

Table 6 (*continued*)

Final conform.	Optimized parameters									
BB [$\chi_1\chi_2$]	ϕ	ψ	ω_0	ω_1	χ_1	χ_2	E_{min} (Hartree)	ΔE (kcal/mol)	ΔE^{stabil} (kcal) γ_L	ΔE^{stabil} (kcal) β_L
α_D [g^+g^-]	59.50	29.35	164.08	−176.20	55.10	−81.81	−684.4040903	13.783	7.3203	6.1890
αa_D [ag^+]	65.49	31.81	168.69	−176.91	−167.04	37.82	−684.4097827	10.211	3.7482	2.6170
α_D [as^-]	66.30	32.61	169.86	−177.78	−157.47	−149.78	−684.4122840	8.641	2.1787	1.0474
α_D [g^-s]	66.36	28.71	166.07	−177.25	−63.19	−18.36	−684.4119363	8.859	2.3968	1.2656
α_D [g^-a]	66.01	30.43	164.61	−177.19	−64.43	−176.83	−684.4166005	5.932	−0.5300	−1.6613
ε_D Backbone conformation										
ε_D [g^+g^+]	53.92	−123.45	−176.20	177.24	51.08	89.57	−684.4079873	11.337	4.8749	3.7436
ε_D [g^+s^-]	57.16	−134.18	−164.86	179.14	69.41	−103.68	−684.4113997	9.196	2.7336	1.6023
ε_D [s^-a]	66.93	−178.82	−158.02	−175.88	−149.86	160.48	−684.4142905	7.382	0.9196	−0.2117
ε_D [s^-g^-]	64.41	−167.41	−160.60	−175.48	−135.38	−50.94	−684.4076898	11.524	5.0616	3.9303

[a] After 200 iterations under B3LYP/6-31G(d) at (TIGHT, Z-MATRIX), the force has converged, but the displacement did not converge completely.

[b] This result was obtained from an optimization fully converged under regular B3LYP/6-31G(d) at (Z-MATRIX).

receptor binding. Rather, it suggests that while the sidechain of the aspartic acid residue is stabilized by its SC/SC hydrogen bond, it is still possible for its backbone to participate in either external or internal stabilizing interactions. These suggestions point to the fact that ab initio studies for single amino acid residues may be useful in experiments involving protein bindings, receptor/ligand recognition, as well as de novo drug designs in a biological system.

The difference in stabilization energy, ΔE^{stabil}, with respect to the β_L and with respect to the γ_L backbone of *N*-acetyl-glycine-*N*′-methylamide is constant (0.66 kcal/mol at RHF/3-21G, 0.031 kcal/mol at RHF/6-31G(d), and 1.13 kcal/mol [50,51] at B3LYP/6-31G(d)), as shown in Tables 2–7. When examining Tables 2–7, one can observe that the L subscripted conformations (i.e. α_L, β_L, δ_L, ε_L, γ_L) of *N*-acetyl-L-aspartic acid *N*′-methylamide are more stabilized than its D subscripted forms (i.e. α_D, δ_D, ε_D, γ_D). Most of the stabilization energies for the L conformers have greater negative values or smaller positive values than those found for the D conformers. This trend, existed in both *endo* and *exo* forms of the aspartic acid residue (Figs. 20–25), shows that the L subscripted conformers are more stabilized while the D subscripted conformers are more 'de-stabilized'. In addition, the stabilization energy calculated with respect to the β_L backbone of glycine diamide was observed to be generally lower than those calculated with respect to the γ_L backbone (Figs. 20, 21, 24 and 25). However, this trend is not observed at the RHF/6-31G(d) level of theory, where the stabilization energy calculated with respect to the γ_L backbone of glycine diamide is lowered than that calculated with respect to the β_L backbone (Figs. 22 and 23).

A correlating trend between hydrogen bond distance and ring size (RS) was observed. Here, it is apparent that the shorter the hydrogen bond distance, the greater the RS. This trend can be observed at all three levels of theory (RHF/3-21G, RHF/6-31G(d), and B3LYP/6-31G(d)) in both the *endo* and the *exo* forms of *N*-acetyl-L-aspartic acid *N*′-methylamide, as shown in Figs. 26 and 27. At RHF/3-21G, the correlation equation for hydrogen bond distance versus ring size shows a least square value of $R^2 = 0.8083$ for the *endo* form (Fig. 26(a)) and $R^2 = 0.8312$ for the *exo* form (Fig. 27(a)). At RHF/6-31G(d), the correlation equation shows a least square value of $R^2 = 0.9300$ for the *endo* form (Fig. 26(b)) and $R^2 = 0.9425$ for the *exo* form (Fig. 27(b)). At B3LYP/6-31G(d), the correlation equation shows a least square value of $R^2 = 0.8443$ [51] for the *endo* form (Fig. 26(c)) and $R^2 = 0.9980$ [50] for the *exo* form (Fig. 27(c)). Clearly,

Table 7
Optimized conformers of *N*-acetyl-L-aspartic acid *N*′-methylamide in its *exo* form for all its stable backbone (γ_L, β_L, δ_L, ε_L, γ_D, δ_D, α_D, and ε_D) conformation computed at the B3LYP/6-31G(d) level of theory. Shown here are the optimized torsional angles, computed energy values, relative energies, and stabilization energies

Final conform.	Optimized parameters										
BB [$\chi_1\chi_2$]	ϕ	ψ	ω_0	ω_1	χ_1	χ_2	χ_3	E_{min} (Hartree)	ΔE (kcal/mol)	ΔE^{stabil} (kcal) γ_L	ΔE^{stabil} (kcal) β_L
γ_L Backbone conformation											
γ_L [g^+g^+]	−81.06	63.58	−171.12	−179.73	50.73	82.28	−13.95	−684.4265160	−0.290	−12.6619	−13.7932
γ_L [g^+g^+]	−81.91	63.80	−170.70	−179.40	50.58	82.31	−13.98	−684.4266579	−0.379	−12.7509	−13.8822
γ_L [ag^-]	−83.16	64.17	−172.10	−179.20	−165.32	−70.57	4.41	−684.4208809	3.246	−9.1258	−10.2571
γ_L [g^-s^-]	−84.07	70.53	−169.26	−176.36	−45.91	−121.27	0.59	−684.4126227	8.428	−3.9437	−5.0750
β_L Backbone conformation											
β_L [g^+g^+][a,b]	−156.59	−176.43	177.82	−171.12	64.56	72.14	−1.65	−684.4058456	12.681	0.3090	−0.8223
β_L [g^+s^-]	158.11	−139.74	172.36	179.88	63.71	−90.93	6.92	−684.4201077	3.731	−8.6406	−9.7719
β_L [*aa*]	−167.29	170.92	174.39	179.24	−159.70	167.29	−3.78	−684.4161709	6.202	−6.1702	−7.3015
β_L [s^-g^+]	−169.92	−177.45	175.01	−179.22	−130.05	74.37	−4.45	−684.4237651	1.436	−10.9357	−12.0669
δ_L Backbone conformation											
δ_L [s^-g^+][a,b]	−161.43	45.11	−176.35	173.71	−118.31	48.09	4.66	−684.4099383	10.113	−2.2592	−3.3905
δ_L [g^-s]	−135.40	25.16	−177.58	174.07	−67.01	−15.76	14.84	−684.4103060	9.882	−2.4900	−3.6212
ε_L Backbone conformation											
ε_L [g^-g^+]	−94.47	149.36	160.78	177.79	−63.25	43.99	−5.09	−684.4102974	9.888	−2.4846	−3.6158
γ_D Backbone conformation											
γ_D [g^+g^+]	64.96	−61.81	168.52	175.34	60.23	67.68	−17.12	−684.4033200	14.266	1.8938	0.7625
γ_D [s^+g^-]	79.72	−53.75	−177.65	−174.22	107.66	−75.40	6.66	−684.4073279	11.751	−0.6212	−1.7524
γ_D [*aa*]	74.38	−70.80	−179.62	175.29	−154.73	−154.72	4.80	−684.4035338	14.132	1.7597	0.6284
γ_D [ag$^-$]	70.34	−81.17	177.02	172.78	−176.52	−70.85	4.12	−684.4078146	11.446	−0.9266	−2.0579
γ_D [s^-g^-]	70.12	−28.28	167.77	−175.15	−143.16	−35.94	−3.53	−684.4144381	7.289	−5.0829	−6.2142
γ_D [g^-a]	73.63	−44.57	167.30	−177.58	−63.68	176.48	−0.54	−684.4098022	10.198	−2.1738	−3.3051
δ_D Backbone conformation											
δ_D [g^+a][a,b]	−160.74	−48.85	175.72	−176.93	52.48	−164.30	3.41	−684.4071457	11.865	−0.5068	−1.6381
δ_D [g^+g^-][a,b]	−152.24	−46.34	162.79	−174.56	62.86	−42.90	−3.04	−684.4046175	13.452	1.0796	−0.0516
δ_D [s^-g^+]	−166.96	−52.06	172.53	−173.85	−121.06	55.27	4.53	−684.4070418	11.930	−0.4416	−1.5729
δ_D [g^-s][a,b]	−135.56	−70.97	168.84	−177.26	−79.12	2.05	12.10	−684.4055002	12.898	0.5257	−0.6055
α_D Backbone conformation											
α_D [g^+g^+]	51.02	50.87	158.65	−173.41	57.95	78.07	−13.34	−684.4118612	8.906	−3.4659	−4.5971
α_D [g^+g^-]	49.91	35.67	175.22	−176.17	42.68	−69.95	7.37	−684.3904410	22.348	9.9755	8.8442
α_D [s^-g^-]	68.57	27.90	165.45	−178.48	−147.48	−61.61	0.62	−684.4145135	7.242	−5.1302	−6.2615
α_D [g^-a]	66.58	30.54	164.64	−177.60	−64.08	−177.94	0.92	−684.4094323	10.430	−1.9417	−3.0730

(*continued on next page*)

Table 7 (*continued*)

Final conform.	Optimized parameters										
BB [$\chi_1\chi_2$]	ϕ	ψ	ω_0	ω_1	χ_1	χ_2	χ_3	E_{min} (Hartree)	ΔE (kcal/mol)	ΔE^{stabil} (kcal) γ_L	ΔE^{stabil} (kcal) β_L
ε_D Backbone conformation											
ε_D [*aa*]	68.83	176.68	−157.00	−176.55	−152.00	171.32	−0.35	−684.4069842	11.967	−0.4055	−1.5368
ε_D [g^-g^+]	85.36	163.60	−152.58	178.97	−62.34	93.43	−7.44	−684.4096079	10.320	−2.0519	−3.1832

[a] After 200 iterations under B3LYP/6-31G(d) at (TIGHT, Z-MATRIX), the force has converged, but the displacement did not converge completely.
[b] This result was obtained from an optimization fully converged under regular B3LYP/6-31G(d) at (Z-MATRIX).

this trend concerning hydrogen bond distance and ring size is unmistakably evident at all three levels of theory.

Furthermore, a strikingly significant correlation was found between the torsional angles (χ_1, χ_2, χ_3, ω_0, ω_1, ϕ, and ψ) optimized at the one level of theory and those optimized at another level of theory (Fig. 28). Specifically, only minute deviation was found between torsional angle values found at RHF/3-21G when compared to those found at RHF/6-31G(d) or at B3LYP/6-31G(d) levels. For example, when correlating the torsional angles optimized at RHF/6-31G(d) against those optimized at RHF/3-21G for the *endo* form of the aspartic acid residue, the correlation has a strikingly high least square value of $R^2 = 0.9956$ (Fig. 28(a)). When correlating the torsional angles optimized at B3LYP/6-31G(d) against those optimized at RHF/6-31G(d) for the *endo* form, yet another high correlation with a least square value of $R^2 = 0.9981$ was found (Fig. 28(b)). Lastly, when correlating the torsional angles optimized at B3LYP/6-31G(d) against those optimized at RHF/3-21G, a strong correlation that has a least square value of $R^2 = 0.9703$ was found (Fig. 28(c)). Although the trend observed at B3LYP/6-31G(d) versus RHF/3-21G was slightly less significant, the correlation was clearly strong and undoubtedly apparent. In a similar fashion, the torsional angles found for the *exo* form of *N*-acetyl-L-aspartic acid *N*′-methylamide at the different levels of theory correlated strongly against one another: $R^2 = 0.9910$ for RHF/6-31G(d) versus RHF/3-21G (Fig. 28(d)), $R^2 = 0.9958$ for B3LYP/6-31G(d) versus RHF/6-31G(d) (Fig. 28(e)), and $R^2 = 0.9923$ for B3LYP/6-31G(d) versus RHF/3-21G (Fig. 28(f)). To test the validity of this observation, optimization results for the torsional angles found in both *endo* and *exo* forms of *N*-acetyl-L-aspartic acid *N*′-methylamide were collectively correlated between the different levels of theory. In order to perform the correlation, the χ_3 torsional angles were removed from the data pool. This is because the only true difference between *endo* and *exo* lies in the hydroxyl group. The results obtained were quite remarkable (Fig. 29). When both *endo* and *exo* optimization results were combined, very high correlation values were obtained between

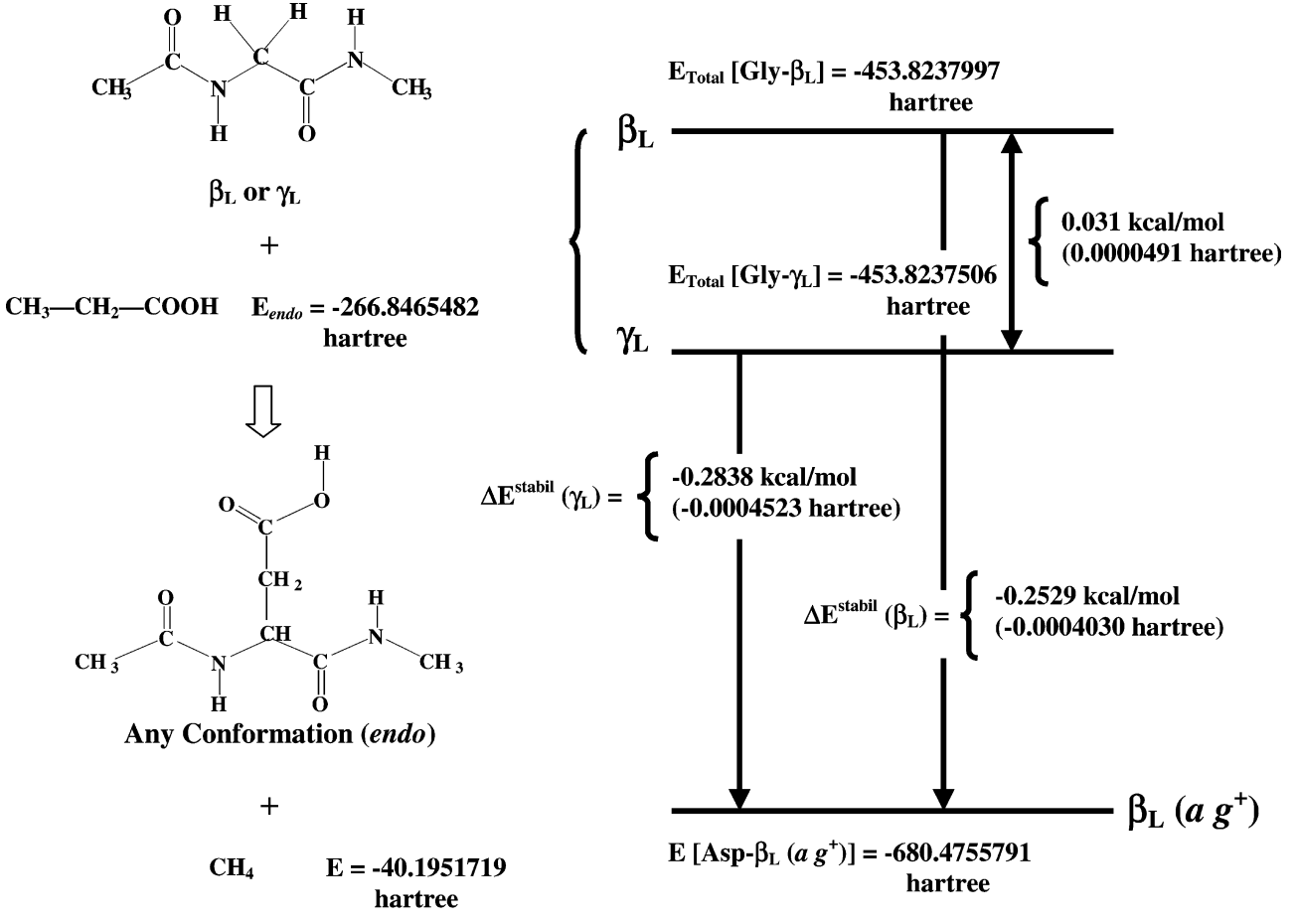

Fig. 6. An example demonstrating how stabilization energies for all stable conformers were calculated using *N*-acetyl-glycine-*N*′-methylamide with respect to the γ_L or β_L conformers of *N*-acetyl-L-aspartic acid *N*′-methylamide. The *endo* form of *N*-acetyl-L-aspartic acid *N*′-methylamide was used in this example. Here, the stabilization energy for the ag^+ conformer found at the β_L backbone conformation at RHF/6-31G(d) was calculated.

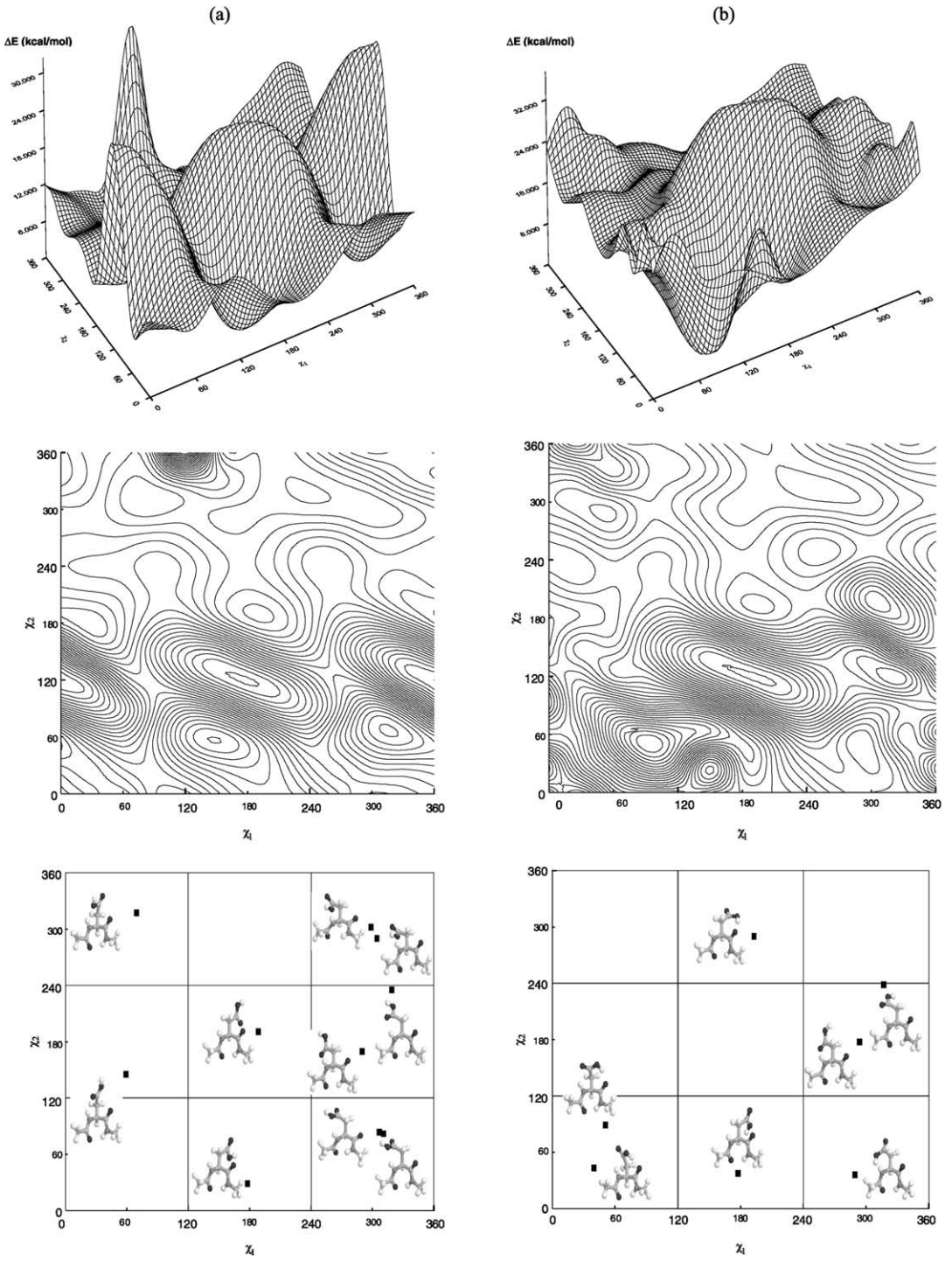

Fig. 7. Double-scan PES, $E = E(\chi_1, \chi_2)$, generated for the γ_L backbone conformation of (a) the *endo* form and (b) the *exo* form of *N*-acetyl-L-aspartic acid *N'*-methylamide at RHF/3-21G. (Top) landscape representation; (middle) contour representation; (bottom) topology diagram with ball-and-stick representation of stable conformers found. Torsional angles X_1 on X_2 are given in degrees.

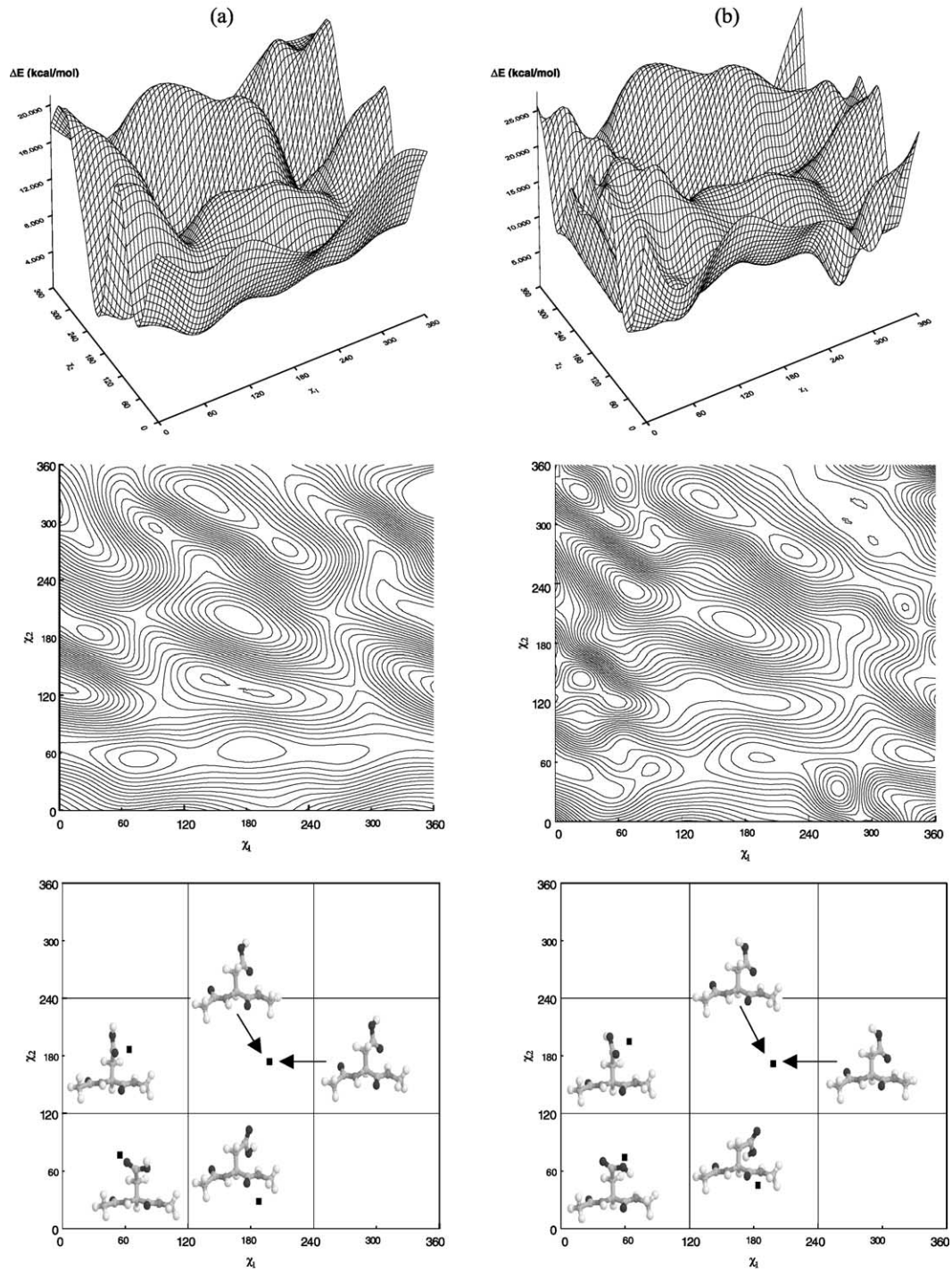

Fig. 8. Double-scan PES, $E = E(\chi_1, \chi_2)$, generated for the β_L backbone conformation of (a) the *endo* form and (b) the *exo* form of *N*-acetyl-L-aspartic acid *N*′-methylamide at RHF/3-21G. (Top) landscape representation; (middle) contour representation; (bottom) topology diagram with ball-and-stick representation of stable conformers found. Torsional angles X_1 on X_2 are given in degrees.

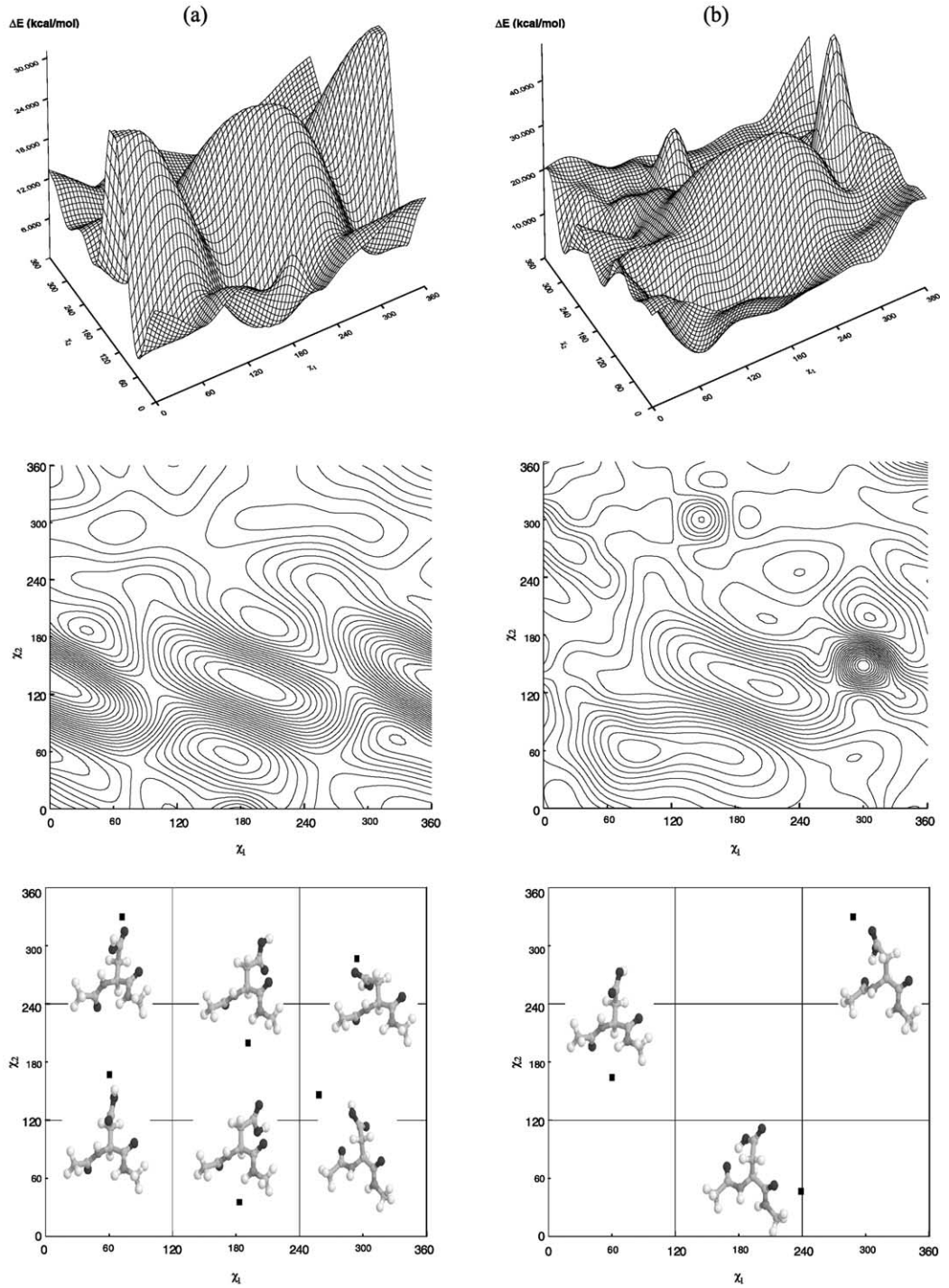

Fig. 9. Double-scan PES, $E = E(\chi_1, \chi_2)$, generated for the δ_L backbone conformation of (a) the *endo* form and (b) the *exo* form of *N*-acetyl-L-aspartic acid *N*′-methylamide at RHF/3-21G. (Top) landscape representation; (middle) contour representation; (bottom) topology diagram with ball-and-stick representation of stable conformers found. Torsional angles X_1 on X_2 are given in degrees.

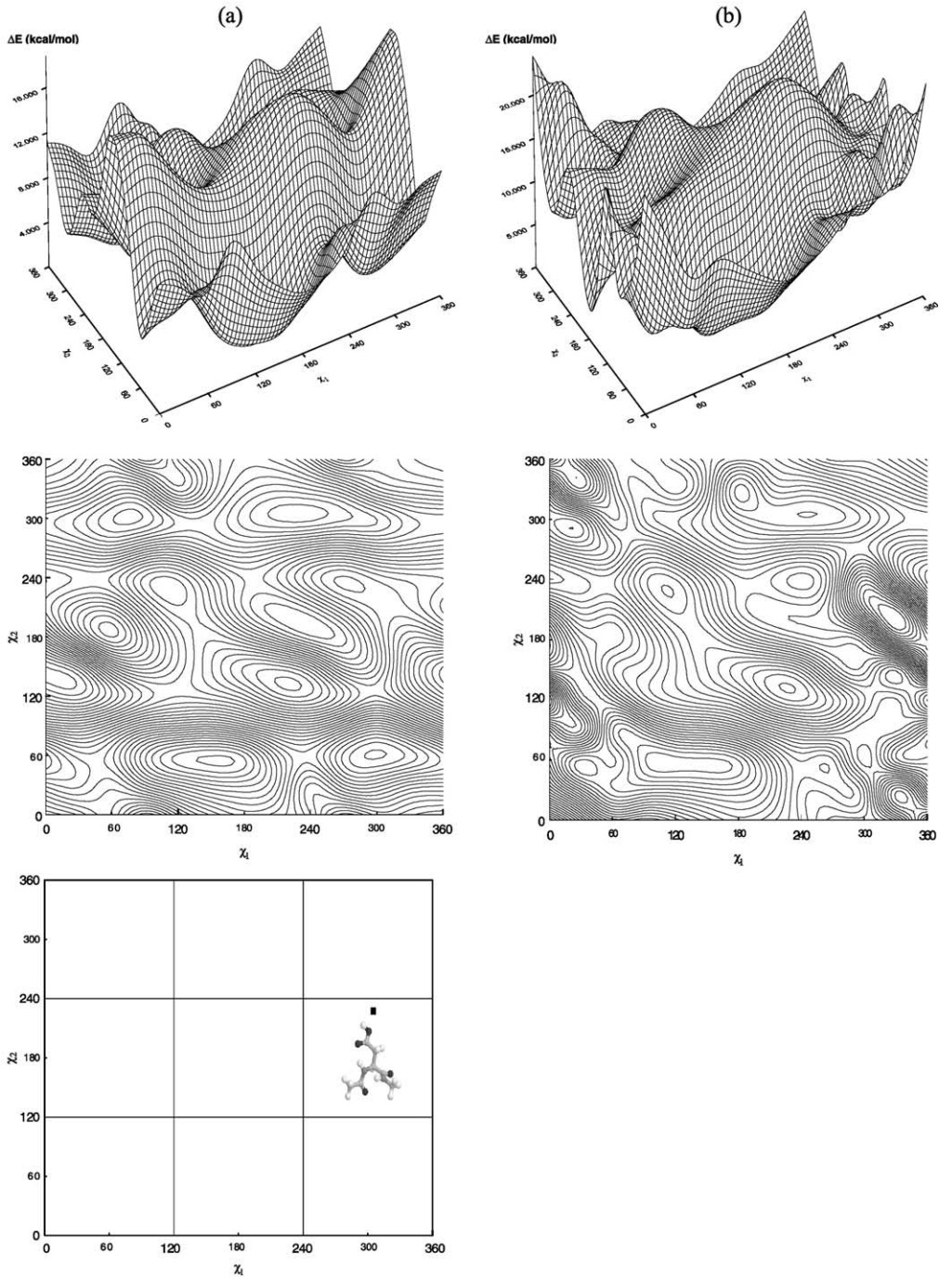

Fig. 10. Double-scan PES, $E = E(\chi_1, \chi_2)$, generated for the α_L backbone conformation of (a) the *endo* form and (b) the *exo* form of *N*-acetyl-L-aspartic acid *N'*-methylamide at RHF/3-21G. (Top) landscape representation; (middle) contour representation; (bottom) topology diagram with ball-and-stick representation of stable conformers found. Note that no stable conformers could be found for the *exo* form of *N*-acetyl-L-aspartic acid *N'*-methylamide in the α_L backbone conformation (and hence there is no topology diagram for the *exo* form in this backbone). Torsional angles X_1 on X_2 are given in degrees.

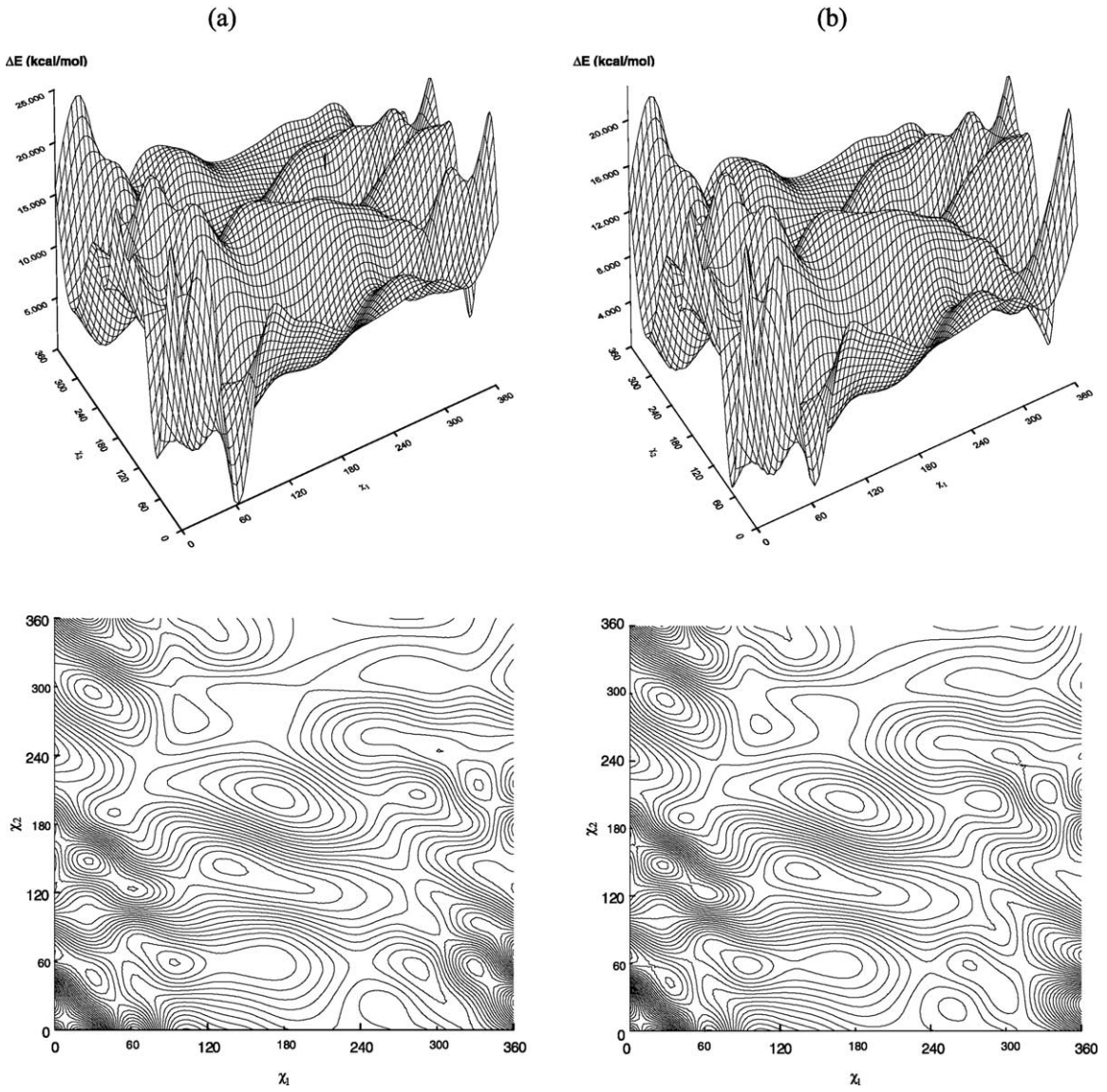

Fig. 11. Double-scan PES, $E = E(\chi_1, \chi_2)$, generated for the ε_L backbone conformation of (a) the *endo* form and (b) the *exo* form of *N*-acetyl-L-aspartic acid *N*′-methylamide at RHF/3-21G. (Top) landscape representation; (middle) contour representation; (bottom) topology diagram with ball-and-stick representation of stable conformers found. Note that no stable conformers could be found for both *endo* and *exo* forms of *N*-acetyl-L-aspartic acid *N*′-methylamide in the ε_L backbone conformation (and hence there are no topology diagrams for both the *endo* and the *exo* forms in this backbone). Torsional angles X_1 on X_2 are given in degrees.

the different levels of theory: $R^2 = 0.9937$ for RHF/6-31G(d) versus RHF/3-21G (Fig. 29(a)); $R^2 = 0.9967$ for B3LYP/6-31G(d) versus RHF/6-31G(d) (Fig. 29(b)); and $R^2 = 0.9914$ for B3LYP/6-31G(d) versus RHF/3-21G (Fig. 29(c)). And lastly, optimized ΔE values in kcal/mol for all *endo* and *exo* conformers were correlated between each level of theory (Fig. 30). Again, high correlation values were obtained between the different levels of theory: $R^2 = 0.9424$ for RHF/6-31G(d) versus

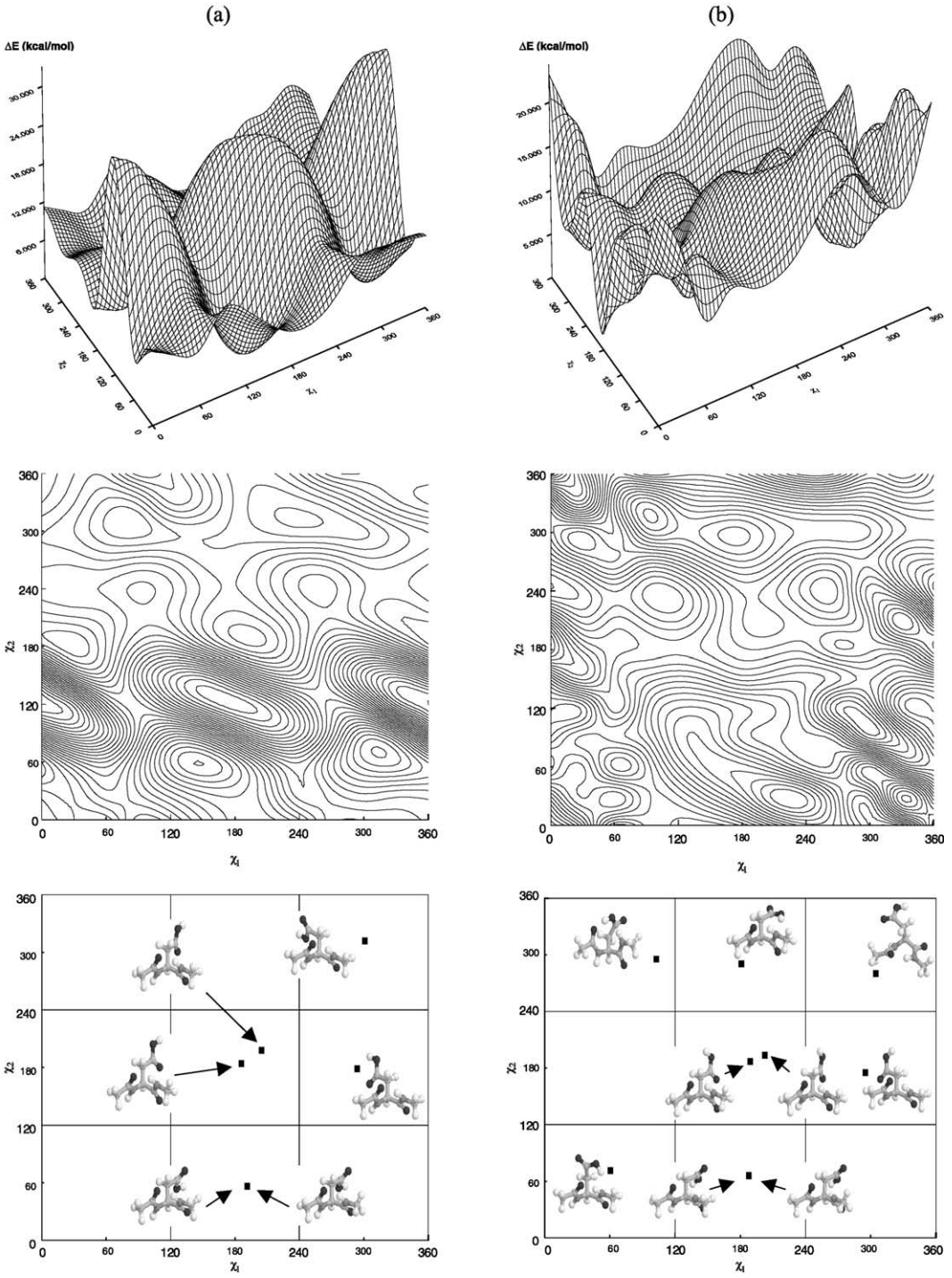

Fig. 12. Double-scan PES, $E = E(\chi_1, \chi_2)$, generated for the γ_D backbone conformation of (a) the *endo* form and (b) the *exo* form of *N*-acetyl-L-aspartic acid *N'*-methylamide at RHF/3-21G. (Top) landscape representation; (middle) contour representation; (bottom) topology diagram with ball-and-stick representation of stable conformers found. Torsional angles X_1 on X_2 are given in degrees.

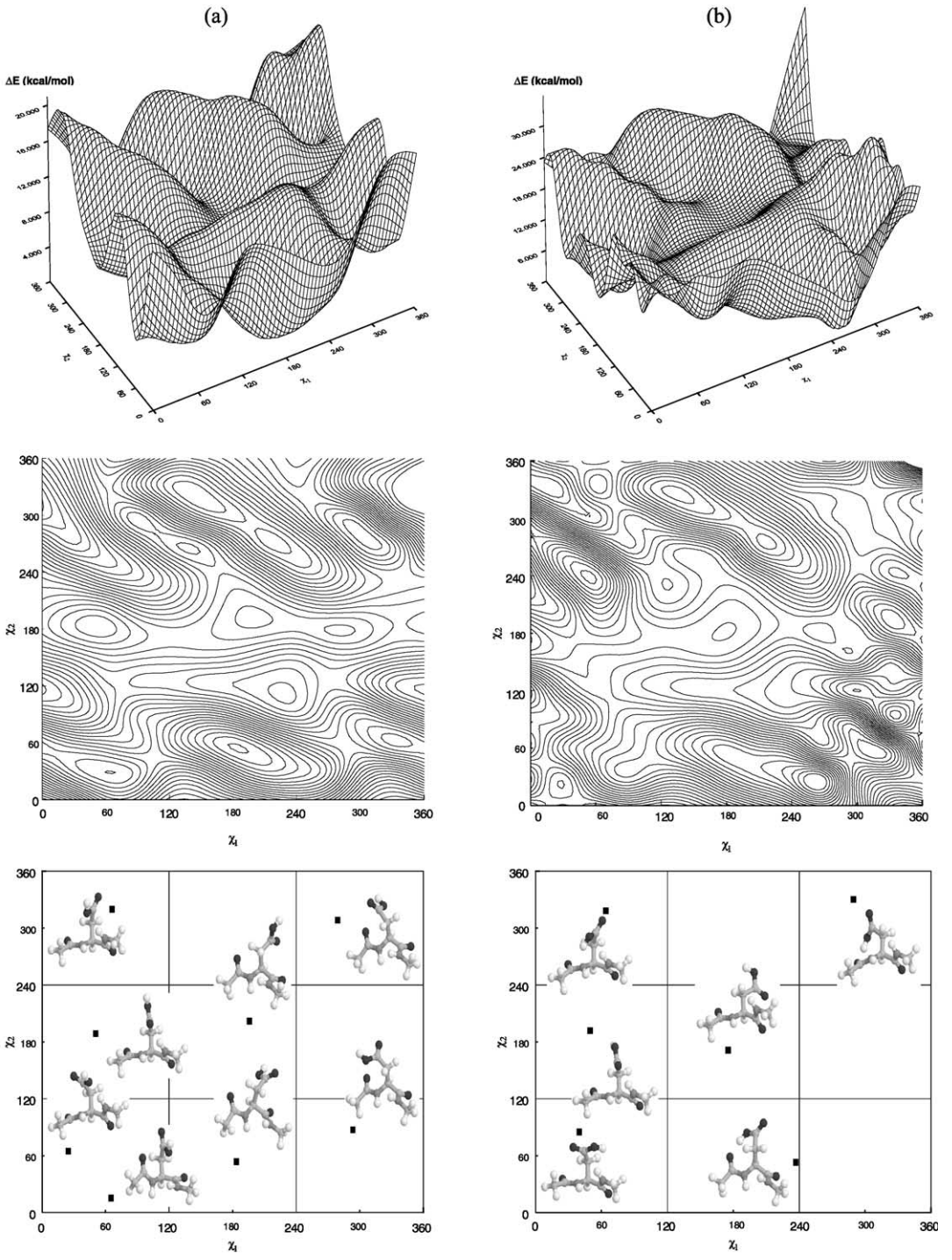

Fig. 13. Double-scan PES, $E = E(\chi_1, \chi_2)$, generated for the δ_D backbone conformation of (a) the *endo* form and (b) the *exo* form of *N*-acetyl-L-aspartic acid *N*′-methylamide at RHF/3-21G. (Top) landscape representation; (middle) contour representation; (bottom) topology diagram with ball-and-stick representation of stable conformers found. Torsional angles X_1 on X_2 are given in degrees.

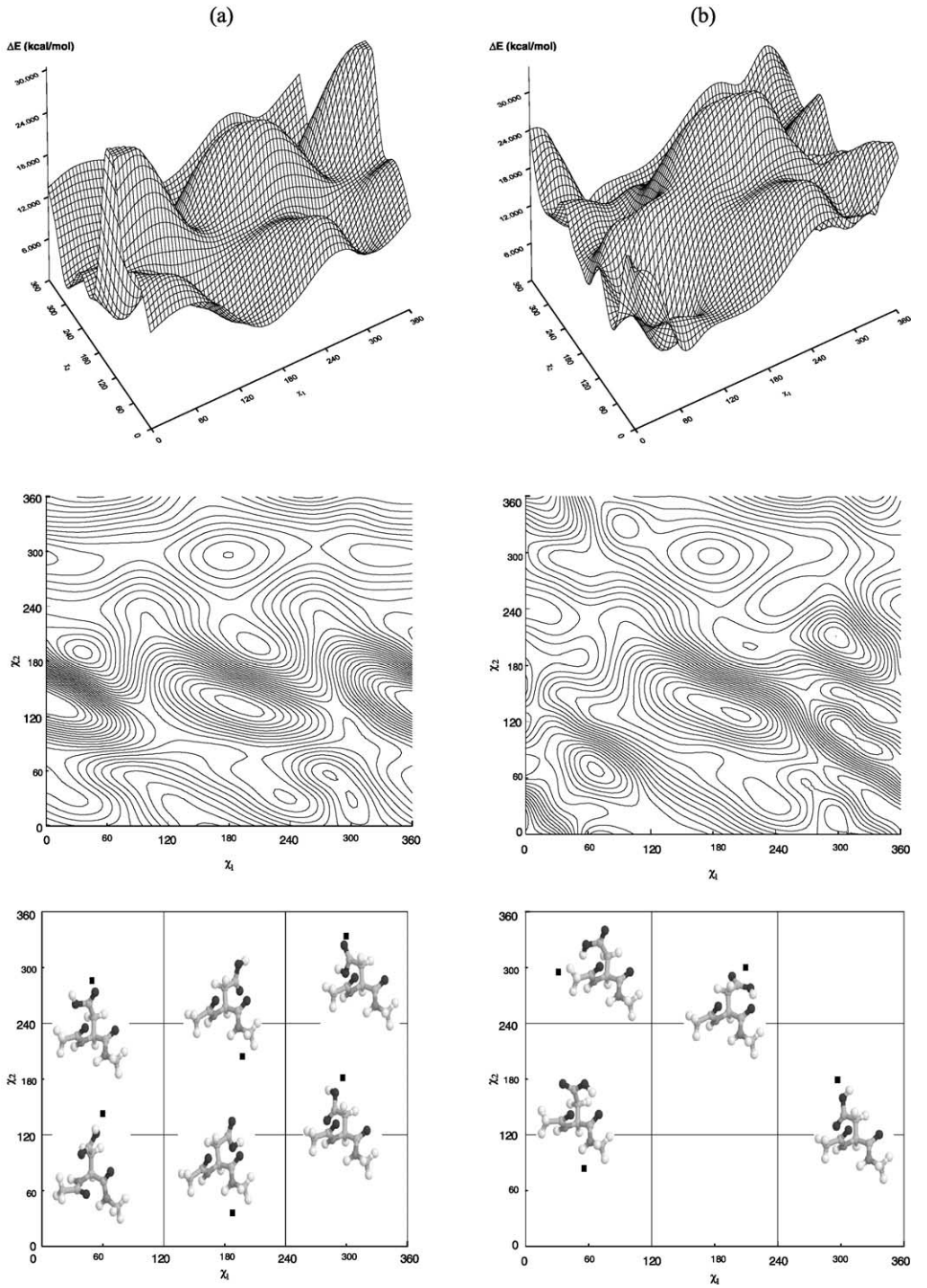

Fig. 14. Double-scan PES, $E = E(\chi_1, \chi_2)$, generated for the α_D backbone conformation of (a) the *endo* form and (b) the *exo* form of *N*-acetyl-L-aspartic acid *N'*-methylamide at RHF/3-21G. (Top) landscape representation; (middle) contour representation; (bottom) topology diagram with ball-and-stick representation of stable conformers found. Torsional angles X_1 on X_2 are given in degrees.

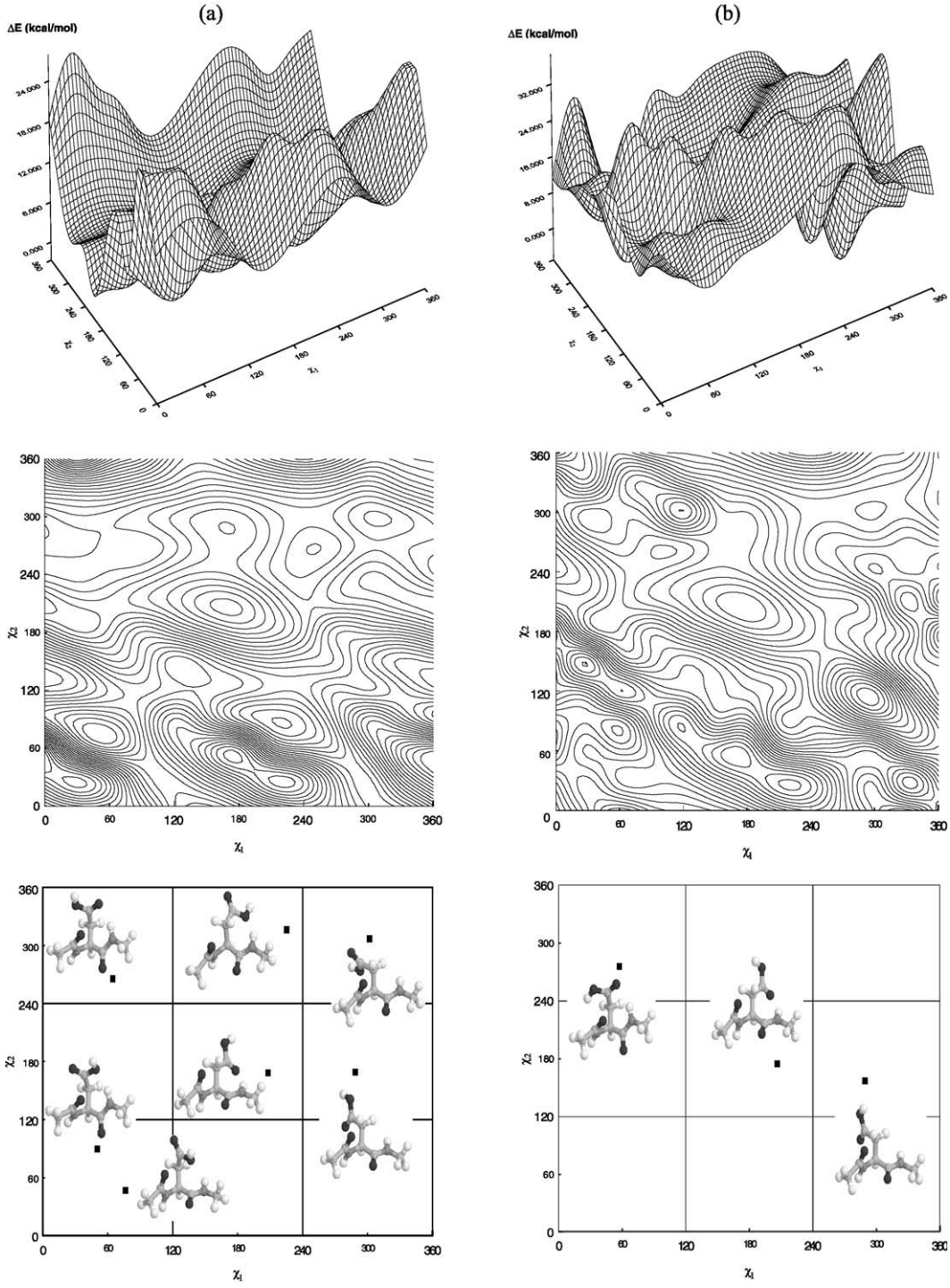

Fig. 15. Double-scan PES, $E = E(\chi_1, \chi_2)$, generated for the ε_D backbone conformation of (a) the *endo* form and (b) the *exo* form of *N*-acetyl-L-aspartic acid *N'*-methylamide at RHF/3-21G. (Top) landscape representation; (middle) contour representation; (bottom) topology diagram with ball-and-stick representation of stable conformers found. Torsional angles X_1 on X_2 are given in degrees.

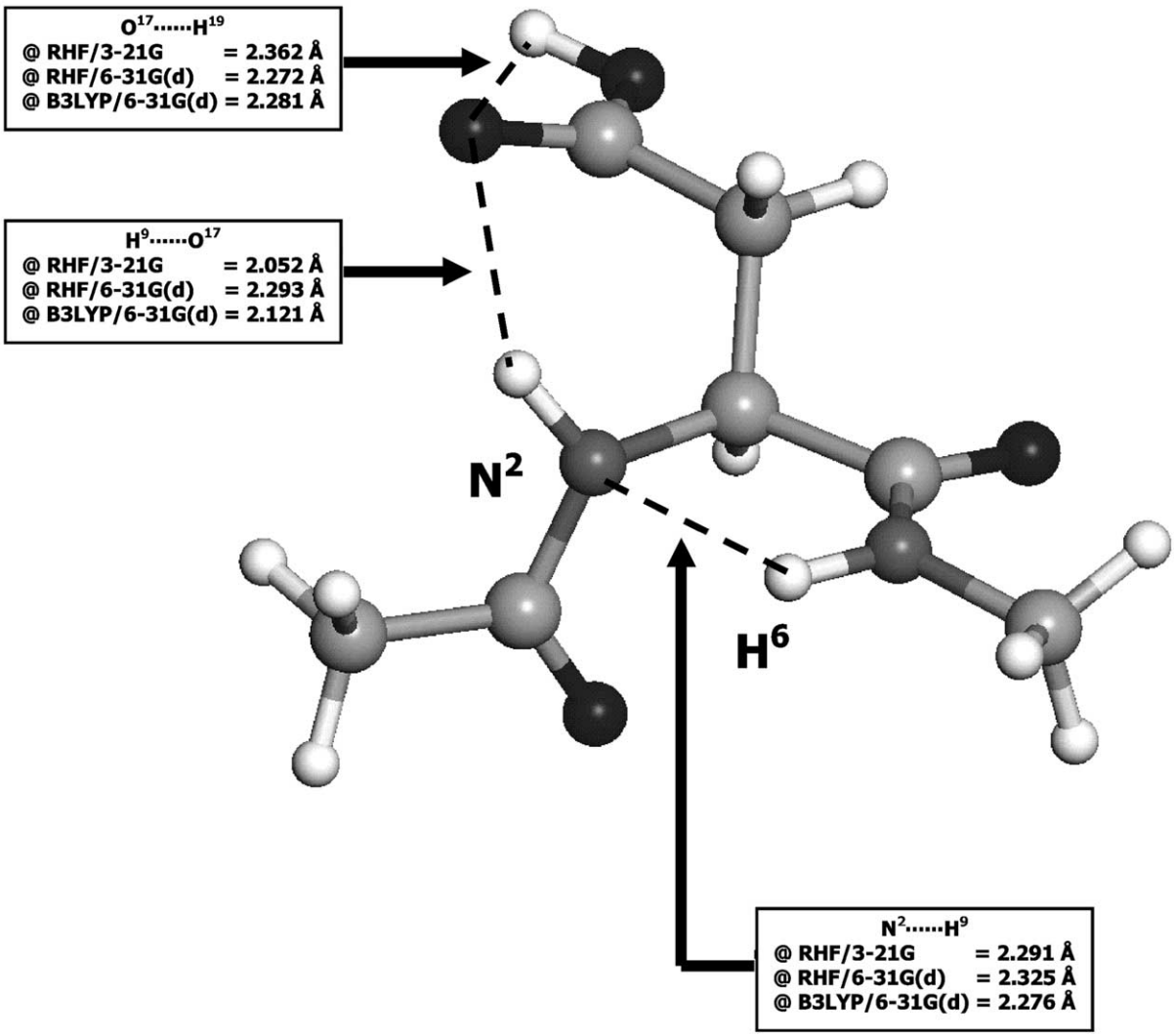

Fig. 16. A pictorial representation of the stable $g^{-}s^{-}$ conformer found at the α_L backbone of the *endo* form of *N*-acetyl-L-aspartic acid *N'*-methylamide.

RHF/3-21G (Fig. 30(a)); $R^2 = 0.9108$ for B3LYP/6-31G(d) versus RHF/6-31G(d) (Fig. 30(b)); and $R^2 = 0.9434$ B3LYP/6-31G(d) versus RHF/3-21G (Fig. 30(c)).

Although the correlations for optimization results (be it torsional angles or ΔE values) between different levels of theories are strong, one limitation for lower-level optimizations is that they are not selective enough for identifying stable conformers. For example, it is clear that some conformers found at the RHF/3-21G level of theory are not found at the B3LYP/6-31G(d) level. With that said however, the strong correlation between the torsional angles (χ_1, χ_2, χ_3, ω_0, ω_1, ϕ, ψ) and between the ΔE values, for both *endo* and *exo* forms, optimized at the different levels of theory undoubtedly suggest that the optimization results did not deviate greatly among the three levels of theory. This observation suggests that calculations performed

Sidechain-Sidechain Interaction (SC/SC)

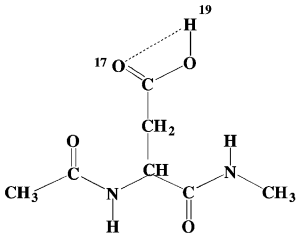

Intramolecular H-bonded
Interaction Type: **1**
Distance: O^{17}····· H^{19}
Ring Size: 4

Backbone-Backbone Interactions (BB/BB)

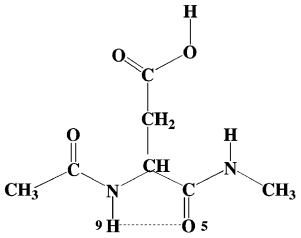

Intramolecular H-bonded
Interaction Type: **2A**
Distance: O^{5}····· H^{9}
Ring Size: 5

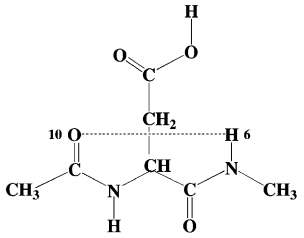

Intramolecular H-bonded
Interaction Type: **2B**
Distance: O^{10}····· H^{6}
Ring Size: 7

Sidechain-Backbone Interactions (SC/BB)

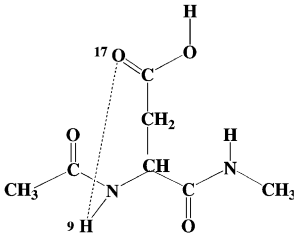

Intramolecular H-bonded
Interaction Type: **3A**
Distance: O^{17}····· H^{9}
Ring Size: 6

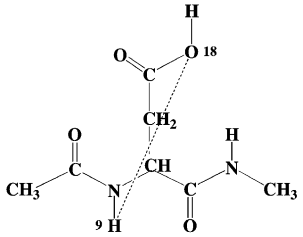

Intramolecular H-bonded
Interaction Type: **3B**
Distance: O^{18}····· H^{9}
Ring Size: 6

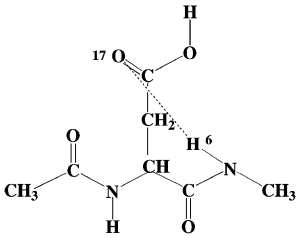

Intramolecular H-bonded
Interaction Type: **3C**
Distance: O^{17}····· H^{6}
Ring Size: 7

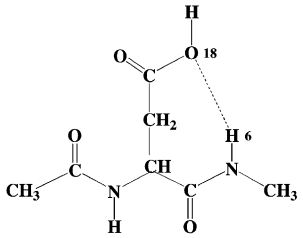

Intramolecular H-bonded
Interaction Type: **3D**
Distance: O^{18}····· H^{6}
Ring Size: 7

Fig. 17. Classification of traditional hydrogen bond interactions for the *endo* form of *N*-acetyl-L-aspartic acid *N'*-methylamide.

Table 8
The relative distances of potential hydrogen bonds of *N*-acetyl-L-aspartic acid *N*′-methylamide in its *endo* form for all its stable backbone (γ_L, β_L, δ_L, α_L, γ_D, δ_D, α_D, and ε_D) conformations computed at the RHF/3-21G level of theory. No conformers were found for the ε_L backbone and hence no hydrogen bond distances for the ε_L backbone could be tabulated

Final conform.	Interaction type			Distance (Å)						
BB [$\chi_1\chi_2$]	SC/SC	BB/BB	SC/BB	O17 − H19	H9 − O17	H9 − O18	H9 − O5	H6 − O10	H6 − O17	H6 − O18
γ_L Backbone conformation										
γ_L [g^+s^+]	1	2B	3A	2.359	2.007	3.878	3.497	2.065	4.826	5.763
γ_L [g^+g^-]	1	2B	3B	2.355	3.936	2.007	3.505	2.068	5.742	4.716
γ_L [*as*]	1	2B	–	2.371	4.880	4.610	3.644	2.032	5.664	4.141
γ_L [*aa*]	1	2B	–	2.369	4.715	4.867	3.588	2.060	4.207	5.789
γ_L [g^-g^+]	1	2B	3B	2.356	3.651	2.134	3.710	1.969	5.678	5.424
γ_L [g^-g^+]	1	–	3B	2.357	3.777	2.274	4.175	3.119	5.768	4.872
γ_L [g^-a]	1	2B	–	2.365	3.371	3.942	3.677	2.008	4.899	6.157
γ_L [g^-s^-]	1	2B	3A	2.354	2.069	3.813	3.752	1.950	5.374	5.950
γ_L [g^-g^-]	1	2B	–	2.371	2.798	3.672	3.673	2.006	5.717	5.047
γ_L [g^-g^-]	1	–	–	2.377	3.532	3.974	3.917	3.311	5.714	5.220
β_L Backbone conformation										
β_L [g^+g^+]	1	2A	–	2.376	3.497	3.620	2.101	5.011	5.017	3.576
β_L [g^+a]	1	2A	–	2.365	2.971	4.584	2.110	5.077	3.769	4.315
β_L [*as*]	1	2A	3D	2.349	5.408	4.849	2.077	5.011	3.427	2.070
β_L [*aa*]	1	2A	3C	2.356	4.933	5.472	2.047	5.079	1.962	3.795
β_L [*aa*]	1	2A	3C	2.357	4.934	5.470	2.044	5.053	1.963	3.791
δ_L Backbone conformation										
δ_L [g^+a]	1	–	3A	2.361	2.150	3.993	3.708	3.532	3.992	5.656
δ_L [g^+g^-]	1	–	3B	2.347	4.049	2.104	3.663	3.370	5.598	4.034
δ_L [ag^+]	1	–	–	2.368	5.117	4.750	3.675	3.593	5.791	4.676
δ_L [a*a*]	1	–	–	2.363	4.854	5.157	3.566	3.613	4.655	5.903
δ_L [s^-s^+]	1	–	–	2.359	4.786	4.968	3.520	4.209	5.008	6.100
δ_L [g^-g^-]	1	–	–	2.383	3.664	4.407	3.733	3.770	5.568	5.311
α_L Backbone conformation										
α_L [g^-s^-]	1	–	3A	2.362	2.052	3.856	4.385	3.092	4.569	5.589
γ_D Backbone conformation										
γ_D [ag^+]	1	2B	–	2.374	5.507	4.443	3.913	1.916	4.312	4.850
γ_D [ag^+]	1	2B	–	2.374	5.508	4.442	3.899	1.918	4.304	4.836
γ_D [a*a*]	1	2B	–	2.365	4.545	5.543	3.719	1.951	4.691	4.560
γ_D [a*a*]	1	2B	–	2.366	4.779	5.560	3.586	2.008	4.033	4.301
γ_D [g^-a]	1	2B	–	2.368	2.918	4.615	3.932	1.884	4.949	5.060
γ_D [g^-g^-]	1	2B	–	2.357	4.122	3.313	3.869	1.896	4.830	5.040
δ_D Backbone conformation										
δ_D [sg^+]	1	–	3D	2.336	3.844	2.992	3.484	4.886	3.864	1.877
δ_D [g^+s]	1	–	–	2.350	5.238	3.901	3.939	3.787	4.878	2.796
δ_D [g^+a]	1	–	3C	2.349	2.955	4.609	3.576	4.745	1.927	3.886
δ_D [g^+g^-]	1	–	3D	2.321	4.735	2.955	3.555	4.593	3.411	2.060

(*continued on next page*)

Table 8 (*continued*)

Final conform.	Interaction type			Distance (Å)						
BB [$\chi_1\chi_2$]	SC/SC	BB/BB	SC/BB	O17 − H19	H9 − O17	H9 − O18	H9 − O5	H6 − O10	H6 − O17	H6 − O18
δ_D [ag^+]	1	–	–	2.374	5.429	4.897	3.545	4.405	4.467	4.885
δ_D [a*a*]	1	–	–	2.362	4.949	5.585	3.450	4.397	4.807	4.671
δ_D [g^-g^+]	1	–	–	2.365	4.916	3.781	3.526	4.793	5.157	4.253
δ_D [g^-g^-]	1	–	–	2.389	4.896	4.668	3.454	4.548	4.897	5.056
α_D Backbone conformation										
α_D [g^+s^+]	1	–	–	2.355	3.264	4.710	4.289	2.886	4.898	5.780
α_D [g^+g^-]	1	–	–	2.336	4.754	3.281	4.411	2.985	5.333	4.994
α_D [ag^+]	1	–	–	2.358	5.497	4.435	4.375	3.210	5.795	4.757
α_D [a*a*]	1	–	–	2.361	4.507	5.459	4.372	3.264	4.853	5.886
α_D [g^-s]	1	–	–	2.339	4.092	2.736	4.389	3.135	6.046	4.903
α_D [g^-a]	1	–	–	2.360	2.560	4.323	4.395	3.140	4.962	6.167
ε_D Backbone conformation										
ε_D [g^+g^+]	1	–	–	2.402	5.057	4.602	3.022	4.722	4.487	2.986
ε_D [g^+g^+]	1	–	3D	2.377	3.954	4.793	3.369	2.891	3.701	1.921
ε_D [g^+s^-]	1	–	3C	2.365	4.972	4.061	3.254	3.147	1.966	3.674
ε_D [*aa*]	1	–	3C	2.354	4.756	5.503	2.962	4.736	1.971	3.742
ε_D [s^-g^-]	1	–	3D	2.350	5.170	4.706	2.953	4.516	3.881	1.950
ε_D [g^-a]	1	–	–	2.365	3.321	4.766	3.171	4.695	4.311	4.698
ε_D [g^-g^-]	1	–	–	2.356	4.175	3.509	3.076	4.516	5.022	4.141

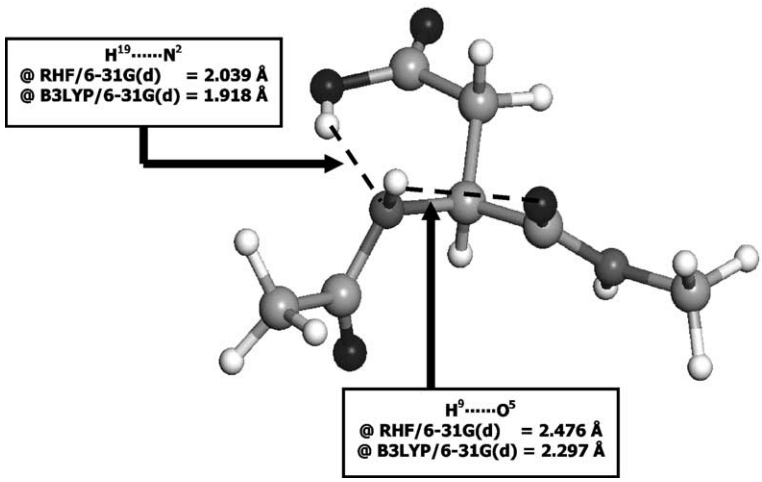

Fig. 18. A pictorial representation of the stable g^-g^+ conformer found at the α_L backbone of the *exo* form of *N*-acetyl-L-aspartic acid *N*′-methylamide. Note that at RHF/3-21G this g^-g^+ conformer does not exist in the ε_L backbone.

Backbone-Backbone Interactions
(BB/BB)

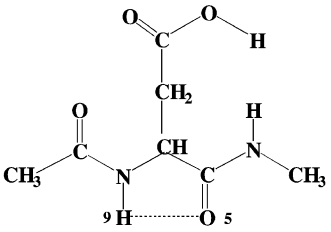

Intramolecular H-bond
Interaction Type: **1A**
Distance: $O^{5}\cdots\cdots H^{9}$
Ring Size: 5

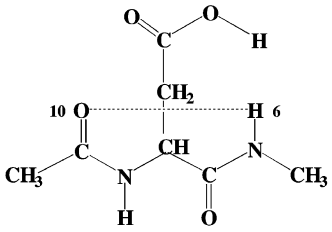

Intramolecular H-bond
Interaction Type: **1B**
Distance: $O^{10}\cdots\cdots H^{6}$
Ring Size: 7

Sidechain-Backbone Interactions
(SC/BB)

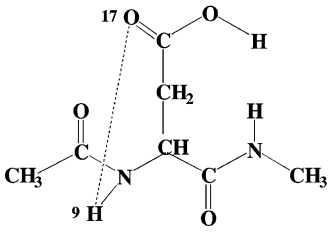

Intramolecular H-bond
Interaction Type: **2A**
Distance: $O^{17}\cdots\cdots H^{9}$
Ring Size: 6

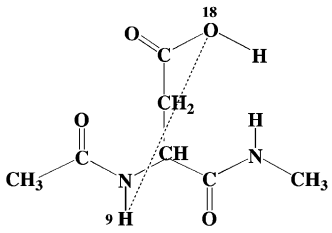

Intramolecular H-bond
Interaction Type: **2B**
Distance: $O^{18}\cdots\cdots H^{9}$
Ring Size: 6

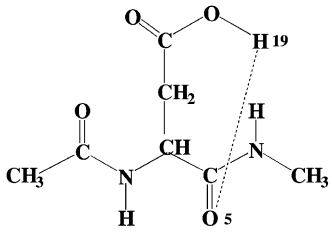

Intramolecular H-bond
Interaction Type: **2C**
Distance: $O^{5}\cdots\cdots H^{19}$
Ring Size: 7

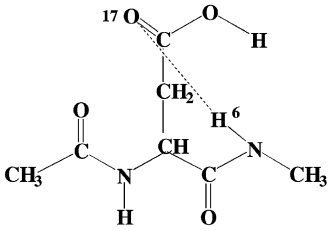

Intramolecular H-bond
Interaction Type: **2D**
Distance: $O^{17}\cdots\cdots H^{6}$
Ring Size: 7

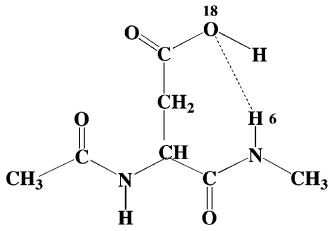

Intramolecular H-bond
Interaction Type: **2E**
Distance: $O^{18}\cdots\cdots H^{6}$
Ring Size: 7

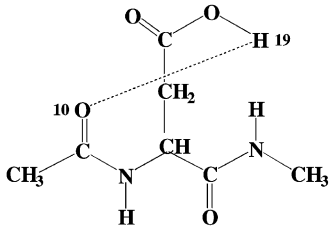

Intramolecular H-bond
Interaction Type: **2F**
Distance: $O^{10}\cdots\cdots H^{19}$
Ring Size: 8

Fig. 19. Classification of traditional hydrogen bond interactions for the *exo* form of *N*-acetyl-L-aspartic acid *N*′-methylamide.

Table 9
The relative distances of potential hydrogen bonds of *N*-acetyl-L-aspartic acid *N'*-methylamide in its *exo* form for all its stable backbone (γ_L, β_L, δ_L, γ_D, δ_D, α_D, and ε_D) conformations computed at the RHF/3-21G level of theory. No conformers were found for the α_L and ε_L backbones and hence no hydrogen bond distances for the α_L and ε_L backbones could be tabulated

Final conform.	Interaction type		Distance (Å)							
BB [χ_1 χ_2]	BB/BB	SC/BB	H9–O5	H9–O17	H9–O18	H19–O5	H6–O10	H6–O17	H6–O18	H19–O10
γ_L Backbone conformation										
γ_L [g^+g^+]	1B	2C	3.411	3.170	2.405	1.681	2.106	6.014	4.817	4.946
γ_L [g^+g^+]	1B	2A, 2C	3.821	2.152	3.395	1.714	1.913	5.340	5.059	5.470
γ_L [ag^+]	1B	–	3.602	4.823	4.787	3.490	2.052	5.662	4.420	4.357
γ_L [ag^-]	1B	2C	3.697	4.785	4.764	1.706	1.954	5.593	4.803	5.432
γ_L [g^-g^+]	1B	–	3.354	4.522	3.109	4.604	2.107	5.967	5.044	3.366
γ_L [g^-a]	1B	2A	3.790	2.033	3.789	4.946	1.932	5.350	5.988	5.916
γ_L [g^-s^-]	1B	–	3.719	3.084	3.987	4.703	1.992	4.928	6.217	6.411
β_L Backbone conformation										
β_L [g^+g^+]	1A	–	2.143	3.610	3.748	3.048	5.041	4.868	3.445	5.296
β_L [g^+a]	1A	–	2.083	3.059	4.558	5.611	5.108	3.623	4.445	4.326
β_L [ag^+]	1A	2E	2.132	5.262	4.939	4.869	4.911	3.110	2.204	3.567
β_L [aa]	1A	2D	2.020	4.913	5.556	5.732	5.095	1.928	3.780	4.509
β_L [aa]	1A	2D	2.024	4.912	5.558	5.743	5.121	1.928	3.782	4.505
δ_L Backbone conformation										
δ_L [g^+a]	–	2A	3.744	2.102	3.990	3.885	3.571	3.918	5.605	6.176
δ_L [s^-g^+]	–	2F	3.421	5.474	4.627	4.822	4.136	5.835	4.987	1.717
δ_L [g^-g^-]	–	2F	3.678	4.535	4.245	4.790	3.793	6.128	5.153	1.730
γ_D Backbone conformation										
γ_D [g^+g^+]	1B	–	3.988	4.398	4.847	3.458	1.800	3.958	2.668	2.991
γ_D [s^+g^-]	–	2E, 2F	3.236	5.550	4.640	4.726	2.952	3.126	1.962	1.583
γ_D [ag^+]	1B	–	3.809	5.485	4.731	3.859	1.945	4.011	4.902	5.296
γ_D [ag^+]	1B	–	3.799	5.489	4.733	3.838	1.945	4.005	4.886	5.292
γ_D [aa]	1B	–	3.675	4.559	5.597	5.286	1.966	4.597	4.625	4.646
γ_D [aa]	1B	–	3.585	4.716	5.625	5.483	2.010	4.156	4.392	4.612
γ_D [a g^-]	1B	–	3.653	5.199	5.198	3.102	1.910	4.779	3.274	3.892
γ_D [g^-a]	1B	–	3.951	2.882	4.579	5.685	1.883	4.936	5.128	4.477
γ_D [g^-g^-]	1B	–	3.983	3.405	3.740	4.383	1.873	4.581	5.288	5.245
δ_D Backbone conformation										
δ_D [g^+g^+]	–	2E	3.553	3.441	3.690	3.962	4.743	3.406	2.164	5.245
δ_D [g^+a]	–	2D	3.578	2.944	4.600	5.670	4.726	1.906	3.890	4.340
δ_D [g^+g^-]	–	2E	3.474	4.788	3.069	4.419	4.754	3.243	2.080	3.323
δ_D [aa]	–	2F	3.413	5.549	4.671	4.763	4.565	4.970	5.095	1.698
δ_D [s^-g^+]	–	–	3.220	4.788	5.583	5.647	4.707	3.612	4.295	4.649
δ_D [g^-s]	–	2F	3.502	4.751	4.351	4.694	4.933	4.680	5.000	1.671
α_D Backbone conformation										
α_D [g^+g^+]	–	2C	4.389	3.639	4.604	1.783	3.105	5.414	4.983	3.021
α_D [g^+g^-]	–	–	4.390	4.766	3.293	4.855	3.013	5.487	5.060	3.332
α_D [ag$^-$]	–	2C	4.391	4.793	4.995	1.668	3.116	5.998	5.045	4.492
α_D [g^-a]	–	–	4.393	2.548	4.314	4.796	3.159	4.947	6.205	4.789
ε_D Backbone conformation										
ε_D [g^+g^-]	–	2D	3.293	4.935	3.879	5.114	3.021	2.067	3.659	3.080
ε_D [aa]	–	2D	2.957	4.718	5.604	5.756	4.782	1.983	3.696	4.515
ε_D [g^-a]	–	–	3.163	3.447	4.701	5.752	4.815	4.178	4.928	3.876

Table 10
The relative distances of potential hydrogen bonds of *N*-acetyl-L-aspartic acid *N′*-methylamide in its *endo* form for all its stable backbone (γ_L, β_L, δ_L, α_L, γ_D, δ_D, α_D, and ε_D) conformations computed at the RHF/6-31G(d) level of theory. No conformers were found for the ε_L backbone and hence no hydrogen bond distances for the ε_L backbone could be tabulated

Final conform.	Interaction type			Distance (Å)						
BB [$\chi_1\chi_2$]	SC/SC	BB/BB	SC/BB	O17–H19	H9–O17	H9–O18	H9–O5	H6–O10	H6–O17	H6–O18
γ_L Backbone conformation										
γ_L [g^+s^+]	1	2B	3A	2.263	2.125	3.956	3.550	2.182	4.931	5.842
γ_L [g^+g^-]	1	2B	3B	2.260	4.028	2.166	3.505	2.206	5.854	4.906
γ_L [*as*]	1	2B	–	2.270	4.868	4.676	3.486	2.220	5.723	4.182
γ_L [*aa*]	1	2B	–	2.271	4.739	4.872	3.391	2.285	4.146	5.740
γ_L [g^-s^+]	1	2B	–	2.266	3.868	2.898	3.497	2.196	5.222	5.764
γ_L [g^-a]	1	2B	–	2.268	3.430	3.954	3.547	2.186	4.922	6.156
γ_L [g^-g^-]	1	2B	–	2.272	2.634	3.838	3.643	2.144	5.645	5.325
γ_L [g^-g^-]	1	2B	–	2.272	2.619	3.847	3.656	2.143	5.632	5.341
β_L Backbone conformation										
β_L [g^+s^+]	1	2A	–	2.269	2.811	3.997	2.345	4.777	5.321	4.561
β_L [g^+a]	1	2A	–	2.269	3.059	4.606	2.188	5.033	3.866	4.433
β_L [ag^+]	1	2A	–	2.256	5.319	4.924	2.181	4.917	3.677	2.391
β_L [*aa*]	1	2A	3C	2.264	4.955	5.442	2.136	4.988	2.123	3.929
δ_L Backbone conformation										
δ_L [g^+s]	1	–	–	2.256	4.149	2.303	3.753	3.701	5.710	4.111
δ_L [g^+a]	1	–	3A	2.266	2.271	4.062	3.777	3.723	4.058	5.678
δ_L [ag^+]	1	–	–	2.268	5.108	4.825	3.642	3.822	5.880	4.800
δ_L [g^-g^+]	1	–	–	2.257	4.514	3.147	3.822	3.691	5.827	5.314
δ_L [g^-s^-]	1	–	–	2.275	3.112	4.326	3.868	3.714	5.361	5.680
α_L Backbone conformation										
α_L [g^-s^-]	1		3A	2.272	2.293	3.826	4.324	3.045	4.965	5.791
γ_D Backbone conformation										
γ_D [ag^+]	1	2B	–	2.275	5.469	4.562	3.871	2.052	4.316	4.997
γ_D [*aa*]	1	2B	–	2.269	4.732	5.568	3.361	2.232	4.047	4.166
γ_D [g^-a]	1	2B	–	2.270	2.836	4.534	4.062	1.998	5.084	5.350
γ_D [g^-g^-]	1	2B	–	2.262	4.150	3.345	3.932	2.000	4.971	5.185
δ_D Backbone conformation										
δ_D [g^+s]	1	–	–	2.254	5.285	4.014	3.852	3.863	4.858	2.833
δ_D [g^+g^+]	1	–	–	2.245	4.455	3.520	3.654	4.759	4.253	2.369
δ_D [g^+a]	1	–	3C	2.259	2.966	4.579	3.672	4.876	2.080	4.041
δ_D [g^+g^-]	1	–	3D	2.236	4.755	3.001	3.630	4.790	3.641	2.273
δ_D [ag^+]	1	–	–	2.277	5.260	5.083	3.508	4.658	4.068	4.879
δ_D [as^-]	1	–	–	2.272	5.263	5.075	3.502	4.644	4.991	3.834
δ_D [g^-s^+]	1	–	–	2.273	4.925	3.965	3.530	4.919	5.193	4.491
δ_D [g^-g^-]	1	–	–	2.290	3.947	4.673	3.605	4.969	4.541	5.118
α_D Backbone conformation										
α_D [g^+s^+]	1	–	–	2.271	3.329	4.573	4.394	2.815	5.132	5.109
α_D [g^+g^-]	1	–	–	2.254	4.753	3.390	4.393	2.792	5.247	5.026
α_D [ag^+]	1	–	–	2.262	5.373	4.411	4.370	3.064	5.885	4.969
α_D [*aa*]	1	–	–	2.266	4.416	5.353	4.366	3.149	5.027	5.911
α_D [g^-a]	1	–	–	2.264	2.538	4.257	4.378	3.005	5.063	6.183
α_D [g^-g^-]	1	–	–	2.253	3.871	2.943	4.377	2.967	5.912	5.160

(*continued on next page*)

Table 10 (*continued*)

Final conform.	Interaction type			Distance (Å)						
BB [$\chi_1\chi_2$]	SC/SC	BB/BB	SC/BB	O17–H19	H9–O17	H9–O18	H9–O5	H6–O10	H6–O17	H6–O18
ε_D Backbone conformation										
ε_D [g^+g^+]	1	–	3D	2.277	4.155	4.870	3.134	3.109	3.865	2.123
ε_D [g^+s^-]	1	–	3C	2.270	5.021	4.343	2.968	3.322	2.071	3.785
ε_D [s^-a]	1	–	3C	2.262	4.739	5.502	2.774	4.732	2.100	3.765
ε_D [s^-g^-]	1	–	3D	2.259	5.102	4.811	2.744	4.429	3.999	2.130

Table 11
The relative distances of potential hydrogen bonds of *N*-acetyl-L-aspartic acid *N'*-methylamide in its *exo* form for all its stable backbone (γ_L, β_L, δ_L, ε_L, γ_D, δ_D, α_D, and ε_D) conformations computed at the RHF/6-31G(d) level of theory. No conformers were found for the α_L backbone and hence no hydrogen bond distances for the α_L backbone could be tabulated

Final conform.	Interaction type		Distance (Å)							
BB [$\chi_1\chi_2$]	BB/BB	SC/BB	H9–O5	H9–O17	H9–O18	H19–O5	H6–O10	H6–O17	H6–O18	H19–O10
γ_L Backbone conformation										
γ_L [g^+g^+]	1B	2C	3.837	2.346	3.447	1.884	2.056	5.493	5.155	5.589
γ_L [ag^-]	1B	2C	3.623	4.773	4.777	1.874	2.118	5.479	4.851	5.545
γ_L [g^-a]	1B	–	3.754	2.819	3.945	4.631	2.114	5.023	6.220	6.358
γ_L [g^-s^-]	1B	–	3.764	2.383	3.840	4.744	2.096	5.518	5.604	5.255
β Backbone conformation										
β_L [g^+g^+]	1A	–	2.219	3.568	3.907	3.199	4.952	4.974	3.672	5.442
β_L [g^+a]	1A	–	2.125	3.360	4.503	5.614	5.163	3.229	4.374	4.243
β_L [aa]	1A	2D	2.117	4.939	5.521	5.538	5.021	2.083	3.916	4.727
β_L [s^-g^+]	1A	2F	2.153	5.341	4.836	5.207	5.016	2.467	3.838	1.947
δ_L Backbone conformation										
δ_L [g^+a]	–	2A	3.793	2.223	4.073	3.818	3.753	4.030	5.617	6.016
δ_L [s^-g^+]	–	2F	3.505	5.421	4.701	4.741	4.155	5.801	5.148	1.892
δ_L [g^-g^-]	–	2F	3.854	4.104	3.843	4.613	3.713	6.024	5.310	2.069
ε_L Backbone conformation										
ε_L [g^-g^+]	–	–	2.476	4.694	3.345	4.445	3.806	4.957	5.093	3.501
γ_D Backbone conformation										
γ_D [g^+g^+]	1B	–	3.933	4.266	4.826	3.654	1.918	4.058	2.795	3.161
γ_D [s^+g^-]	–	2F	3.694	5.435	4.859	4.661	2.319	3.628	2.663	1.815
γ_D [ag^+]	1B	–	3.743	5.444	4.828	3.885	2.090	3.973	4.969	5.318
γ_D [ag^+]	1B	–	3.760	5.447	4.822	3.850	2.082	3.992	4.972	5.321
γ_D [aa]	1B	–	3.353	4.707	5.619	5.548	2.232	4.088	4.268	4.626
γ_D [ag^-]	1B	–	3.553	5.035	5.236	3.299	2.074	4.836	3.444	4.151
γ_D [g^-a]	1B	–	4.135	2.762	4.471	5.224	2.024	5.112	5.527	4.602
δ_D Backbone conformation										
δ_D [g^+a]	–	2D	3.675	2.967	4.580	5.467	4.855	2.069	4.054	4.580
δ_D [g^+a]	–	2D	3.685	2.928	4.559	5.463	4.857	2.071	4.044	4.600
δ_D [g^+g^-]	–	–	3.503	4.782	3.271	4.551	4.810	3.322	2.430	3.407
δ_D [s^-g^+]	–	2F	3.458	5.539	4.772	4.699	4.644	4.987	5.226	1.866
δ_D [g^-s]	–	2F	3.551	4.800	4.233	4.611	5.035	4.693	5.036	1.862

Table 11 (*continued*)

Final conform.	Interaction type		Distance (Å)							
BB [$\chi_1\chi_2$]	BB/BB	SC/BB	H9–O5	H9–O17	H9–O18	H19–O5	H6–O10	H6–O17	H6–O18	H19–O10
α_D Backbone conformation										
α_D [g^+g^+]	–	2C	4.367	3.643	4.557	1.942	2.993	5.462	4.988	3.225
α_D [g^+g^-]	–	–	4.377	4.809	3.585	4.868	2.706	5.191	5.122	3.389
α_D [s^-g^-]	–	2C	4.377	4.539	4.970	1.823	3.067	5.955	5.177	4.657
α_D [g^-a]	–	–	4.376	2.520	4.250	4.728	3.042	5.047	6.217	4.814
ε_D Backbone conformation										
ε_D [s^+g^-]	–	2F	2.799	5.496	4.771	3.584	4.631	2.408	3.291	1.766
ε_D [s^-a]	–	2D	2.777	4.707	5.591	5.775	4.791	2.112	3.717	4.503
ε_D [g^-s^+]	–	2F	2.807	4.315	4.130	4.781	5.021	4.387	5.224	1.958

Table 12
The relative distances of potential hydrogen bonds of *N*-acetyl-L-aspartic acid *N*′-methylamide in its *endo* form for all its stable backbone (γ_L, β_L, δ_L, α_L, γ_D, δ_D, α_D, and ε_D) conformations computed at the B3LYP/6-31G(d) level of theory. No conformers were found for the ε_L backbone and hence no hydrogen bond distances for the ε_L backbone could be tabulated

Final conform.	Interaction type			Distance (Å)						
BB [$\chi_1\chi_2$]	SC/SC	BB/BB	SC/BB	O17–H19	H9–O17	H9–O18	H9–O5	H6–O10	H6–O17	H6–018
γ_L Backbone conformation										
γ_L [g^+s^+]	1	2B	3A	2.274	2.056	3.924	3.565	2.030	4.945	5.833
γ_L [g^+g^-]	1	2B	3B	2.276	4.026	2.109	3.554	2.053	5.858	4.893
γ_L [as]	1	2B	–	2.282	4.911	4.701	3.632	2.044	5.761	4.260
γ_L [aa]	1	2B	–	2.283	4.774	4.895	3.588	2.066	4.277	5.797
γ_L [g^-s^+]	1	2B	–	2.281	3.778	2.419	3.747	1.986	5.506	5.566
γ_L [g^-a]	1	2B	–	2.280	3.638	3.859	3.720	2.004	4.922	6.155
γ_L [g^-s^-]	1	2B	3A	2.275	2.097	3.807	3.834	1.952	5.416	5.873
β_L Backbone conformation										
β_L [g^+s^+]	1	2A	–	2.281	2.906	4.064	2.261	4.891	5.233	4.343
β_L [g^+a][a,b]	1	2A	–	2.282	3.161	4.713	2.117	5.099	3.719	4.322
β_L [ag^+]	1	2A	3D	2.266	5.406	4.935	2.120	4.999	3.587	2.196
β_L [aa]	1	2A	3C	2.270	4.988	5.509	2.074	5.040	1.984	3.864
δ_L Backbone conformation										
δ_L [g^+s]	1	–	3B	2.270	4.129	2.215	3.832	3.543	5.674	4.065
δ_L [g^+a][a,b]	1	–	3A	2.275	2.179	4.031	3.850	3.588	4.038	5.649
δ_L [ag^+]	1	–	–	2.282	5.107	4.838	3.784	3.617	5.887	4.899
δ_L [g^-g^+]	1	–	–	2.271	4.514	3.111	3.921	3.649	5.828	5.281
δ_L [g^-s^-]	1	–	–	2.286	2.950	4.333	3.978	3.641	5.245	5.773
α_L Backbone conformation										
α_L [g^-s^-][a,b]	1	–	3A	2.281	2.121	3.843	4.397	3.014	4.822	5.831
γ_D Backbone conformation										
γ_D [ag^+]	1	2B	–	2.288	5.505	4.611	3.941	1.927	4.230	4.972
γ_D [as^-][a,b]	1	2B	–	2.282	4.558	5.581	3.754	1.957	4.856	4.483
γ_D [g^-a]	1	2B	–	2.282	2.787	4.517	4.096	1.873	4.856	5.279
γ_D [g^-g^-]	1	2B	–	2.271	4.307	3.193	3.992	1.894	4.856	5.111

(*continued on next page*)

Table 12 (*continued*)

Final conform.	Interaction type			Distance (Å)						
BB [$\chi_1\chi_2$]	SC/SC	BB/BB	SC/BB	O17–H19	H9–O17	H9–O18	H9–O5	H6–O10	H6–O17	H6–018
δ_D Backbone conformation										
δ_D [g^+g^+][a,b]	1	–	3D	2.250	4.467	3.351	3.623	4.853	4.126	2.078
δ_D [g^+a][a,b]	1	–	3C	2.265	3.075	4.664	3.624	4.874	1.961	3.961
δ_D [g^+g^-]	1	–	3D	2.247	4.876	3.084	3.608	4.760	3.630	2.151
δ_D [ag^+]	1	–	–	2.288	5.341	5.097	3.554	4.602	4.205	4.952
δ_D [as^-]	1	–	–	2.282	5.154	5.363	3.573	4.532	5.105	4.349
δ_D [g^-g^-][a,b]	1	–	–	2.303	4.032	4.740	3.570	5.004	4.531	5.101
α_D Backbone conformation										
α_D [g^+s^+]	1	–	–	2.283	3.329	4.602	4.456	2.800	5.109	5.092
α_D [g^+g^-]	1	–	–	2.268	4.793	3.475	4.453	2.713	5.081	4.996
α_D [ag^+]	1	–	–	2.274	5.453	4.439	4.428	3.070	5.888	4.999
α_D [as^-]	1	–	–	2.278	4.445	5.421	4.424	3.143	5.063	5.913
α_D [g^-s]	1	–	–	2.261	4.199	2.721	4.438	2.974	6.132	5.031
α_D [g^-a]	1	–	–	2.275	2.528	4.295	4.437	2.993	5.048	6.198
ε_D Backbone conformation										
ε_D [g^+g^+]	1	–	3D	2.293	4.062	4.881	3.321	2.932	3.782	2.030
ε_D [g^+s^-]	1	–	3C	2.279	5.051	4.461	2.990	3.281	1.942	3.740
ε_D [s^-a]	1	–	3C	2.268	4.856	5.512	2.783	4.718	1.966	3.800
ε_D [s^-g-]	1	–	3D	2.273	5.203	4.879	2.763	4.444	3.960	2.025

[a] After 200 iterations under B3LYP/6-31G(d) at (TIGHT, Z-MATRIX), the force has converged, but the displacement did not converge completely.

[b] This result was obtained from an optimization fully converged under regular B3LYP/6-31G(d) at (Z-MATRIX).

Table 13

The relative distances of potential hydrogen bonds of *N*-acetyl-L-aspartic acid *N'*-methylamide in its *exo* form for all its stable backbone (γ_L, β_L, δ_L, ε_L, γ_D, δ_D, α_D, and ε_D) conformations computed at the B3LYP/6-31G(d) level of theory. No conformers were found for the α_L backbone and hence no hydrogen bond distances for the α_L backbone could be tabulated

Final conform.	Interaction type		Distance (Å)							
BB [$\chi_1\chi_2$]	BB/BB	SC/BB	H9–O5	H9–O17	H9–O18	H19–O5	H6–O10	H6–O17	H6–O18	H19–O10
γ_L Backbone conformation										
γ_L [g^+g^+]	1B	2C	3.906	2.344	3.376	1.749	1.917	5.528	5.068	5.421
γ_L [g^+g^+]	1B	2C	3.899	2.342	3.371	1.748	1.916	5.515	5.065	5.430
γ_L [ag^-]	1B	2C	3.776	4.780	4.809	1.746	1.940	5.610	4.866	5.454
γ_L [g^-s^-]	1B	2A	3.880	2.044	3.796	4.863	1.929	5.381	5.973	5.902
β_L Backbone conformation										
β_L [g^+g^+][a,b]	1A	–	2.175	3.850	3.943	3.124	5.015	4.888	3.465	5.396
β_L [g^+s^-]	1A	2D, 2F	2.156	4.717	4.271	5.117	5.000	1.977	3.699	1.717
βb_L [aa]	1A	2D	2.046	4.983	5.598	5.767	5.090	1.937	3.847	4.422
β_L [s^-g^+]	1A	2F	2.133	5.371	4.819	5.168	5.023	2.434	3.829	1.827
δ_L Backbone conformation										
δ_L [s^-g^+][a,b]	–	2F	3.532	5.467	4.663	4.779	4.121	5.934	5.150	1.773
δ_L [g^-s]	–	2F	3.844	4.562	4.047	4.677	3.770	6.205	5.302	1.841

Table 13 (*continued*)

Final conform.	Interaction type		Distance (Å)							
BB [$\chi_1\chi_2$]	BB/BB	SC/BB	H9–O5	H9–O17	H9–O18	H19–O5	H6–O10	H6–O17	H6–O18	H19–O10
ε_L Backbone conformation										
ε_L [g^-g^+]	1A	–	2.297	4.853	3.402	4.295	4.115	5.002	5.195	3.253
γ_D Backbone conformation										
γ_D [g^+g^+]	1B	–	4.044	4.364	4.806	3.506	1.810	4.106	2.731	3.086
γ_D [s^+g^-]	1B	2F	3.776	5.537	4.829	4.588	2.225	3.746	2.565	1.713
γ_D [*aa*]	1B	–	3.677	4.549	5.637	5.103	1.975	4.773	4.615	4.654
γ_D [ag^-]	1B	–	3.678	5.186	5.266	3.181	1.934	4.846	3.378	3.970
γ_D [s^-g^-]	1B	2C	4.214	4.995	4.763	1.716	1.896	5.732	4.943	5.059
γ_D [g^-a]	1B	–	4.140	2.740	4.465	5.415	1.876	5.060	5.391	4.661
δ_D Backbone conformation										
δ_D [g^+a][a,b]	–	2D	3.620	3.076	4.641	5.666	4.848	1.942	3.960	4.337
δ_D [g^+g^-][a,b]	–	2E	3.497	4.848	3.182	4.451	4.853	3.305	2.248	3.376
δ_D [s^-g^+]	–	2F	3.450	5.599	4.753	4.740	4.693	5.019	5.204	1.745
δ_D [g^-s][a,b]	–	2F	3.425	5.149	4.371	4.654	5.131	4.703	5.027	1.717
α_D Backbone conformation										
α_D [g^+g^+]	–	2C	4.422	3.685	4.547	1.812	3.005	5.525	4.956	3.173
α_D [g^+g^-]	–	–	4.430	4.908	3.525	4.794	2.764	5.396	5.086	3.222
α_D [s^-g^-]	–	2C	4.438	4.677	4.988	1.711	3.000	6.042	5.158	4.608
α_D [g^-a]	–	–	4.435	2.514	4.288	4.733	3.024	5.034	6.237	4.866
ε_D Backbone conformation										
ε_D [*aa*]	–	2D	2.792	4.800	5.647	5.834	4.824	1.986	3.740	4.491
ε_D [g^-g^+]	–	2F	2.727	4.660	4.241	4.776	5.273	4.242	5.246	1.760

[a] After 200 iterations under B3LYP/6-31G(d) at (TIGHT, Z-MATRIX), the force has converged, but the displacement did not converge completely.

[b] This result was obtained from an optimization fully converged under regular B3LYP/6-31G(d) at (Z-MATRIX).

at lower levels (i.e. at RHF/3-21G) may still be significant. If this is the case, then ab initio computational studies can be carried out with less time and less energy in the future. This way, computations on amino acids, peptides, molecules and proteins can be carried out with even higher efficiency, enhancing research development in pharmacological and biomedical studies.

6. Conclusions

Using quantum chemical calculations at the RHF/3-21G, RHF/6-31G(d), and B3LYP/6-31G(d) ab initio levels, the conformation preference for both the *endo* and the *exo* forms of *N*-acetyl-L-aspartic acid *N*′-methylamide were determined. At RHF/3-21G, a total of 49 stable conformers was found for the *endo* form and a total of 37 stable conformers for the *exo* form. At RHF/6-31G(d), a total of 40 stable conformers was found for the *endo* form and a total of 31 stable conformers for the *exo* form. And lastly at B3LYP/6-31G(d), a total of 37 stable conformers for the *endo* form and a total of 27 stable conformers for the *exo* form were found. All relative energies, including the stabilization exerted by the sidechain on the backbone, were calculated for all stable conformers.

Various SC/SC (HO···O=C), BB/BB (N–H···O=C) and BB/SC (N–H···O=C; N–H···OH)

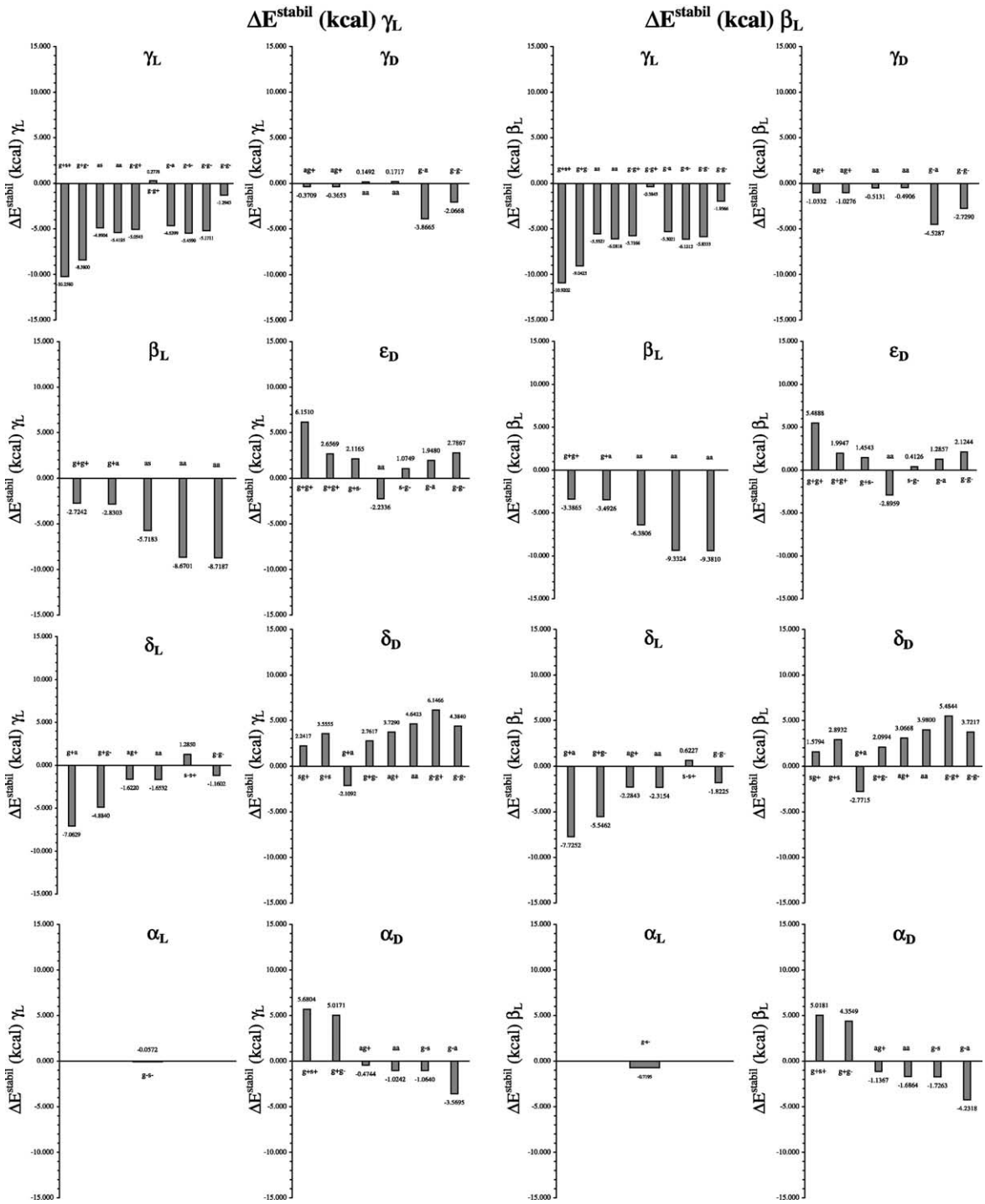

Fig. 20. Computed stabilization energies at RHF/3-21G for the *endo* form of *N*-acetyl-L-aspartic acid *N'*-methylamide with respect to the γ_L and β_L backbone conformation of *N*-acetyl-glycine-*N'*-methylamide.

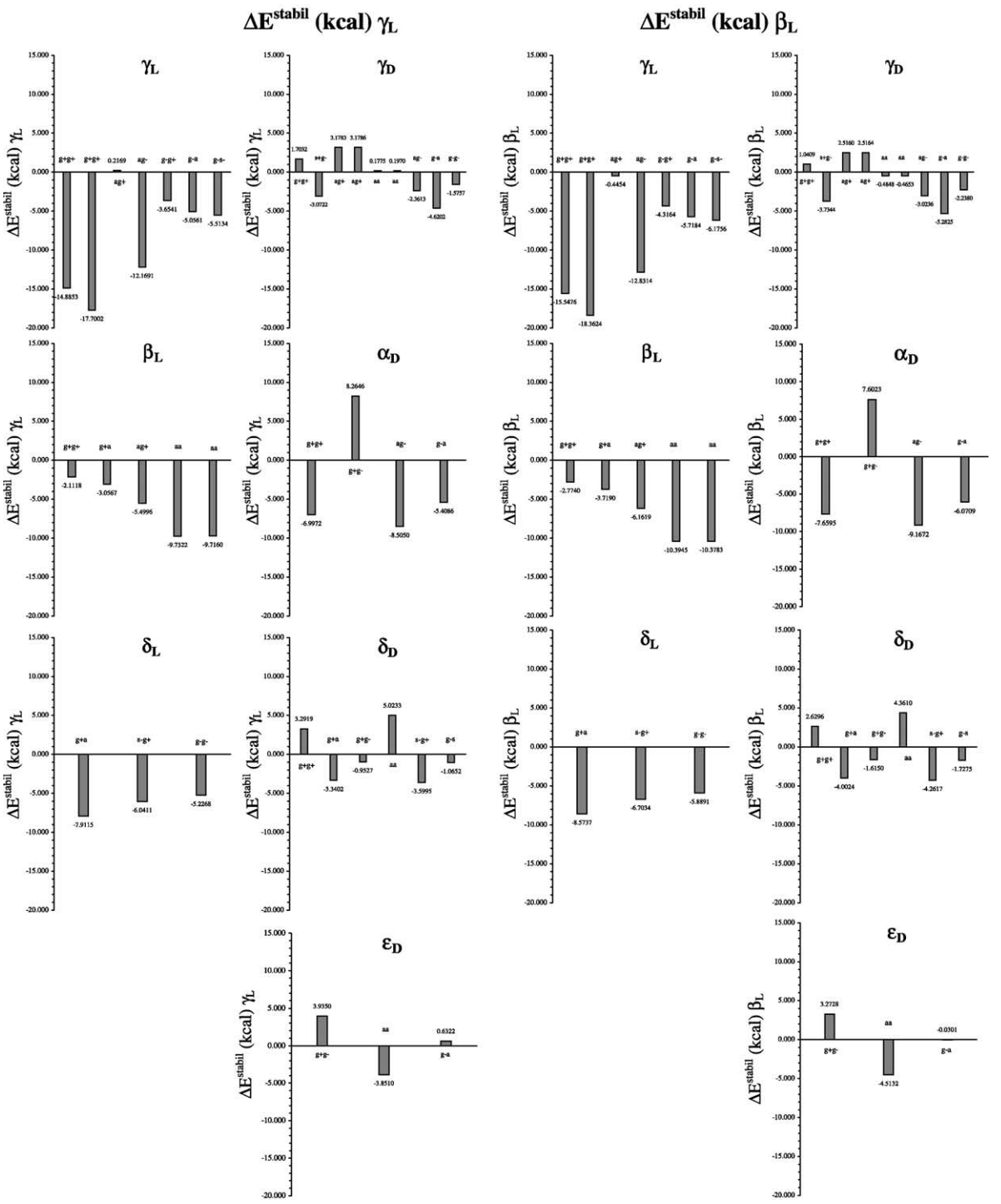

Fig. 21. Computed stabilization energies at RHF/3-21G for the *exo* form of *N*-acetyl-L-aspartic acid *N*′-methylamide with respect to the γ_L and β_L backbone conformation of *N*-acetyl-glycine-*N*′-methylamide.

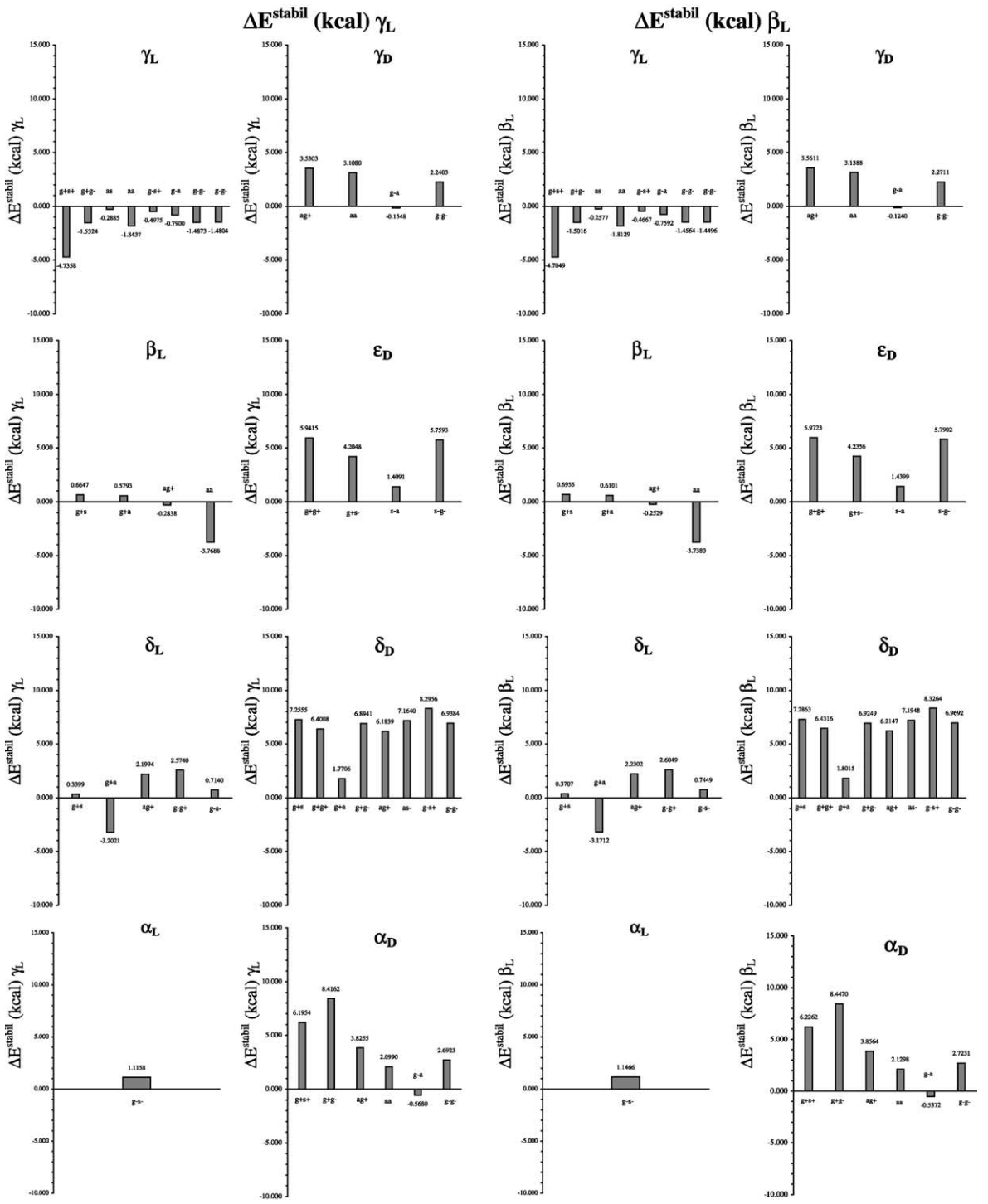

Fig. 22. Computed stabilization energies at RHF/6-31G(d) for the *endo* form of *N*-acetyl-L-aspartic acid *N'*-methylamide with respect to the γ_L and β_L backbone conformation of *N*-acetyl-glycine-*N'*-methylamide.

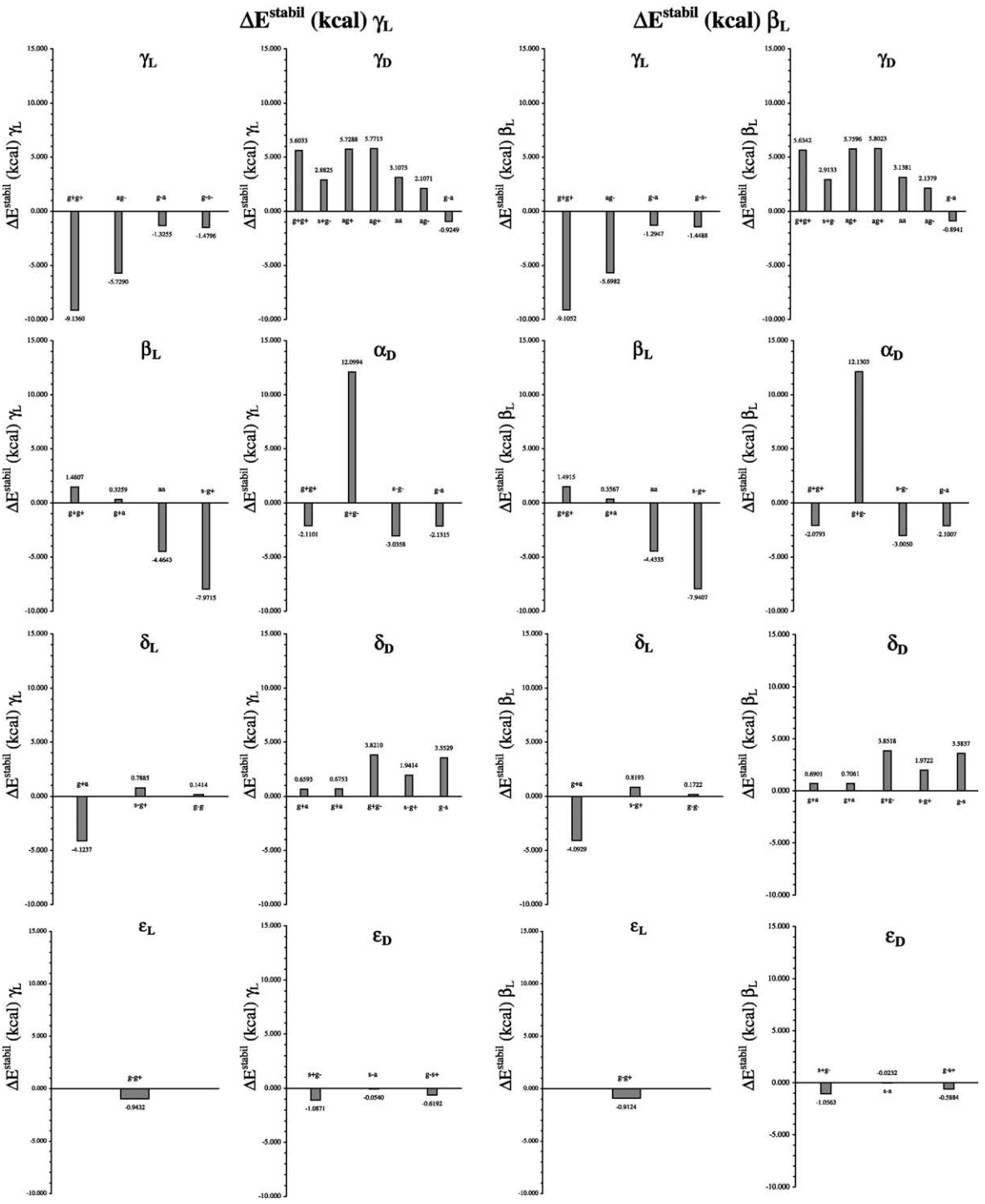

Fig. 23. Computed stabilization energies at RHF/6-31G(d) for the *exo* form of *N*-acetyl-L-aspartic acid *N'*-methylamide with respect to the γ_L and β_L backbone conformation of *N*-acetyl-glycine-*N'*-methylamide.

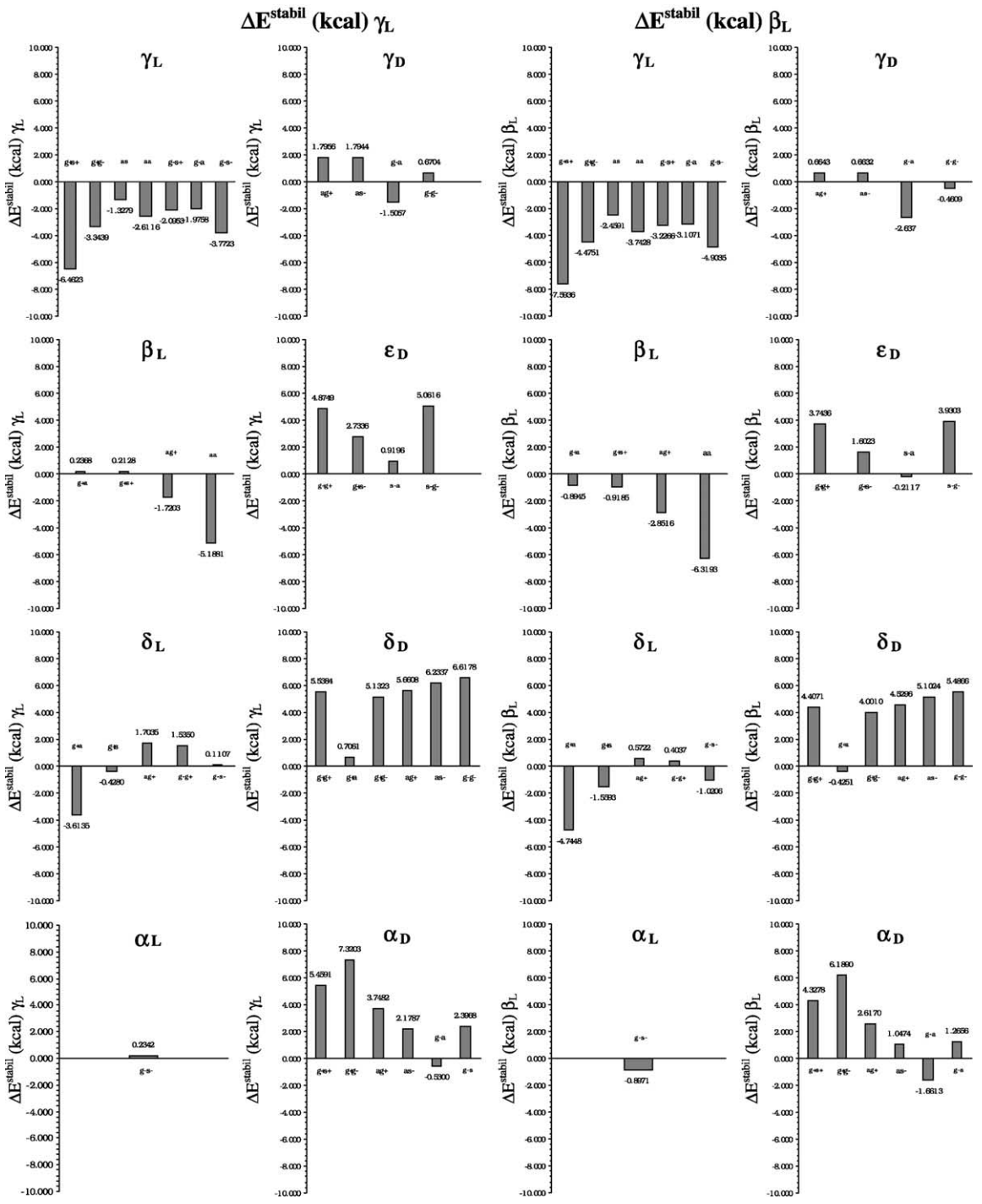

Fig. 24. Computed stabilization energies at B3LYP/6-31G(d) for the *endo* form of *N*-acetyl-L-aspartic acid *N'*-methylamide with respect to the γ_L and β_L backbone conformation of *N*-acetyl-glycine-*N'*-methylamide.

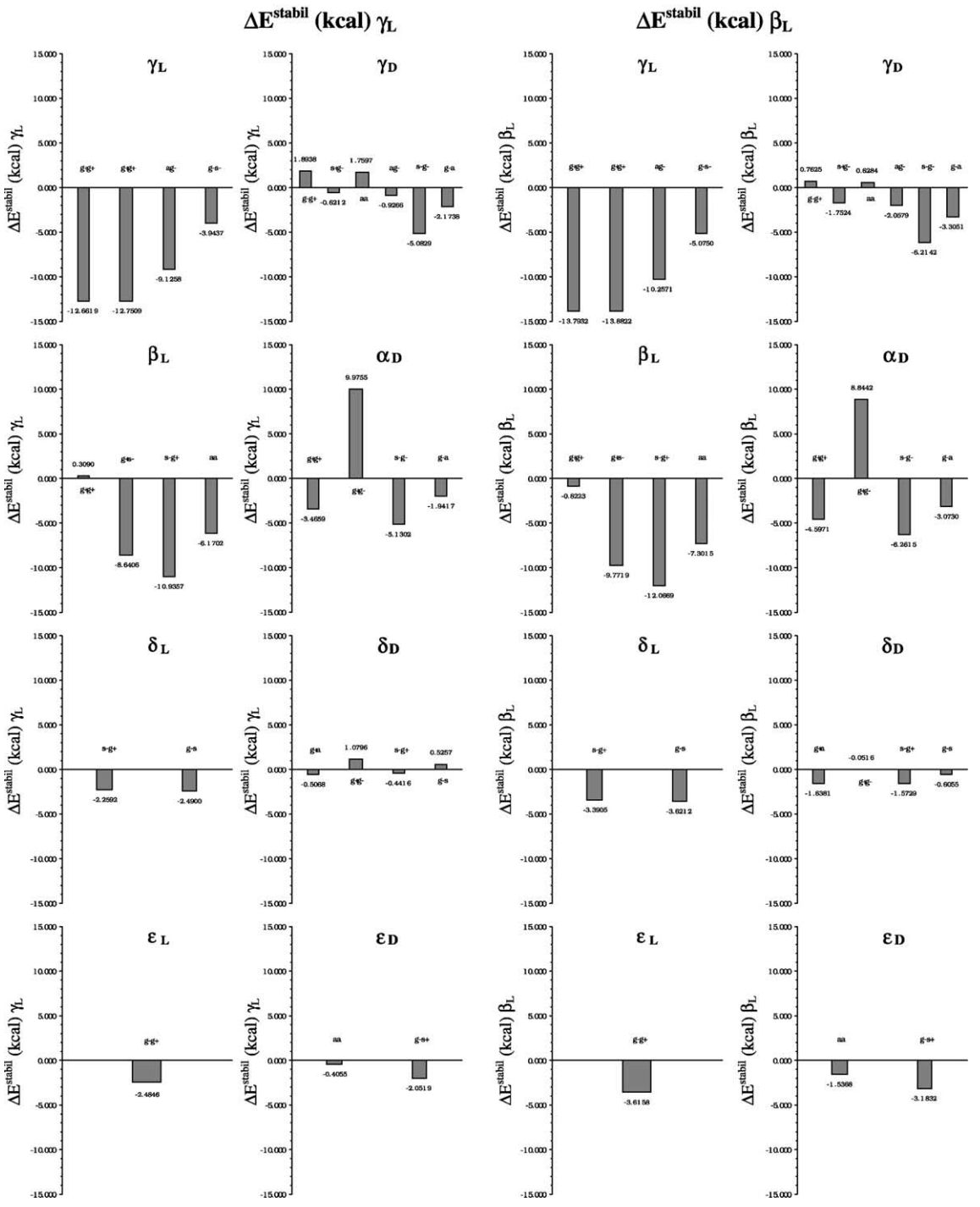

Fig. 25. Computed stabilization energies at B3LYP/6-31G(d) for the *exo* form of *N*-acetyl-L-aspartic acid *N*′-methylamide with respect to the γ_L and β_L backbone conformation of *N*-acetyl-glycine-*N*′-methylamide.

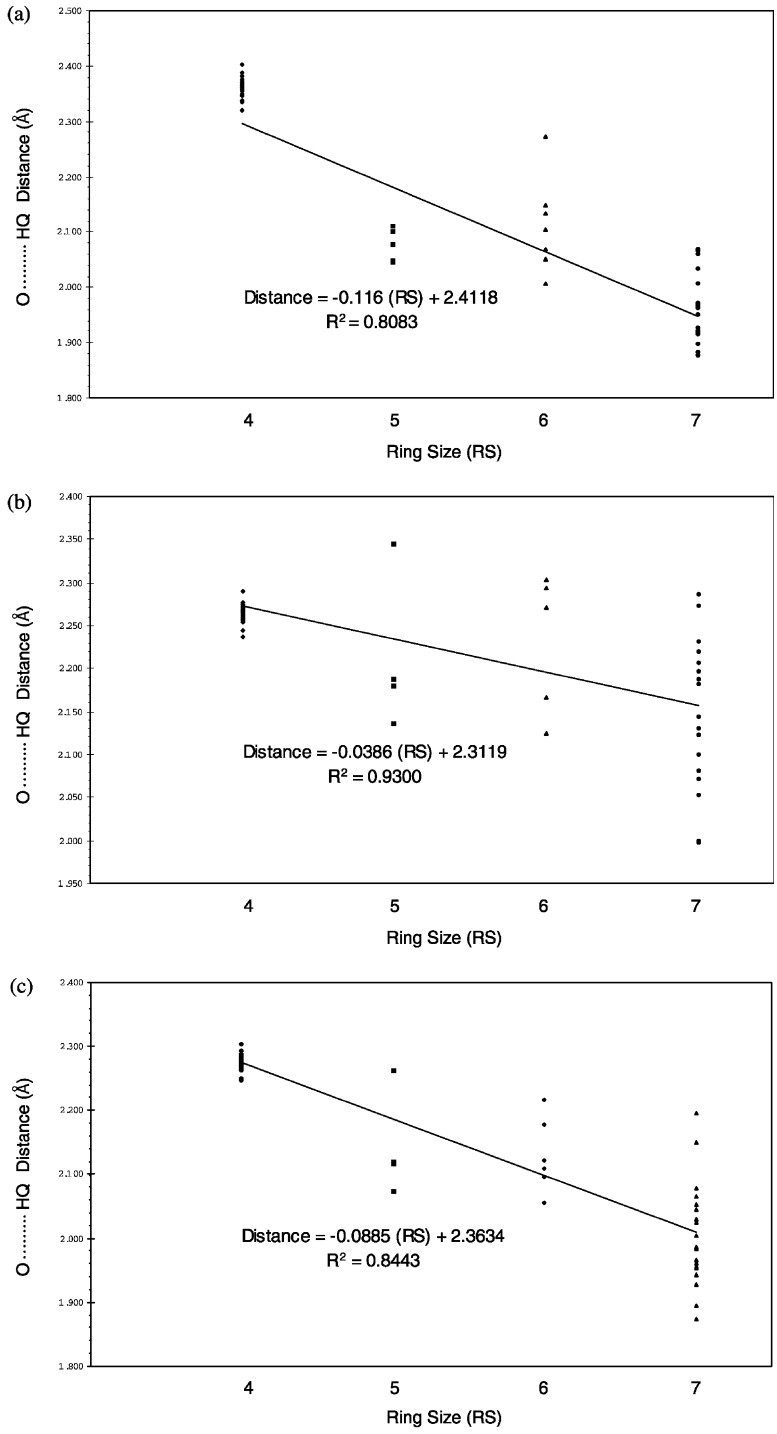

Fig. 26. Trends illustrating the correlation between hydrogen-bonded distance and ring size (RS) for the *endo* form of *N*-acetyl-L-aspartic acid *N'*-methylamide at (a) RHF/3-21G; (b) RHF/6-31G(d); and (c) B3LYP/6-31G(d) levels of theory. Note: HQ may be H–N or H–O.

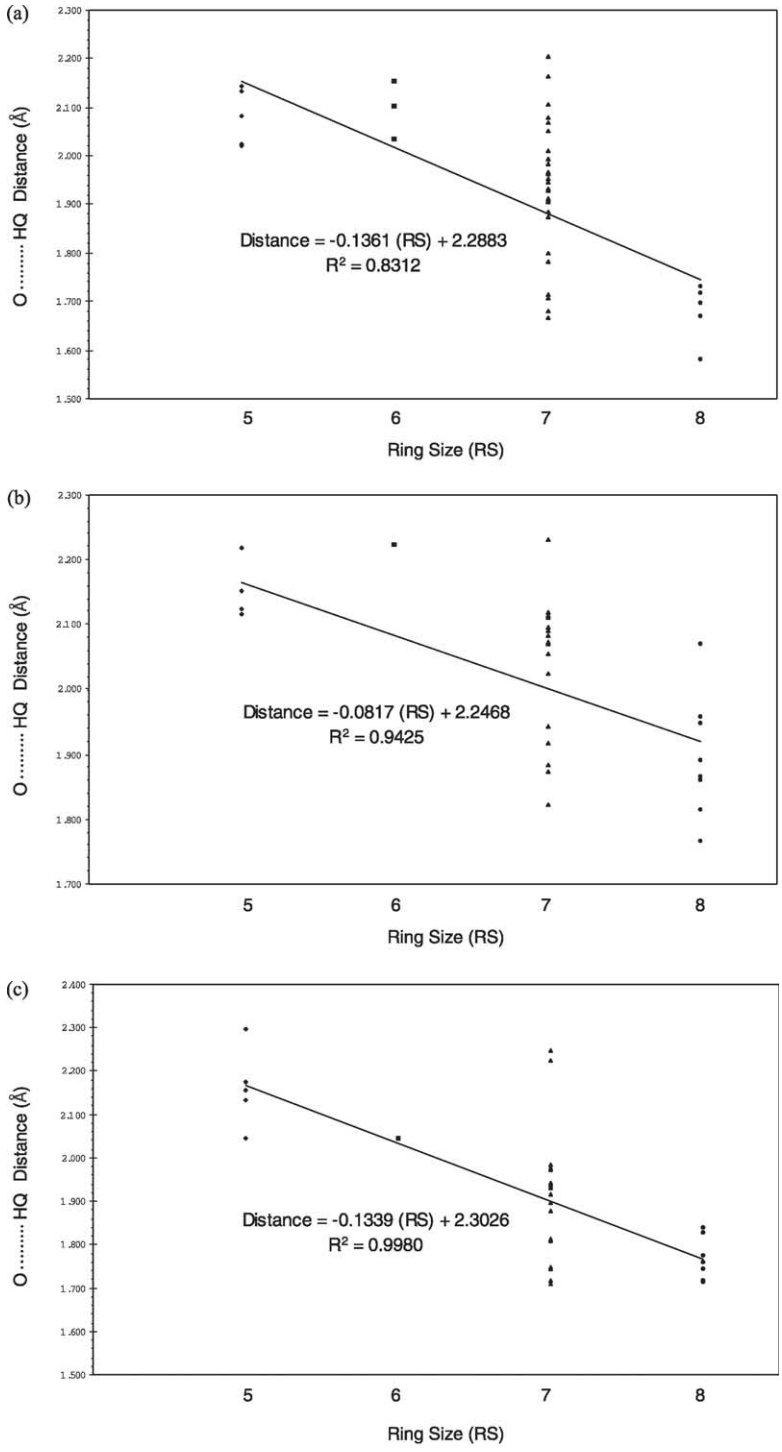

Fig. 27. Trends illustrating the correlation between hydrogen-bonded distance and ring size (RS) for the *exo* form of *N*-acetyl-L-aspartic acid *N'*-methylamide at (a) RHF/3-21G; (b) RHF/6-31G(d); and (c) B3LYP/6-31G(d) levels of theory. Note: HQ may be H–N or H–O.

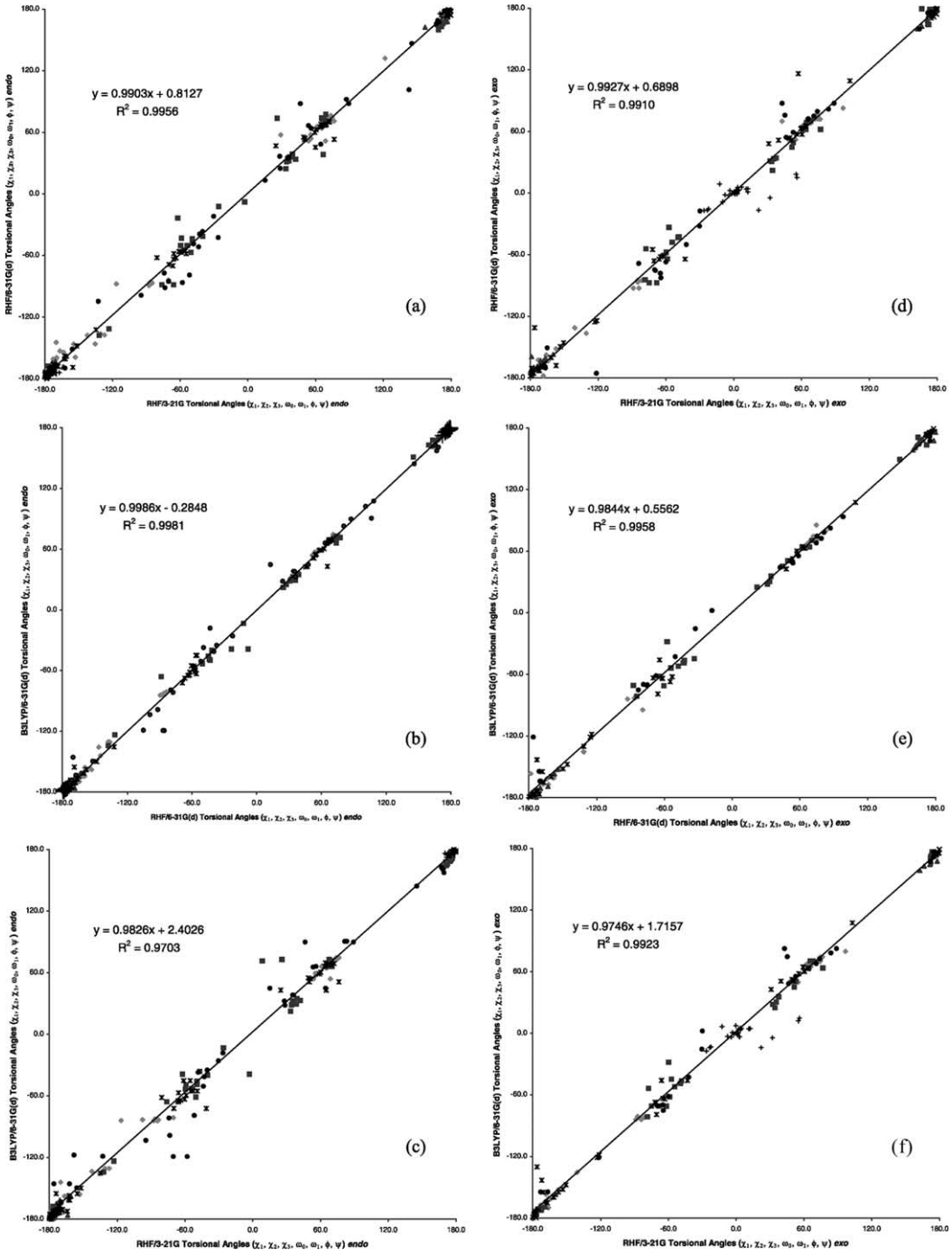

Fig. 28. A graph showing the correlation between the torsional angles (χ_1, χ_2, χ_3, ω_0, ω_1, ϕ, ψ) optimized for *N*-acetyl-L-aspartic acid *N*′-methylamide: (a) RHF/6-31G(d) vs. RHF/3-21G for the *endo* form; (b) B3LYP/6-31G(d) vs. RHF/6-31G(d) for the *endo* form; (c) B3LYP/6-31G(d) vs. RHF/3-21G for the *endo* form; (d) RHF/6-31G(d) vs. RHF/3-21G for the *exo* form; (e) B3LYP/6-31G(d) vs. RHF/6-31G(d) for the *exo* form; (f) B3LYP/6-31G(d) vs. RHF/3-21G for the *exo* form.

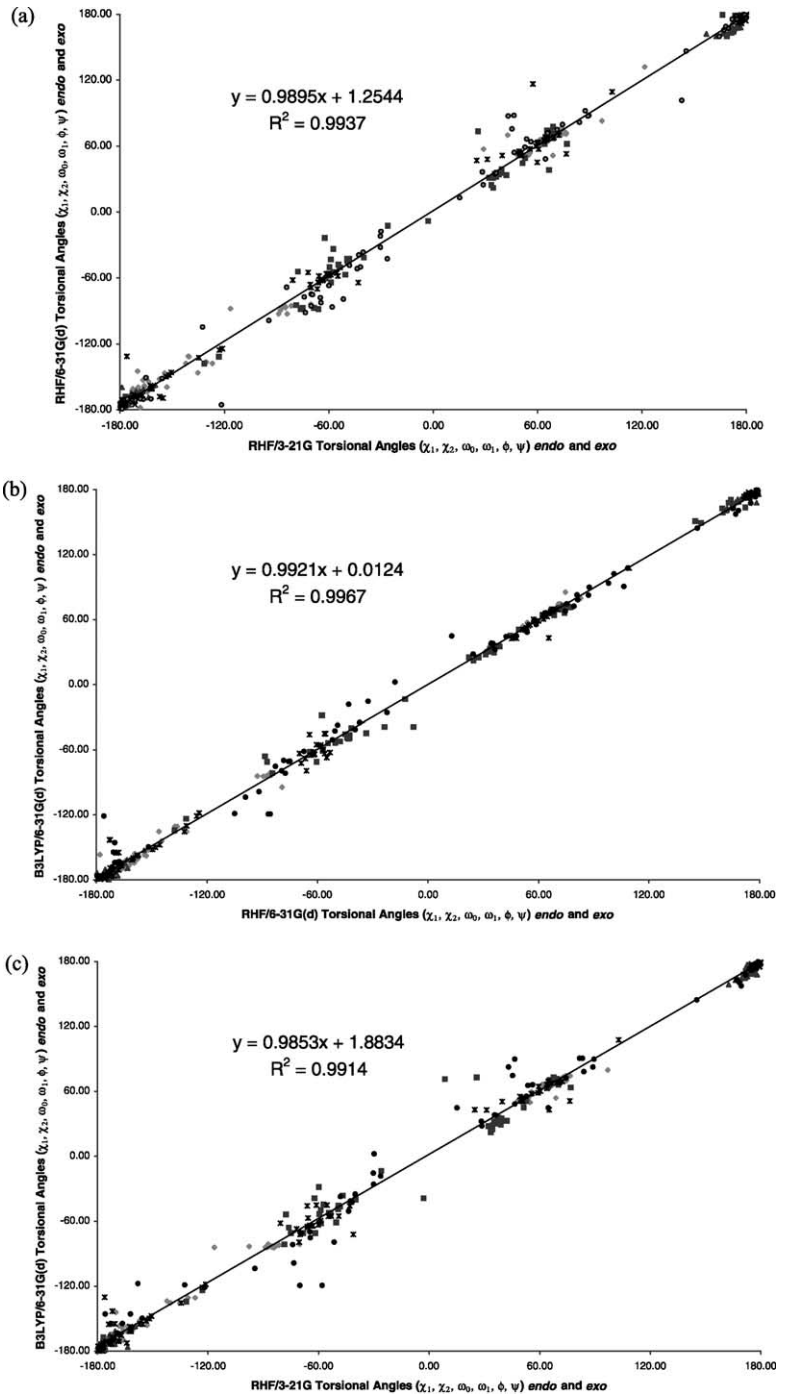

Fig. 29. A graph showing the correlation between the torsional angles (χ_1, χ_2, ω_0, ω_1, ϕ, ψ) optimized at the different levels of theory for *N*-acetyl-L-aspartic acid *N*′-methylamide: (a) RHF/6-31(d) vs. RHF/3-21G; (b) B3LYP/6-31G(d) vs. RHF/6-31G(d); (c) B3LYP/6-31G(d) vs. RHF/3-21G. Note that the χ_3 results have been omitted in this plot and that the optimization results for both *endo* and *exo* forms of *N*-acetyl-L-aspartic acid *N*′-methylamide were combined to generate the plots.

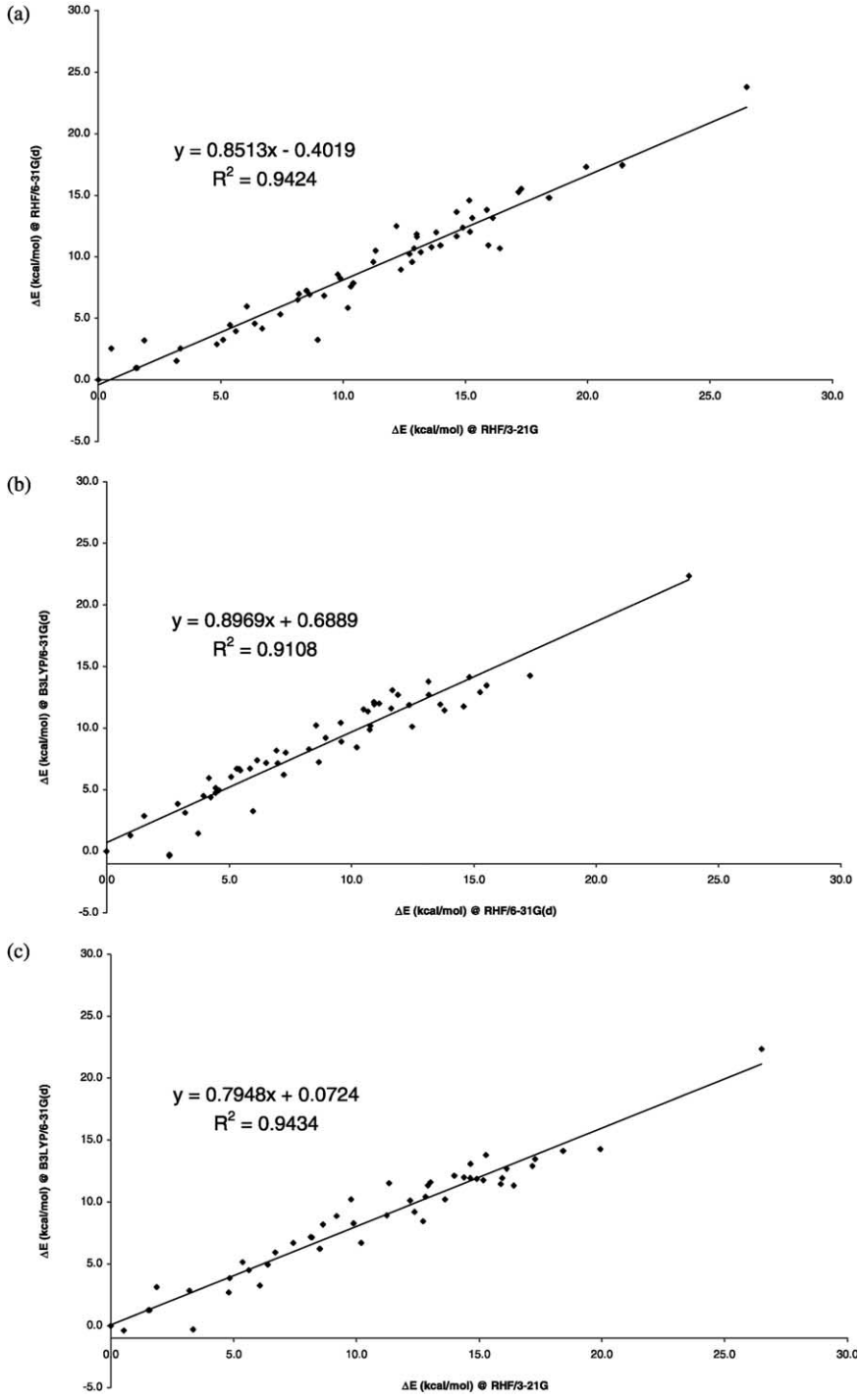

Fig. 30. A graph showing the correlation between the ΔE values (kcal/mol) optimized at the different levels of theory for *N*-acetyl-L-aspartic acid *N*′-methylamide: (a) RHF/6-31(d) vs. RHF/3-21G; (b) B3LYP/6-31G(d) vs. RHF/6-31G(d); (c) B3LYP/6-31G(d) vs. RHF/3-21G. Note that optimization results for both *endo* and *exo* forms of *N*-acetyl-L-aspartic acid *N*′-methylamide were combined to generate the plots.

were analyzed. There was no SC/SC interaction in the carboxyl group of the *exo* aspartic acid residue, indicating that the sidechain may involve with external hydrogen bonding to stabilize the amino acid or with other stabilizing forces in a larger molecule. Both internal and external hydrogen bondings are significant when the aspartyl residue participates in intra- or inter-molecular interactions, such as in the RGD tripeptide. This way, the presence or absence of these stabilizing forces may directly affect the folding pattern of a peptide segment such as the RGD moiety. In this work, the stable g^-s^- and g^-g^+ found, respectively, at the α_L and ε_L backbones may represent novel geometries in which the aspartyl residue partakes during such peptide folding. In addition, while the BB/BB interaction can be considered as an internal stabilizing factor for the *exo* forms of the aspartic acid residue, its sidechain can participate in external interactions with other substrates. This phenomenon can be applied to the docking of a specific molecule to receptors that express the aspartic acid residue on its surface.

There also exists a trend between the hydrogen bond distance and ring size for both the *endo* and *exo* forms of *N*-acetyl-L-aspartic acid *N*′-methylamide at all three levels of theory; where the shorter the hydrogen bond distance, the greater the RS. Finally, there is a remarkably high correlation between torsional angles ($R^2 = 0.9937$ for RHF/6-31G(d) versus RHF/3-21G; $R^2 = 0.9967$ for B3LYP/6-31G(d) versus RHF/6-31G(d); $R^2 = 0.9914$ for B3LYP/6-31G(d) versus RHF/3-21G) and between ΔE values ($R^2 = 0.9424$ for RHF/6-31G(d) versus RHF/3-21G; $R^2 = 0.9108$ for B3LYP/6-31G(d) versus RHF/6-31G(d); $R^2 = 0.9434$ B3LYP/6-31G(d) versus RHF/3-21G) optimized at different levels of theory, suggesting that ab initio calculations carried at lower levels, such as RHF/3-21G, are still significant.

Acknowledgements

The authors would like to express their gratitude for the generous allocation of CPU time provide by the National Cancer Institute (NCI) at the Frederick Biomedical Supercomputing Center.

References

[1] M.L. Lopez-Rodriguez, B. Vicente, X. Deupi, S. Barrondo, M. Olivella, M.J. Morcillo, B. Behamu, J.A. Ballesteros, J. Salles, L. Pardo, Mol. Pharmacol. 62 (2002) 15.
[2] M.T. Makhija, V.M. Kulkarni, J. Comput. Aid. Mol. Des. 15 (2001) 961.
[3] I. Halperin, B. Ma, H. Wolfson, R. Nussinov, Proteins 47 (2002) 409.
[4] M. Glick, D.D. Robinson, G.H. Grant, W.G. Richards, J. Am. Chem. Soc. 124 (2002) 2337.
[5] J. Zhu, H. Fan, H. Liu, Y. Shi, J. Comput. Aid. Mol. Des. 15 (2001) 979.
[6] R. Bitetti-Putzer, D. Joseph-McCarthy, J.M. Hogle, M. Karplus, J. Comput. Aid. Mol. Des. 15 (2001) 935.
[7] A.W. Ravna, O. Edvardsen, J. Mol. Graph. Model. 20 (2001) 133.
[8] O.A. Santos-Filho, R.K. Mishra, A.J. Hopfinger, J. Comput. Aid. Mol. Des. 15 (2001) 787.
[9] A. Percel, J.G. Ángyán, M. Kajtár, W. Viviani, J.L. Rivail, J.F. Marcoccia, I.G. Csizmadia, J. Am. Chem. Soc. 113 (1991) 6256.
[10] M.A. McAllister, A. Perczel, P. Császár, W. Viviani, J.L. Rivail, I.G. Csizmadia, J. Mol. Struct. (Theochem) 288 (1993) 161.
[11] M.A. McAllister, A. Perczel, P. Császár, I.G. Csizmadia, J. Mol. Struct. (Theochem) 288 (1993) 181.
[12] A. Perczel, M.A. McAllister, P. Császár, I.G. Csizmadia, Can. J. Chem. 72 (1994) 2050.
[13] M. Cheung, M.E. McGovern, T. Jin, D.C. Zhao, M.A. McAllister, A. Perczel, P. Császár, I.G. Csizmadia, J. Mol. Struct. (Theochem) 309 (1994) 151.
[14] A.M. Rodriguez, H.A. Baldoni, F. Suvire, R. Nieto-Vasquez, G. Zamarbide, R.D. Enriz, Ö. Farkas, A. Perczel, I.G. Csizmadia, J. Mol. Struct. (Theochem) 455 (1998) 275.
[15] M. Berg, S.J. Salpietro, A. Perczel, Ö. Farkas, I.G. Csizmadia, J. Mol. Struct. (Theochem) 504 (2000) 127.
[16] M.A. Zamora, H.A. Baldoni, J.A. Bombasaro, M.L. Mak, A. Perczel, Ö. Farkas, R.D. Enriz, J. Mol. Struct. (Theochem) 540 (2001) 271.
[17] M.A. Zamora, H.A. Baldoni, A.M. Rodriguez, R.D. Enriz, C.P. Sosa, A. Perczel, A. Kucsman, O. Farkas, E. Deretey, J.C. Vank, I.G. Csizmadia, Can. J. Chem. 80 (2002) 832.
[18] A. Perczel, Ö. Farkas, I.G. Csizmadia, J. Am. Chem. Soc. 117 (1995) 1653.
[19] H.A. Baldoni, G.N. Zamarbide, R.D. Enriz, E.A. Jauregui, Ö. Farkas, A. Perczel, S.J. Salpietro, I.G. Csizmadia, J. Mol. Struct. (Millennium Volume) 500 (2000) 97.
[20] Ö. Farkas, M.A. McAllister, J.H. Ma, A. Perczel, M. Hollósi, I.G. Csizmadia, J. Mol. Struct. (Theochem) 369 (1996) 105.
[21] A. Perczel, Ö. Farkas, I.G. Csizmadia, Can. J. Chem. 75 (1997) 1120.
[22] I. Jakli, A. Perczel, Ö. Farkas, M. Hollosi, I.G. Csizmadia, J. Mol. Struct. (Theochem) 455 (1998) 303.
[23] H.A. Baldoni, A.M. Rodriguez, G. Zamarbide, R.D. Enriz, Ö. Farkas, P. Csaszar, L.L. Torday, C.P. Sosa, I. Jakli, A. Perczel,

M. Hollosi, I.G. Csizmadia, J. Mol. Struct. (Theochem) 465 (1999) 79.
[24] J.C. Vank, C.P. Sosa, A. Perczel, I.G. Csizmadia, Can. J. Chem. 78 (2000) 395.
[25] A. Perczel, Ö. Farkas, I.G. Csizmadia, J. Comput. Chem. 17 (1996) 821.
[26] A. Perczel, Ö. Farkas, I.G. Csizmadia, J. Am. Chem. Soc. 118 (1996) 7809.
[27] I. Jakli, A. Perczel, Ö. Farkas, C.P. Sosa, I.G. Csizmadia, J. Comput. Chem. 21 (2000) 626.
[28] W. Viviani, J.-L. Rivail, A. Perczel, I.G. Csizmadia, J. Am. Chem. Soc. 115 (1993) 8321.
[29] S.J. Salpietro, A. Perczel, Ö. Farkas, R.D. Enriz, I.G. Csizmadia, J. Mol. Struct. (Theochem) 497 (2000) 39.
[30] S. Hatse, K. Princen, L.O. Gerlach, G. Bridger, G. Henson, E. De Clercq, T.W. Schwartz, D. Schols, Mol. Pharmacol. 60 (2001) 164.
[31] C. Demougeot, P. Garnier, C. Mossiat, N. Bertrand, M. Giroud, A. Beley, C. Marie, J. Neurochem. 77 (2001) 408.
[32] K. Chlebovská, O. Chlebovský, Mech. Ageing Dev. 108 (1999) 127.
[33] P. Fedoročko, N.O. Macková, Z. Šándorčínová-Hoferová, Z. Sedláková-Hoferová, P. Solár, O. Chlebovský, Mech. Ageing Dev. 119 (2000) 159.
[34] J.A. Contreras, M. Karlsson, T. Østerlund, H. Laurell, A. Svensson, C. Holm, J. Biol. Chem. 271 (1996) 31426.
[35] G.F. Short III, A.L. Laikhter, M. Lodder, Y. Shayo, T. Arslan, S.M. Hecht, Biochemistry 39 (2000) 8768.
[36] R. Hu, J. Bekisz, H. Schmeisser, P. McPhie, K. Zoon, J. Immunol. 167 (2001) 1482.
[37] R. Hoffmann, D.J. Craik, K. Bokonyi, I. Varga, L. Otvos Jr., J. Pept. Sci. 5 (1999) 442.
[38] D. Saadat, D.H. Harrison, Biochemistry 37 (1998) 10074.
[39] J. Rotonda, M. Garcia-Calvo, H.G. Bull, W.M. Geissler, B. McKeever, N.A. Thornberry, J.W. Becker, Chem. Biol. 8 (2001) 357.
[40] M.J. Collins, E.R. Waite, A.C. van Duin, Philos. Trans. R. Soc. Lond. B, Biol. Sci. 354 (1999) 51.
[41] M.A. Berg, G.A. Chass, E. Deretey, A.K. Füzéry, B.M. Fung, D.Y.K. Fung, H. Henry-Riyad, A.C. Lin, M.L. Mak, A. Mantas, M. Patel, I.V. Repyakh, M. Staikova, S.J. Salpietro, T.-H. Tang, J.C. Vank, Ö. Perczel, L.L. Farkas, Z. Torday, I.G. Székely, J. Mol. Struct. (Theochem) 500 (2000) 5.
[42] E. Ruoslahti, M.D. Pierschbacher, Science 238 (1987) 491.
[43] M.K. Magnusson, S.S. Hong, P. Boulanger, L. Lindholm, J. Virol. 75 (2001) 7280.
[44] N. Okada, Y. Tsukada, S. Nakagawa, H. Mizuguchi, K. Mori, T. Saito, T. Fujita, A. Yamamoto, T. Hayakawa, T. Mayumi, Biochem. Biophys. Res. Commun. 282 (2001) 173.
[45] C. Hay, H. De Leon, J.D. Jafari, J.L. Jakubczak, C.A. Mech, P.L. Hallenbeck, S.K. Powell, G. Liau, S.C. Stevenson, J. Vasc. Res. 38 (2001) 315.
[46] C.D. Anuradha, S. Kanno, S. Hirano, Cell Biol. Toxicol. 16 (2000) 275.
[47] H. Ghandehari, R. Sharan, W. Rubas, W.M. Killing, J. Pharm. Pharm. Sci. 4 (2001) 32.
[48] M.J. Frisch, G.W. Trucks, H.B. Schlegel, P.M.W. Gill, B.G. Johnson, M.A. Robb, J.R. Cheeseman, T. Keith, G.A. Petersson, J.A. Montgomery, K. Raghavachari, M.A. Al-Laham, V.G. Zakrzewski, J.V. Ortiz, J.B. Foresman, J. Cioslowski, B.B. Stefanov, A. Nanayakkara, M. Challacombe, C.Y. Peng, P.Y. Ayala, W. Chen, M.W. Wong, J.L. Andres, E.S. Replogle, R. Gomperts, R.L. Martin, D.J. Fox, J.S. Binkley, D.J. Defrees, J. Baker, J.P. Stewart, M. Head-Gordon, C. Gonzalez, J.A. Pople, GAUSSIAN 94, Revision D.2, Gaussian Inc., Pittsburgh, PA, 1995.
[49] M.J. Frisch, G.W. Trucks, H.B. Schlegel, G.E. Scuseria, M.A. Robb, J.R. Cheeseman, V.G. Zakrzewski, J.A. Montgomery, Jr., R.E. Stratmann, J.C. Burant, S. Dapprich, J.M. Millam, A.D. Daniels, K.N. Kudin, M.C. Strain, O. Farkas, J. Tomasi, V. Barone, M. Cossi, R. Cammi, B. Mennucci, C. Pomelli, C. Adamo, S. Clifford, J. Ochterski, G.A. Petersson, P.Y. Ayala, Q. Cui, K. Morokuma, D.K. Malick, A.D. Rabuck, K. Raghavachari, J.B. Foresman, J. Cioslowski, J.V. Ortiz, A.G. Baboul, B.B. Stefanov, G. Liu, A. Liashenko, P. Piskorz, I. Komaromi, R. Gomperts, R.L. Martin, D.J. Fox, T. Keith, M.A. Al-Laham, C.Y. Peng, A. Nanayakkara, C. Gonzalez, M. Challacombe, P.M.W. Gill, B.G. Johnson, W. Chen, M.W. Wong, J.L. Andres, M. Head-Gordon, E.S. Replogle, J.A. Pople, GAUSSIAN 98, Revision A.x, Gaussian Inc., Pittsburgh, PA, 1998.
[50] J.C.P. Koo, G.A. Chass, A. Perczel, Ö. Farkas, L.L. Torday, A. Varro, J.G. Papp, I.G. Csizmadia, Eur. Phys. J. D. 20 (2002) 499–511.
[51] J.C.P. Koo, G.A. Chass, A. Perczel, Ö. Farkas, L.L. Torday, A. Varro, J.G. Papp, I.G. Csizmadia, J. Phys. Chem. A 106 (2002) 6999.
[52] M. Tarditi, M.W. Klipfel, A.M. Rodriguez, F.D. Suvire, G.A. Chasse, Ö. Farkas, A. Perczel, R.D. Enriz, J. Mol. Struct. (Theochem) 545 (2001) 29.
[53] M.F. Masman, M.G. Amaya, A.M. Rodriguez, F.D. Suvire, G.A. Chasse, Ö. Farkas, A. Perczel, R.D. Enriz, J. Mol. Struct. (Theochem) 543 (2001) 203.
[54] M.N. Barroso, E.S. Cerutti, A.M. Rodriguez, E.A. Jauregui, Ö. Farkas, A. Perczel, R.D. Enriz, J. Mol. Struct. (Theochem) 548 (2001) 21.